ABSTRACT

The central theme of this thesis is the high temperature physical chemistry of metal sulphates , and the aspects dealt with in parts one and two are , respectively , decomposition kinetics and phase diagrams.

The original investigations in part one are concerned with the isothermal decomposition (loss of SO_3) in high vacuum of packed or aggregated MSO_4 powder (M = Cu^{2+} , Ni^{2+} , Zn^{2+} , Fe^{3+}). Weight loss versus time plots were analysed to obtain rate laws and the correlation of these data with observations of reaction morphology is discussed. It was found that the decomposition of powder packed in a small Pt cup occurred by the thickening of a band of oxide which formed on the exposed surface. This mode of reaction , as opposed to the independent decomposition of each grain , implies intergranular interaction and mechanisms for this are proposed.

Part one contains an account of the physicochemical principles of decomposition reactions , which aims to clarify some of those aspects not fully discussed in existing texts on this topic.

The original investigations in part two deal with the determination of phase diagrams of decomposable sulphate systems. Differential thermal analysis (DTA) apparatus capable of operating with an SO_3 atmosphere is described and this , together with quenching techniques , was used to study two problematic systems. The SO_3 atmosphere suppresses decomposition and so extends the temperature range in which a sulphate is chemically stable. A polymorphic transition of $ZnSO_4$, which is usually obscured by decomposition , is fully characterised here. The study of the previously undetermined phase diagram for the system Ag_2SO_4-$BeSO_4$ includes some observations of the kinetics of the phase change involved.

HIGH TEMPERATURE STUDIES OF METAL SULPHATES

A Thesis

presented for the degree of

DOCTOR OF PHILOSOPHY

in the Faculty of Science of the

University of St. Andrews

by

Edmund Gimzewski

United College of
St. Salvator and St. Leonard
St. Andrews.

May 1981.

CERTIFICATE

I hereby certify that Edmund Gimzewski has spent eleven terms of research work under my supervision, has fulfilled the Conditions of Resolution of the University Court, 1967, No. 1 and of Ordinance General No. 12 (St. Andrews), and is qualified to submit the accompanying thesis in application for the degree of Doctor of Philosophy.

P.A.H. Wyatt
Director of Research.

DECLARATION

I declare that this thesis is my own composition , that the work of which it is a record has been carried out by me , and that it has not been submitted in any previous application for a Higher Degree.

This thesis describes results of research carried out at the Department of Chemistry , University of St. Andrews , under the supervision of Professor P.A.H.Wyatt since the 1st of October 1978.

E.Gimzewski

ACKNOWLEDGEMENTS

I would like to express my gratitude to all those members of the teaching and technical staff of the Chemistry Department of the University of St. Andrews who have helped me during the course of this work. In particular , I thank Professor P.A.H.Wyatt for many stimulating discussions and Z.M.Zochowski for his invaluable practical help and encouragement.

Mention must also be made of the considerable assistance of A.S.Edwards from the Gatty Marine Laboratory and C.H.Donaldson and R.A.Batchelor from the Department of Geology.

SUMMARY

The central theme of this thesis is the high temperature physical chemistry of metal sulphates , and the aspects dealt with in parts one and two are , respectively , decomposition kinetics and phase diagrams.

The original investigations in part one are concerned with the isothermal decomposition (loss of SO_3) in high vacuum of packed or aggregated MSO_4 powder (M = Cu^{2+} , Ni^{2+} , Zn^{2+} , Fe^{3+}). Weight loss versus time plots were analysed to obtain rate laws and the correlation of these data with observations of reaction morphology is discussed. It was found that the decomposition of powder packed in a small Pt cup occurred by the thickening of a band of oxide which formed on the exposed surface. This mode of reaction , as opposed to the independent decomposition of each grain , implies intergranular interaction and mechanisms for this are proposed.

Part one contains an account of the physicochemical principles of decomposition reactions , which aims to clarify some of those aspects not fully discussed in existing texts on this topic.

The original investigations in part two deal with the determination of phase diagrams of decomposable sulphate systems. Differential thermal analysis (DTA) apparatus capable of operating with an SO_3 atmosphere is described and this , together with quenching techniques , was used to study two problematic systems. The SO_3 atmosphere suppresses decomposition and so extends the temperature range in which a sulphate is chemically stable. A polymorphic transition of $ZnSO_4$, which is usually obscured by decomposition , is fully characterised here. The study of the previously undetermined phase diagram for the system Ag_2SO_4-$BeSO_4$ includes some observations of the kinetics of the phase change involved.

Part two reviews experimental techniques and describes the thermodynamic basis of phase diagrams with particular reference to recent computer calculation methods. These accounts aim to provide a comprehensive but readable introduction to this technologically very important branch of solid-state chemistry.

CONTENTS

THE PHYSICOCHEMICAL PRINCIPLES OF DECOMPOSITION REACTIONS

INTRODUCTION

The complete characterisation of a decomposition reaction in the solid state presents a considerable challenge to the physical chemist. These reactions are of type $AB_{(s)} \rightarrow A_{(s)} + B_{(g)}$, where the solid product is a distinct phase and does not form a solid solution with the reactant. It follows that there will be a phase boundary or interface between the solids A and AB, which moves into the undecomposed reactant with an evolution of gas in the opposite direction[1]. A section of such an interface is shown in fig. 1.

The course of these reactions can be divided into three sections : (1) the appearance of nuclei of the product phase on the surface of the reactant; (11) the growth of these nuclei; (111) the termination of reaction when an interface reaches the periphery of the sample or meets another interface. These stages are illustrated in fig. 2 for a single cube of reactant into which the nuclei grow three-dimensionally at hemispherical interfaces.

Most studies of decomposition reactions have been carried out under conditions in which each particle of the reactant mass decomposes independently. Such a mass may consist of a single crystal or loosely packed ground crystals, some workers preferring the latter because diffusion paths for gas release are shorter. There is little satisfactory data on the decomposition of packed or aggregated powders, probably because of a desire by workers to establish first the kinetics and mechanisms for materials of well-defined structure and texture. The data presented in this work highlight the co-operative nature of the decomposition of powders, which manifests itself by reaction at a single macroscopic interface.

Although the following exposition of the physicochemical principles of decomposition reactions will concern itself with the case of a cube of isotropic crystal, the concepts and equations will be seen later to

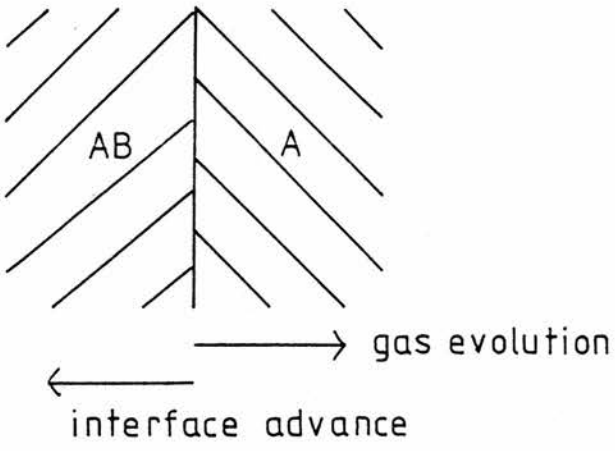

Fig. 1. A section of the interface during a decomposition reaction.

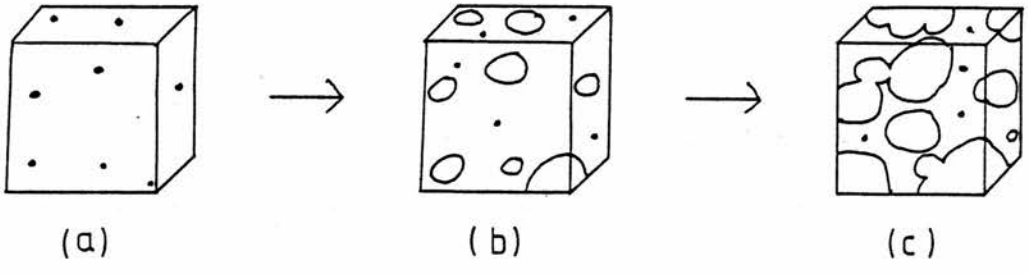

Fig. 2. The decomposition of a cube of crystal.
(a) the appearance of nuclei of product on the surface; (b) the growth of these nuclei; (c) the overlap of growing nuclei.

be applicable to powders. This exposition attempts to provide a much-needed unified account of solid-state decompositions and draws upon the traditional treatment of the subject as reviewed by Jacobs, Tompkins and Young [2-4], and the recent work of Searcy and Beruto [5]. The lay-out is as follows.

First, nucleation of one solid phase in another is described in thermodynamic terms. The next part deals with the growth of nuclei and discusses fully the effects of self-cooling and back reaction. There follows a section in which the rate laws for nucleation and growth are coupled to generate equations for weight loss as a function of time. Then some consideration is given to the reaction interface at an atomic level and to transformations of the product layer. Finally, a brief account is given of the techniques used to obtain kinetic data.

NUCLEATION

The bulk measurable properties of a solid, liquid or gas, correspond to the average of all the accessible quantum states for that system, and the probability of states which differ only slightly from the average is extremely small[6]. For most practical purposes these fluctuations about the mean can be ignored but there are processes whose occurrence is directly attributable to them[7]. These processes involve the creation of a new phase as in the liquefaction of a gas, the melting of a solid, polymorphic transformations, etc.

In decomposition reactions there is the creation of new solid and gas phases and the fluctuations of interest here are in atomic configurations. Small regions of the reactant can have an instantaneous arrangement of bonds which is characteristic of the products and these regions can either relax to a more probable structure or act as centres (nuclei) of growth of the new solid phase, depending on their free energy.

The free energy change for the creation of nuclei has contributions from two sources[2,8]. First, there is the free energy change for the reaction $AB_{(s)} \longrightarrow A_{(s)} + B_{(g)}$, which will be written ΔG_R and will have units of energy per unit volume. Second, there will be a free energy change associated with the creation of the reactant-product interface. This surface free energy, ΔG_s, has units of energy per unit area and can be imagined as the work done in joining a crystal face of AB to that of A in such a way that the interfacial atoms in lattice A are matched one-to-one with the atoms of the A sublattice in AB. The free energy change for the formation of a spherical nucleus of product of radius r can now be written as

$$\Delta G = 4\pi r^2 \Delta G_s + \frac{4}{3}\pi r^3 \Delta G_R \,. \qquad (1)$$

ΔG_s is a positive quantity and ΔG_R will, above a certain temperature, be negative. The variation of ΔG with r will be the sum of an increasingly

positive and an increasingly negative part, as shown in fig. 3.

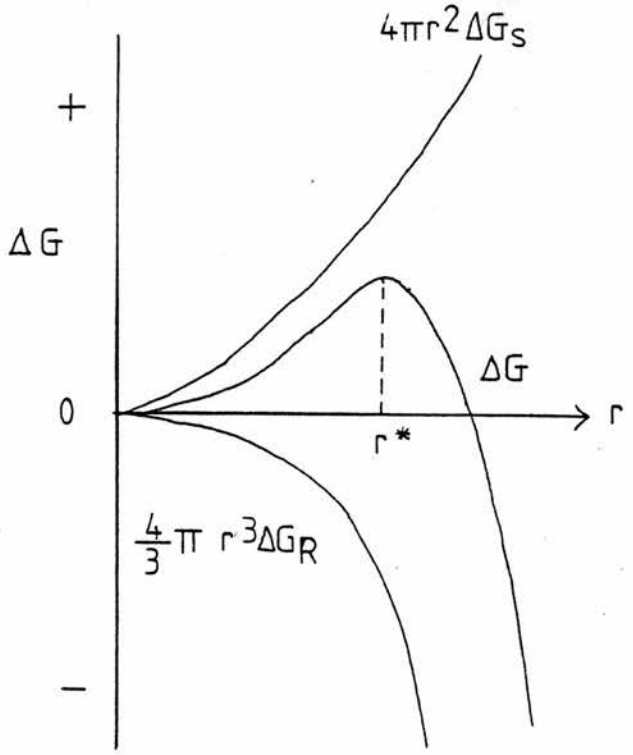

Fig. 3.

Up to a critical radius r^* given by solving

$$\frac{d}{dr}\left(4\pi r^2 \Delta G_s + \frac{4}{3}\pi r^3 \Delta G_R\right) = 0 \qquad (2)$$

there will be an increase in G for the growth of the nucleus because $dG/dr > 0$. The nucleus will relax to a more probable atomic configuration of the reactant. When, however, a fluctuation gives rise to a nucleus with $r > r^*$, then $dG/dr < 0$ so that growth is thermodynamically favourable.

When such nuclei form in the bulk of a reactant phase, the nucleation is said to be 'homogeneous'. Imperfections or impurity inclusions may facilitate nucleation by decreasing the free energy change for the creation of the reactant-product interface. This will depend upon the relation between the interfacial energies of the solid product phase with respect to the imperfection and with respect to the bulk phase. Nucleation of

this kind is said to be 'heterogeneous' and occurs not only at inclusions but at surfaces, grain boundaries and dislocations. In fact, for decomposition reactions nucleation is always heterogeneous, occurring on the reactant surface, because there are no channels in the bulk of the crystal for the escape of product gas and evidence suggests that the rate of gaseous diffusion through a lattice is very slow[9]. There is direct experimental evidence that nuclei form preferentially at lattice imperfections[10].

Consider the case of nucleation occurring at identical imperfections distributed uniformly over the surface of a cube of crystal. To simplify the argument, each imperfection is regarded as a potential nucleus-forming site and there are N_o of these. It is reasonable that there is an equal probability of each site undergoing a critical fluctuation to give rise to a growth centre, so that the rate of formation of nuclei is comparable to the first order decay of an isotope. If N is the number of nuclei at time t, then

$$\frac{dN}{dt} = k\,(N_o - N) \qquad (3)$$

where k is the rate constant for nucleation. With neglect of the possible ingestion of potential nucleus-forming sites by growth of other nuclei, this equation can be integrated to give

$$N = N_o(1 - e^{-kt}). \qquad (4)$$

For small t, $dN/dt \simeq kN_o$ and this has been observed experimentally for the initiation of dehydration of $CuSO_4 \cdot 5H_2O$[11] and $KCr(SO_4)_2 \cdot 12H_2O$[12]. Full accounts of nucleation are given in the reviews by Jacobs, Tompkins and Young.

GROWTH OF NUCLEI

When a fluctuation has led to the appearance of a nucleus of product with a radius greater than the critical value, the subsequent growth of the nucleus is thermodynamically favourable. Early direct observations of nucleus growth by means of hot-stage microscopy showed the rate of advance of the reactant-product interface to be constant for a constant temperature[3]. Recent work on the decomposition of single crystals of $CaCO_3$ and $BaSO_4$ in high vacuum confirms this observation[13,14]. This law may be expressed in the form

$$-dx/dt = k(T) \qquad (5)$$

where x is a direction normal to the interface and k is the rate constant, which is a function of temperature.

It will now be argued that such a rate law will manifest itself only if two complicating processes do not become important. These are self-cooling and back reaction, and will be discussed for the case of a cube of crystal undergoing isothermal decomposition in a high vacuum. It will be assumed that reaction has been initiated by rapid and complete surface nucleation which produces a cubic reactant-product interface (fig. 4).

Self-cooling

The progress of an endothermic decomposition requires a flow of heat to maintain the reaction. Consider the case shown in fig. 4 in which the reaction interface is a contracting cube. It will be assumed that the temperature of the exterior surface of the sample is maintained at T_o by very rapid heat transfer from the surroundings and that there is no reverse reaction at the interface. The rate of heat flow dq/dt to the interface of area a which occurs through a product layer of thermal conductivity K is the consequence of a temperature gradient dT/dx. These quantities are related by Fourier's heat diffusion law

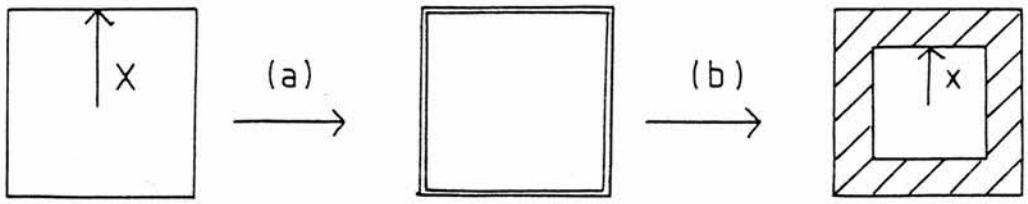

Fig. 4. A section of a cube of crystal decomposing by the contracting cube mechanism.
(a) rapid and complete surface nucleation has resulted in a shell of product; (b) reaction occurs by the contraction of this cubic interface.

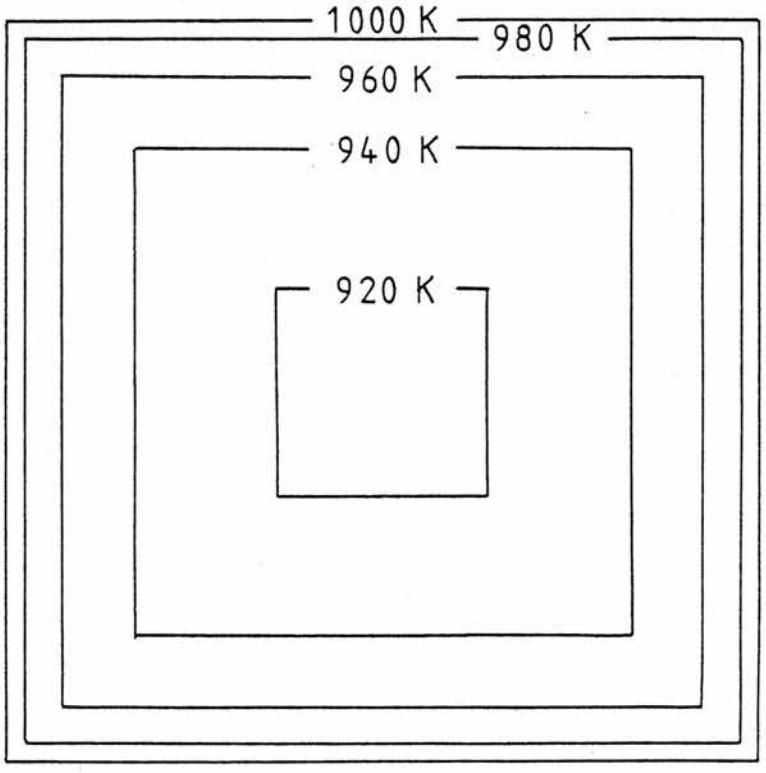

Fig. 5. Self-cooling in a cube of crystal decomposing by the contracting cube mechanism. The interfacial temperature is given for various extents of reaction.

$$-dq/dt = \kappa\, a\, dT/dx \qquad (6)$$

where $a = 24x^2$. The infitesmal amount of heat dq required to decompose a volume dV of the reactant is given by

$$-dq = EdV \qquad (7)$$

where E is the enthalpy of reaction for unit volume of reactant (assumed here to give unit volume of product). Together with the rate equation $-dx/dt = k(T)$, the above relations can be used to determine the interfacial temperature T_i at any extent of reaction. The argument is as follows.

Volume of reactant decomposed $V = 8(X^3-x^3)$

$\therefore dx = -dV/(24x^2) = +(dq/E) / (24x^2)$

$\therefore dq/dx = +24Ex^2 \qquad (8)$

Next, use is made of the equality $dq/dt = dq/dx.dx/dt$ to relate equations 6, 8 and 5.

$-\kappa\, 24x^2\, dT/dx = (+24Ex^2)(-k(T))$

$\therefore dT/dx = Ek(T)/\kappa$

A reasonable expression for k(T) would be $Be^{-\varepsilon/RT}$ where ε is the molar activation energy and B is a constant. Making this substitution and separating the variables (T and x) gives the equation

$$\int_{T_i}^{T_o} e^{\varepsilon/RT}\, dT = (EB/\kappa)\int_{X}^{x} dx = (EB/\kappa)(X-x)$$

The integral of $e^{\varepsilon/RT}$ was solved numerically using a computer. The following values, typical of decomposition reactions, were used to calculate the value of X-x for various T_i.

$E/(J\ m^{-3}) = 6\times10^9$; $\varepsilon/(J\ mol^{-1}) = 2.5\times10^5$;

$B/(m\ s^{-1}) = 10^8$; $\kappa/(J\ s^{-1}m^{-1}K^{-1}) = 1.0$;

$T_o/K = 1000$; $X/m = 10^{-2}$

Fig. 5 shows how T_i varies as the interface advances into the cube.

The effect of the temperature difference is that the interfacial reaction will be occurring at a temperature lower than that of the surroundings and therefore not readily measurable. This introduces an error in temperature measurement. More serious is the possibility that the value of ΔT may increase significantly as the reaction proceeds (i.e. as X-x increases) and cause a deceleration of the interface. Such complications are most likely when the reaction rate is large and the product layer is thick, i.e. a large sample. In fact, when CaO is produced industrially from $CaCO_3$, there can be temperature differences of hundreds of kelvins between the surface and reaction interface in 10 cm diameter spheres[15].

When studying the kinetics of decomposition reactions under isothermal conditions, it is clearly desirable to minimise self-cooling by using suitably small sample masses and low reaction rates.

Reverse reaction

The apparently simple topic of reverse reaction at the interface during a decomposition reaction requires considerable discussion as it is tied up with the subject of gas transport in porous solids[16,17]. The approach adopted will be to look upon the interface as a source of a uniform flux J_o which is a function only of temperature. Microscopic evidence shows that the solid product of a decomposition reaction does not form as a continuous solid but that there is usually considerable pore structure or at least many fissures[3,5,16]. The detailed mechanisms which dictate the texture and crystallographic structure of the product will be dealt with in a later section. For present purposes, the product layer will be regarded as a uniformly porous solid and will be idealised as an array of parallel cylindrical capillaries. The aim will be to show the mechanisms by which gaseous product molecules can return to the interface and become re-incorporated into the reactant phase.

First, however, as background to the discussion, a brief account will be given of gas transport through tubes.

Textbooks generally recognise three types of flow of gases : laminar, turbulent[18] and Knudsen. The latter is sometimes called 'molecular'[19]. Where capillaries are involved, surface flow of gas adsorbed on capillary walls must be considered, particularly at low gas densities.

In laminar flow, the net motion of a molecule results from collisions with other molecules in a fluid in which there is a pressure gradient. For the flow of gas of viscosity η through a tube of radius r and length L, with pressures P_1 and P_2 at the ends, the flowrate is given by Poiseuille's equation for a compressible fluid :

$$\frac{dV}{dt} = \pi (P_2^2 - P_1^2) r^4 / (16 L \eta P_o). \qquad (10)$$

Here $P_2 > P_1$ and P_o is the pressure at which the volume is measured.

The above equation is found to fail when the velocity of a fluid exceeds a certain critical value and then the nature of the flow becomes very complicated. Random local circular currents called vortices develop and there is a large increase in the resistance to flow. Flow of this sort is called 'turbulent'. Flow can be characterised by a number N_R such that when $N_R > 3000$ flow is turbulent. This is the Reynolds number and is given by

$$N_R = 2r\rho u / \eta$$

where ρ is the gas density, η is the gas viscosity and u is the linear velocity which would result from the same volumetric flowrate under laminar conditions. The interparticle spaces in porous solids, however, tend to be so small that turbulent flow conditions never prevail.

In laminar flow the mean free path of a molecule is short compared to the dimensions of the tube, so that the properties of the gas are

determined by the frequency and nature of intermolecular collisions. The question arises as to the nature of the flow when the density of the gas becomes so low that the mean free path has dimensions comparable to the tube. Intermolecular collisions will become rare compared to collisions with walls and the molecules will behave independently in giving rise to the properties of the gas. This can be appreciated by considering the situation represented in fig. 6.

A plate of solid vaporises slowly into a cylinder of length L and radius r, which has a perfect condenser at the other end. That is, molecules which strike the condenser will stick there indefinitely ; in practice this is achieved by a cold trap. When a steady state is reached, the rate of loss of mass from the solid equals the rate of gain for the condenser and it will be assumed that in this condition the gas density in the cylinder will be so low that intermolecular collisions are negligible. Gas transport is now occurring by Knudsen flow.

A molecule breaking away from the solid lattice will travel in a straight line until it strikes the tube wall, from which it will 'rebound' in a direction independent of the direction of incidence. This behaviour is attributed to the molecular roughness of the wall by Lorentz[20] and to an adsorption-re-emission process by Langmuir[21].

A possible series of trajectories for a molecule is shown in fig. 6. There the molecule reached the condenser, but it is also possible that it may be returned to the surface where it can either become part of the lattice structure or undergo an adsorption-re-emission process. For convenience, the probability that a molecule will become incorporated into the parent phase, rather than 'rebound', will be denoted by z , which is often called the 'condensation coefficient'[22].

To quantify the influence of a tube on the flux of molecules

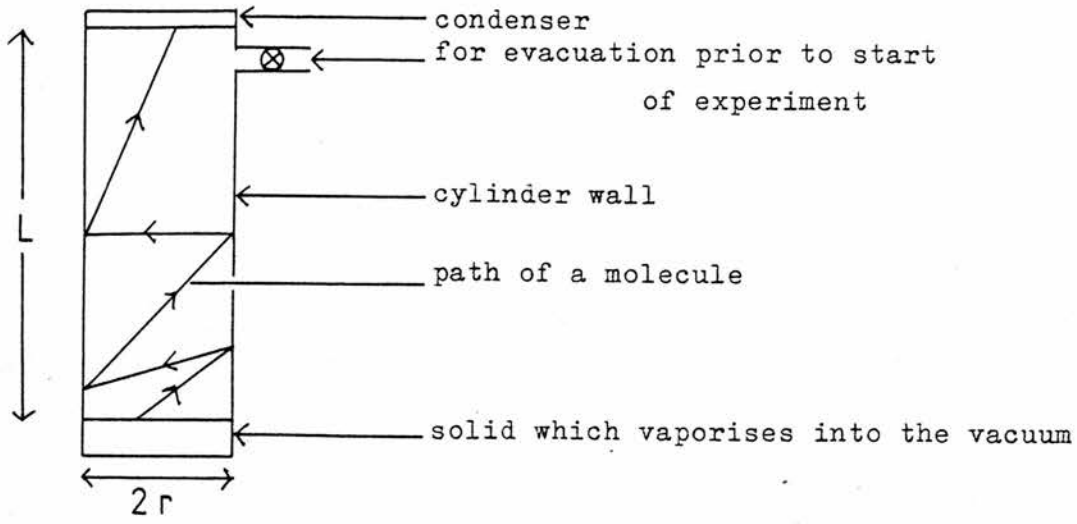

Fig. 6. The vaporisation of a solid into a vacuum.

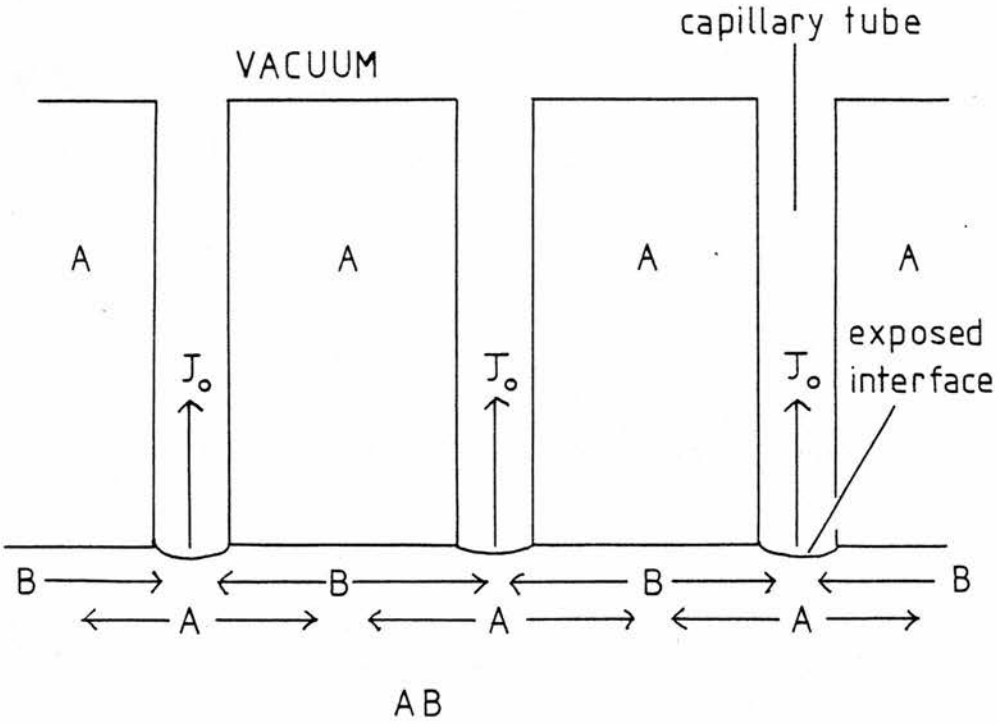

Fig. 7. The model of the reaction interface proposed by Searcy and Beruto.

leaving the surface one can introduce the idea of escape probability[23]. This is defined as the probability P_e that a molecule leaving the surface of the lattice will pass through a tube of length L and radius r to a condenser, and P_e is a function of L/r and z . It transpires that given a formula for P_e for the specific case of z = 1 , the general equation for P_e (L/r , z) can be derived easily[23].

There are two approaches to the calculation of $P_1 = P_e$ (L/r ,z=1): one is analytical and the other is 'experimental'. Clausing[24] has applied the former method and obtained the relations

$$P_1 = 1/(1 + .5L/r) \qquad \text{and}$$

$$P_1 = 1/(1 + .4L/r)$$

in the limits as L/r tends to zero and infinity respectively. The 'experimental' approach[23] uses the Monte Carlo method[25] to generate a series of molecular histories by determining molecular paths from random numbers. P_1 is simply defined as

$$P_1 = \frac{\text{number of histories which end in an escape}}{\text{number of histories followed}}$$

The accuracy of the values of P_1 thus obtained is related to the number N of histories followed , and the standard deviation of the result is given by

$$\sigma = (P_1(1-P_1) / N)^{\frac{1}{2}}$$

Although the Monte Carlo solutions merely confirm the analytical results of Clausing in this case , there are many related situations where an analytical solution is prohibitively difficult and here the Monte Carlo method is an invaluable tool[17].

The derivation of P_e (L/r , z) from P_1 can be made by following the fate of a group of N molecules which break free from the solid lattice. P_1 N molecules will escape and $(1-P_1)N$ will return to the surface of the solid where $z(1-P_1)N$ will become incorporated and

$(1-z)(1-P_1)N$ will 'rebound'. Of these, $(1-P_1)(1-z)(1-P_1)N$ will return to the solid surface. Continuing this analysis leads to the result that the escape probability can be represented by the following geometric series

$$P_e\ (L/r\ ,\ z) = P_1 + P_1(1-z)(1-P_1) + P_1(1-z)^2(1-P_1)^2 + \ldots$$

$$= P_1 \sum_{n=o}^{\infty} \left((1-z)(1-P_1) \right)^n$$

Since $0 < (1-z)(1-P_1) < 1$, the series converges and on rearrangement

$$P_e\ (L/r\ ,\ z) = 1/(1 + 0.4zL/r)$$

The molecular flux, J, at the condenser plate for any L/r ratio can now be related to the flux J_o when no tube impedes Knudsen flow. The formula is

$$J = P_e J_o = J_o/(1 + 0.4zL/r) \qquad (11)$$

It can be shown that the condensation coefficient[22] is given by

$$z = J_o / J(P_{eq}) , \qquad (12)$$

where $J(P_{eq})$ is the flux associated with the equilibrium vapour pressure of the solid, and this provides the means of determining z. Values have been obtained for many metals and vary from 1 to 10^{-5}.

In the discussion of flow so far , the adsorption of gas onto the tube wall has been mentioned only as part of a mechanism to account for the random trajectory of a desorbed molecule. An adsorbed molecule moves in the potential field created by the atoms of the lattice of the solid wall[6]. The relative magnitudes of the wells in this periodic potential, V_o, and the thermal energy of the molecules of the adsorbed phase determine the surface mobility. For $kT > V_o$ there is virtually unimpeded surface migration and , if there is a low surface concentration , the adsorbed phase is comparable to a 2-D ideal gas. It can be shown that for these conditions the surface concentration

C_s is directly proportional to the pressure of gas with which it is in equilibrium[26-29]. If this equilibrium is maintained locally along the length of the tube through which there is gas transport by Knudsen flow, then part of the molecular flux will occur on the surface. This surface contribution will increase as the tube radius decreases since , for a fixed length of tube , the ratio of moles on the surface to moles in the gas phase is inversely proportional to r.

The quantification of these phenomena , however , is still a field of active research[17] and any subsequent discussion of their role in gas transport in decomposition reactions will be essentially qualitative.

To discuss the significance of these modes of flow for the kinetics of decomposition reactions , it is necessary to introduce some model for the interface. The detailed mechanisms of processes occurring at the interface will be considered in a later section but for the present a model proposed by Searcy and Beruto[5] will be used.

In fig. 7 the product layer forms when solid A diffuses along a gradient of chemical potential (not of concentration) from the exposed region of the interface. There is a counter flux of component B from the product-reactant interface towards the exposed region where it is released into the capillary tube.

What is important here is that the mechanism for back reaction due to the effects of the product layer can be discussed by considering the way in which a capillary tube of length L and radius r modifies the flux emanating from the exposed interface. This surface is characterised by a condensation coefficient z , which as before is the probability that a molecule of $B_{(g)}$ will become incorporated into the AB lattice on colliding with the surface. A molecule emerging from the product layer is assumed to be assimilated into the vacuum system so that the situation is identical to the case involving the condenser.

If the steady-state gas density is such that Knudsen flow dominates, the flux J from the tube is related to the flux J_o of molecules of $B_{(g)}$ breaking away from the interface by the equation

$$J = J_o / (1 + .4zL/r) \qquad (13)$$

Two limiting cases of this equation deserve mention. First , when $1 \gg .4zL/r$, $J=J_o$ and there is no back reaction. This condition could be the consequence of a highly irreversible reaction , that is , a very small value of z. Second , when $1 \ll .4zL/r$, $J=J_o r/(.4zL)$. In the present model , z,r and J_o are constants at a constant temperature , and the rate of interface advance $dL/dt \propto J$. It follows that

$$dL/dt \propto L^{-1}$$

and , by integration , $L \propto \sqrt{t}$. This is the so-called 'parabolic' law, frequently encountered in interfacial gas-solid reactions. As $L \rightarrow \infty$, $J \rightarrow 0$ and the forward and reverse fluxes equalise to create equilibrium conditions at the interface.

If, however, the steady-state gas density is such that laminar flow prevails , the flux J form the capillary tube will be

$$J = N_A(dn/dt)/(\pi r^2) = P_i^2 r^2 / (16L\eta kT) \qquad (14)$$

Here P_i is the interfacial pressure, k is Boltzmann's constant, and dn/dt , the moles of gas flowing per second , is obtained from Poiseuille's equation by setting $P_2=P_i$ and $P_1=0$ (vacuum) ; then

$$n = \frac{P_o V}{RT} \quad \therefore \quad \frac{dn}{dt} = \frac{P_o}{RT}\frac{dV}{dt} = \frac{P_o}{RT}\,\frac{\pi P_i^2 r^4}{P_o 16L\eta} = \frac{\pi P_i^2 r^4}{RT16L\eta}$$

It can be shown by a lengthy argument that P_i is a function of L , but for larger values of L it tends to the equilibrium pressure P_{eq}.

$$\therefore J \propto P_{eq}^2 / L \qquad (15)$$

and a parabolic rate law results as for the second limiting case with Knudsen flow.

One way of deciding whether there is Knudsen flow through the product layer is to imagine the system at equilibrium , when the pressure of $B_{(g)}$ will have its maximum value for that temperature. The calculated mean free path can then be compared to the dimensions of interparticle spaces or channels in the sample as measured by microscopy.

Many studies of decomposition kinetics , particularly those employing differential thermal analysis , are carried out in a flowing atmosphere of inert gas , usually N_2. Two consequences of this practice are : first , the product gas on leaving the interface must diffuse through channels in the product layer filled with inert gas ; second , product gas leaving the exterior surface of the product layer may be returned to this layer by collisions with the surrounding inert gas. The former process is uninfluenced by the inert flowrate but the latter is markedly dependent on this and on the volume of inert gas surrounding the sample container in the apparatus. Both processes promote back reaction to an extent which is difficult to quantify. However , some appreciation of the effects of an inert atmosphere can be gained by considering the apparatus shown in fig. 8.

A stream of N_2 of known flowrate passes into a chamber containing a decomposable substance $AB_{(s)}$ held at a temperature at which it loses weight significantly over a period of hours. From the weight loss of the sample over a period during which the rate of weight loss was constant , and the amount of inert gas passed , the partial pressure of $B_{(g)}$ in the chamber is given by

$$P_B = X_B \, P_{atmosphere}$$

where $X_B = \dfrac{\text{moles B lost}}{\text{moles B lost + moles } N_2 \text{ passed}}$

When P_B as calculated above at a particular temperature is plotted

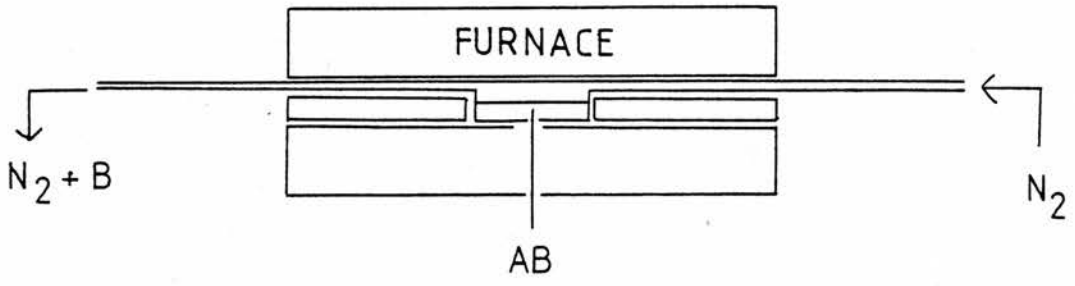

Fig. 8. Apparatus for studying the decomposition rate of a salt in a flowing inert gas.

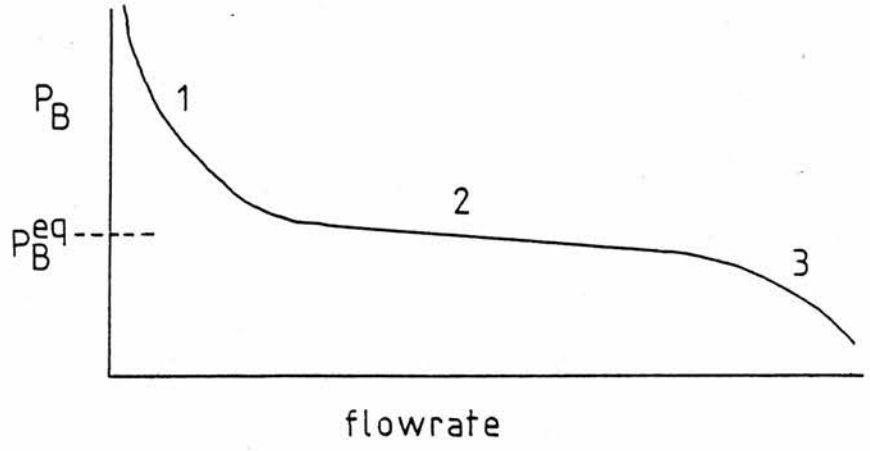

Fig. 9. Dependence of P_B on flowrate.

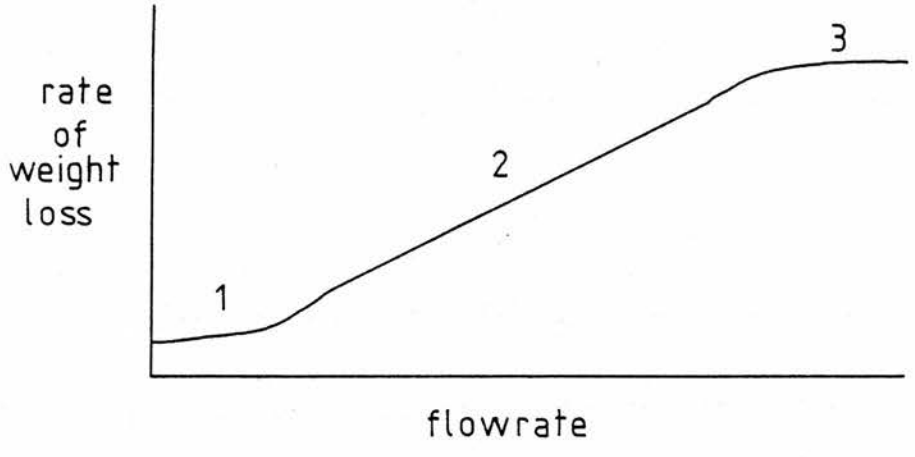

Fig. 10. Dependence of decomposition rate on flowrate.

against flowrate , the plot obtained usually resembles fig. 9. Fig. 10 gives the corresponding rate of weight loss as a function of flowrate.

The interpretation of these regions is as follows. For moderate flowrates (region 2) the equilibrium $AB_{(s)} \rightleftarrows A_{(s)} + B_{(g)}$ is so rapidly reversible that the removal of B in the gas leaving the chamber can be readily compensated for by the forward reaction and P_B equals its equilibrium value in this region. Increasing the flowrate increases proportionally the amount of $B_{(g)}$ removed per minute and this accounts for the upward slope in fig. 10. For higher flowrates (region 3) the removal of $B_{(g)}$ from the chamber cannot be compensated for by the forward reaction and the equilibrium partial pressure can not be sustained. As the flowrate increases in this region , the pressure which the forward reaction can maintain becomes less. At very high flowrates one can imagine a molecule emerging from the product layer and being swept off in the stream of N_2. Only under these conditions can meaningful kinetic measurements be made. There remains , however , the serious complication of back reaction due to collisions of product gas molecules with N_2 in the product layer.

As zero flowrate is approached (region 1) , $B_{(g)}$ can diffuse down the exit tube into the atmosphere through a more or less static N_2 stream. This accounts for the residual rate at zero flowrate and X_B , as defined above , formally equals 1.

The interpretation of such plots for more complicated flow situations adds another difficulty to the study of decomposition kinetics in an inert gas.

The experiment described actually provides a means of determining equilibrium vapour pressures of solids and liquids. It is called the 'transpiration' or 'gas saturation' method and has been applied successfully to simple vaporisation processes[22,30]. Fig. 9 provides

the criterion for equilibrium and has been rigorously derived using diffusion theory[31].

THE VOLUME OF PRODUCT AS A FUNCTION OF TIME

In the previous section , equations were proposed for the rate of interface advance for the cases of no back reaction and a back reaction due to the impedance to flow exerted by the product layer. To account for the experimentally measured weight loss as a function of time , it is necessary to recognise the combined effects of nucleation , the growth of nuclei and the specific geometry of the sample. Consider, for example, the reaction represented in fig. 2. Given the rate equations for the appearance of nuclei at random points on the surface and for their growth , two complications prevent an exact mathematical prediction of the whole course of the reaction. First , there is the disappearance of potential nucleus-forming sites due to the advancing interface of a neighbouring growing nucleus. This reduces the rate of appearance of nuclei. Second , the volume at time t_f of a nucleus of known geometry can readily be obtained by integrating the growth law. However , when two interfaces meet or when an interface reaches the periphery of a sample , the volume of a nucleus becomes a much more complicated function of time.

An exact mathematical treatment is only possible when the above complications are absent , as , for example , during the early stages of a decomposition where the nuclei are few , far apart and small[2]. For such cases , the volume of product at time t_f is given by

$$V(t_f) = \int_0^{t_f} \left(\sigma \left(\int_t^{t_f} \left(\frac{dx}{dt}\right) dt \right)^{\lambda} \left(\frac{dN}{dt}\right) \right) dt \qquad (16)$$

where dN/dt is the rate of appearance of nuclei , dx/dt is the rate of interface advance , and σ and λ are shape factors. For example ,

for a spherical nucleus $\sigma = 4\pi/3$ and $\lambda = 3$. Applications of this equation are dealt with in the reviews by Jacobs, Tompkins and Young.

The much more complicated problem of accounting for ingestion of potential nucleus-forming sites and for overlap of growing nuclei has been tackled by Avrami[32], Erofeyev[33] and Mampel[34].

When a decomposition is initiated by the rapid and complete nucleation of the particle's surface , the subsequent reaction can occur at a contracting envelope (c.f. fig. 4). For future use , the case of a spherical particle of initial radius R decomposing at a contracting spherical interface of radius r will be treated here. It is usual to express the extent of reaction as

$$\alpha = \frac{\text{volume decomposed}}{\text{initial volume of the particle}} = \frac{4/3\ (R^3 - r^3)\pi}{4/3\ R^3 \pi}$$

$$\therefore\ \alpha = 1 - \left(\frac{r}{R}\right)^3 \qquad (17)$$

If the rate of interface advance is $-dr/dt = k$, integration from r=R at t = 0 gives $R-r = kt$ and substitution into eq. 17 gives

$$1 - (1 - \alpha)^{\frac{1}{3}} = kt/R \qquad (18)$$

This equation should be a good description of the decomposition of a sample consisting of many spheres provided that : (1) decomposition starts on each at the same time ; (11) each decomposes independently ; (111) the distribution of their initial radii peaks sharply at r_m. Eq. 18 can then be written as

$$1 - (1 - \alpha)^{\frac{1}{3}} = kt/r_m \qquad (19)$$

and

$$\alpha = \frac{\text{total volume decomposed}}{\text{total volume initially}}$$

MECHANISMS OF PROCESSES AT THE INTERFACE

In the treatment of decomposition reactions given so far , the interface has been regarded simply as a source of gaseous flux and it is now time to consider , at atomic level , the processes occurring there. Two models will be described. The first is based on the idea that gas release at the interface leaves an intact sublattice of product which collapses as the interface moves on. The second model , represented already in fig. 7, regards the creation of two new phases, $A_{(s)}$ and $B_{(g)}$, as the result of solid-state counter diffusion of these two components at the interface. These will be referred to as the 'lattice collapse' and 'counter diffusion' mechanisms.

Lattice collapse

In decompositions the molar volume of the solid product is generally less than that of the reactant. Some values are given in table 1. This inequality has an important consequence if the decomposition of $AB_{(s)}$ to $A_{(s)}$ involves the release of B molecules from the $AB_{(s)}$ lattice leaving an intact sublattice of A molecules. This sublattice will have considerable strain which can be relieved by its fissure to give smaller fragments. The formation and cleavage of a product lattice is shown in fig. 11, and the result here is the formation of blocks of product which can be either amorphous or crystalline , depending on the mechanism of lattice collapse. In the latter case the blocks may be crystallographically oriented. It is also possible that an amorphous product may subsequently crystallise so that only a thin interfacial layer of product may be amorphous[36].

Giovanoli and Brutsch[37] present sound evidence for the lattice collapse mechanism in the decomposition in high vacuum of crystals of γ-FeOOH , where the product formed as perfectly oriented blocks at the reaction interface.

TABLE 1. Comparison of reactant and solid product molar volumes[35].

Reaction	$V_m^{reactant}/m^3$	$V_m^{product}/m^3$
$CaCO_3 \rightarrow CaO + CO_2$	3.4×10^{-5}	1.7×10^{-5}
$MgSO_4 \rightarrow MgO + SO_3$	4.5×10^{-5}	1.1×10^{-5}
$MgCO_3 \rightarrow MgO + CO_2$	2.8×10^{-5}	1.1×10^{-5}

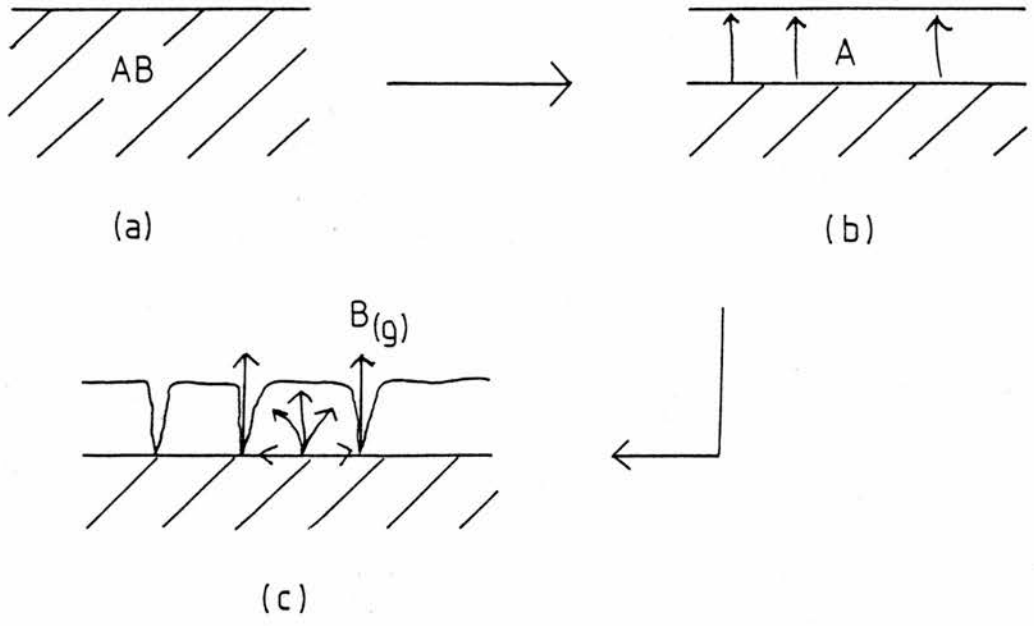

Fig. 11. The lattice collapse model.
(a) reactant; (b) the initially formed solid product is strained; (c) this strain is relieved by fissuring. The arrows indicate possible paths for gas migration.

A difficulty associated with this mechanism lies in accounting for gas transport from the interface. Some paths are suggested in fig. 11.

For the lattice collapse model the rate-controlling step for the forward reaction will consist in molecules of B breaking free of the interfacial layer of the AB lattice. The product layer will only modify this rate by the stress generated at the interface. An attempt has been made by Shannon[38], using activated complex theory , to predict the decomposition rate constants for $MgCO_3$ and $CaCO_3$, assuming the reactant to be unperturbed by the product layer. The treatment is comparable to that used by Schultz and Dekker[39] to predict the vaporisation rates of sulphur and benzene , and utilises the equation[40]

$$k_r = \frac{kT}{h} \frac{Q^{\ddagger}}{Q} e^{-E/RT}$$

Here k_r is the rate constant , $Q^{\ddagger}$ and Q are the partition functions for the activated complex and reactant , k is the Boltzmann constant , T is temperature and E is the molar activation energy , which Shannon takes from experimental data. The principal difficulties encountered were in proposing a reasonable activated complex and in finding the appropriate spectroscopic data from which to construct the partition functions. In particular , it was necessary to decide which of the wide range of vibrational frequencies of a crystal were likely to influence the decomposition rate. Accoustic modes[6], which involve the in-phase motion of large clusters of unit cells , were ignored but optical modes[6] , which involve the out-of-phase motion of one sublattice against another , were considered important. The calculated Arrhenius factors for the two reactions studied agreed well with experimental values , but the real merit in the study is the insight it gives into

the dependence of reaction rate on lattice vibrations.

Counter diffusion mechanism

In the lattice collapse model the interface is the clearly defined region where the AB and A lattices merge , and decomposition is assumed to occur by the release of B atoms from the interfacial surface of AB. An alternative way of constructing the new solid phase is by solid-state diffusion processes in an interfacial region which is really a solid solution of A and B. This model was proposed by Searcy and Beruto[5] and is illustrated in fig. 7. Their argument is that the advance of an interface is only possible if four steps occur at the same rate. With reference to fig. 7 , these are : (1) a flux of that portion of component B which is at the interface between $A_{(s)}$ and $AB_{(s)}$, towards the exposed surface beneath a capillary ; (11) a flux of that portion of component A which is beneath the exposed interface , towards the $AB_{(s)} - A_{(s)}$ interface ; (111) a flux of A across the $AB_{(s)} - A_{(s)}$ interface , which builds $A_{(s)}$; (1V) a gaseous flux J_o of component B from the exposed interface into the capillary tube. Viewing the solid interface as a solid solution , there will be a composition variation such that there is an excess of A near the $A_{(s)} - AB_{(s)}$ interface and a deficit below the exposed interface. The diffusion processes are driven by chemical potential gradients against concentration gradients.

Depending on the relative rates of these four steps , several rate laws can be derived , two of which will be mentioned. First , if the rate constant of solid-state diffusion of component B is smaller than the rate of the surface step for its release , the rate will depend on the rate constant for diffusion. Second , if the surface step releasing B is slower than all other steps , the rate can be shown to be $k \exp(-\Delta G_p/RT)$, where k is the rate constant for the surface step and ΔG_p is the excess free energy of the product.

Searcy and Beruto applied this last equation to their own results for the decomposition in high vacuum of single crystal samples of $CaCO_3$ with only one face exposed. Reaction occurred at a constant rate at a single macroscopic interface and examination of the product showed a 30 μm thick layer of crystallographically distorted CaO at the interface. The rest of the product was crystallographically aligned stable CaO , and scanning electron microscopy showed it to contain pores of 2 μm diameter.

It should be pointed out that the structure and texture of the product is completely consistent with the lattice collapse model if the porosity of the product is attributed to the sintering of crystallites formed by the collapse of the metastable CaO lattice produced at the interface. Sintering is the process in which the small particles constituting a material join together under the influence of heat to form a continuous , porous solid[41,42]. The visible effect is the shrinkage and hardening of the material and the thermodynamic driving force for the process is the reduction in surface free energy (fig. 12).

Fig. 12. Sintering.

TECHNIQUES FOR STUDYING DECOMPOSITION REACTIONS

The ideal study of a decomposition reaction should aim not only to obtain an empirical rate law but should correlate this with the accompanying structural and textural changes. Space groups and unit cell dimensions can be determined by powder X-ray diffraction and this will not only permit the identification of the stable and metastable species involved but will give some indication of the size of particles in the reflecting powder[37,43]. When X-ray diffraction is not available , i.r. spectroscopy can usually identify a pure material conclusively and can distinguish polymorphs[44].

The textures of the solids involved in a decomposition can sometimes be observed continuously during a reaction or , more usually , can be examined by removing the sample at various stages. For reactions occurring below 500 ^{o}C and involving transparent crystals , hot-stage microscopy has been successful in showing the growth of nuclei from the time they become visible and has revealed the preference for nucleation at surface irregularities[16]. For opaque materials, especially those which decompose to give a product with a different colour , examination under reflected light can be informative. A serious limitation with this method is that depth of focus at magnifications greater than x100 is often less than the depth of many surface features. Scanning electron microscopy , however , can produce monochrome pictures of an object with magnifications up to x10 000 without this complication and is probably the most favoured technique for studying surface texture.

Two approaches to obtaining data from which rate laws may be deduced will now be described. The first consists in measuring the amount of reactant decomposed against time at a constant temperature and such methods are called 'isothermal'. The second approach involves differential thermal analysis and consists in relating reaction rate to the effects

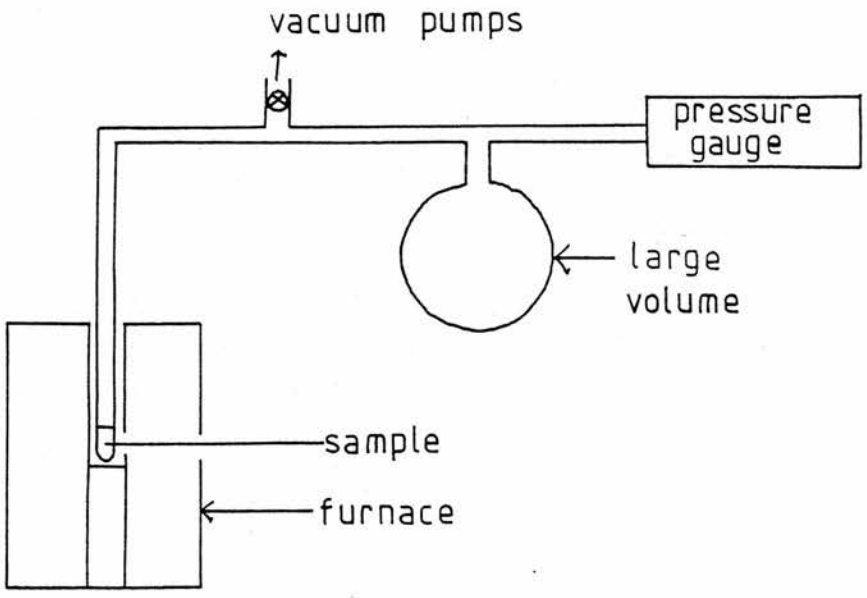

Fig. 13. The gas pressure is a measure of the amount of salt decomposed.

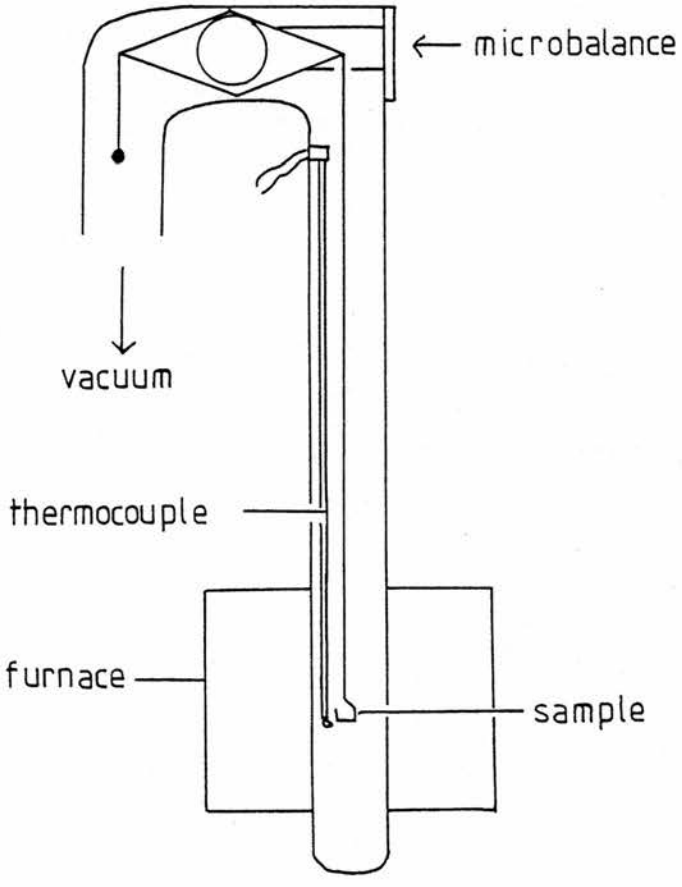

Fig. 14. Apparatus for following the mass of a decomposing salt.

of heat absorption as a sample undergoes decomposition on heating at a constant rate.

One isothermal method follows the rise in pressure created as a solid decomposes into an evacuated closed system of constant volume[45]. The apparatus used is illustrated in fig. 13. The material to be studied is placed in one end of a tube which is initially evacuated and is continuous with a large buffer volume. The temperature of the sample is then raised to and held at a value at which decomposition is measurable. It is necessary that the buffer volume be of such a size that the pressure corresponding to complete decomposition is much less than the equilibrium vapour pressure for the substance at that temperature. It is usual to present the results as the extent of decomposition

$$\alpha(t) = P(t) / P(t=\infty)$$

against time.

A criticism of the method is that there could be an increasing back reaction as the product gas pressure builds up during the decomposition. The method will yield straightforward results only for highly irreversible reactions.

Another technique for following the amount of reactant decomposed uses the apparatus shown in fig. 14. The sample is contained in a small Pt cup and is suspended in the hot zone of a furnace from one arm of an electronic microbalance. The furnace can contain a static or flowing inert atmosphere , or a vacuum may be maintained by constant pumping to remove gas evolved from the sample. As pointed out earlier , back reaction is minimised in high vacuum and the weight loss data should be more amenable to analysis.

The methods mentioned above measure directly the amount of product reacted as a function of time at a constant temperature. For an endothermic reaction the rate of heat absorption by a decomposing

sample will be proportional to the reaction rate according to the relationship

$$dq / dt = \Delta H^{o} \, dn / dt$$

where dq is the amount of heat absorbed to decompose dn moles of reactant and ΔH^{o} is the enthalpy change per mole decomposed. This equation is the basis of attempts to obtain kinetic data by differential thermal analysis (DTA)[46,47]. This technique will be discussed further in part two of this thesis , where it is applied to phase equilibria , but for present purposes , only the features shown in fig. 15 need be considered. The sample and an unreactive reference material are contained in little Pt cups which sit in a ceramic or metallic block. The block is situated in a furnace which is heated at a constant rate , usually about 5 K min^{-1}, and through which passes a stream of inert gas. In the absence of any physical or chemical change , the difference , ΔT , between the temperatures of sample and reference , is approximately zero. When the sample undergoes an endothermic reaction , however , the heat flow to the sample is absorbed as the heat of reaction and its temperature lags behind that of the reference until the process is complete , when ΔT resumes a value of nearly zero. A typical experimental record consists of sample temperature and ΔT against time , as shown in Fig. 16.

One of the most-used theories for obtaining kinetic data from a set of such patterns at a number of heating rates is that proposed by Kissinger[48]. Kissinger argues that the maximum value of ΔT occurs when the reaction rate is greatest , and assumes the rate law to be of the form

$$\frac{d\alpha}{dt} = A \, (1-\alpha)^{n} \exp(-E/RT)$$

Where α is the fraction reacted , A is the Arrhenius factor , E is the molar activation energy and n is the 'order' of the reaction.

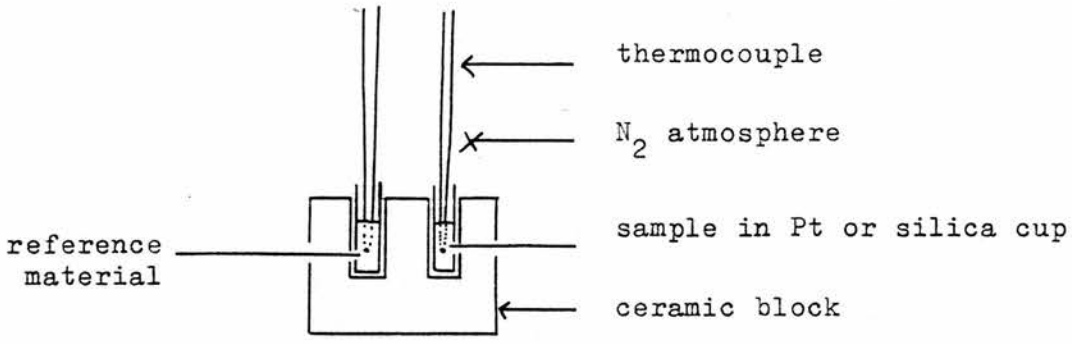

Fig. 15. Typical DTA apparatus.

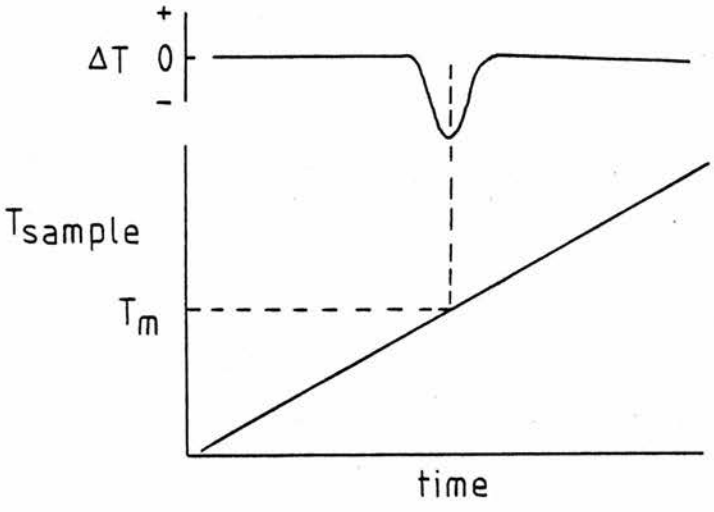

Fig. 16. Typical graphs of T and ΔT for a DTA experiment.

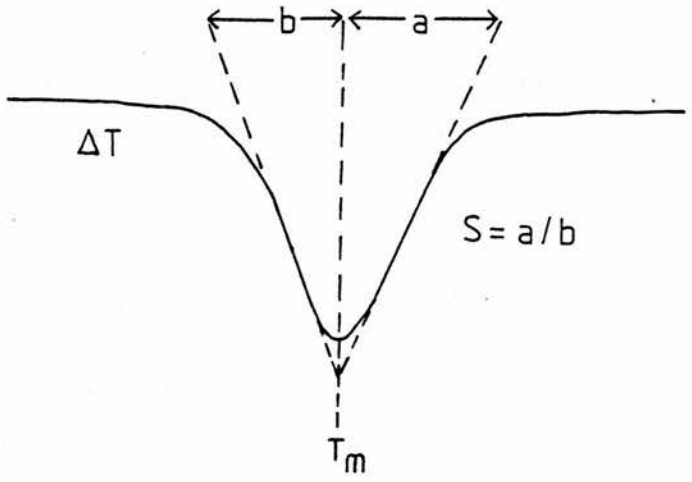

Fig. 17. The method of calculating the asymmetry factor S.

The following equations are derived :

$$\frac{d\ (\ln(\phi/T_m^{\,2}))}{d\ (1/T_m)} = -\frac{E}{R} \quad ; \quad n = 1.26\ S^{\frac{1}{2}}$$

Here ϕ is the heating rate , T_m the sample temperature when ΔT is a maximum , and S is called the 'asymmetry factor'. S is determined for each experiment as the ratio a/b where a and b are obtained by drawing tangents at the two inflection points in the ΔT curve as shown in fig. 17.

These equations are used as follows. Several experiments are run at different heating rates , ϕ , and the corresponding values of T_m are used in a plot of $\ln(\phi/T_m^{\,2})$ against $1/T_m$. The slope of this line gives -E/R. The 'order' n should be the same for each experiment. Some data for $CaCO_3$ are given in table 2 , from which the activation energy is calculated as 183 kJ mol^{-1} and the 'order' is about $\frac{1}{3}$.

TABLE 2. Kinetic data for $CaCO_3$.

Heating rate /°C min^{-1}	T_m/°C	S	n
3.0	871	0.06	0.31
4.5	874	0.09	0.38
6.0	888	0.07	0.33
10.0	911	0.06	0.31
12.5	927	0.07	0.33

The treatment of DTA curves given above is , however , of limited applicability. It is the author's experience that the decomposition of a powder can occur at a single macroscopic interface which moves through the sample as the reaction proceeds. A maximum in ΔT will probably be recorded when the interface happens to be at the thermocouple junction and this need not coincide with the maximum rate. Even for those reactions in which each particle of the reactant mass decomposes independently , the 'order' may change due to overlap of growing nuclei

and , since this occurs towards the end of the reaction , the value of α may be seriously affected. An additional problem is that the conditions used for DTA are such that back reaction may be significant and could contribute to the rate law obtained.

A critical account of the use of DTA as a tool in reaction kinetics is given by Sharp[49].

It is particularly unfortunate that the few texts devoted to solid-state decomposition kinetics[2-4] do not emphasise the care required in choosing a suitable technique. The comparison in figs. 9 and 10 of gas flow methods and the determination of vapour pressures by the transpiration technique , for example , became apparent to the author during exploratory work on the decomposition kinetics of $CaCO_3$ using the apparatus shown in fig. 8. It is hoped that this introduction has clarified this and other points.

ORIGINAL INVESTIGATIONS

OF

SULPHATE POWDERS

THE DECOMPOSITION OF PACKED AND AGGREGATED POWDERS

In the preceding sections the physicochemical principles of decomposition reactions were outlined and it was argued that the most easily interpreted kinetic results are those obtained for small samples with low reaction rates in high vacuum , particularly when gas transport from the reaction interface is by Knudsen flow. With these conditions , back reaction and self-cooling are minimised. It was also emphasised that any rate equation proposed on the basis of physical measurements should be consistent with the observed morphology of the reaction. This is the approach adopted here in the investigation of the decomposition kinetics and mechanisms of some metal sulphate powders.

As pointed out already , almost all of those studies of solid-state decomposition reactions which include a description of the reaction morphology have involved conditions in which each particle of the reactant mass decomposes independently. Under these conditions the kinetics have been successfully explained in terms of the formation , growth and interaction of product nuclei. Although many substances have been decomposed as powders , little attempt has been made to correlate the kinetics with the reaction morphology and , in addition , conditions have been such that back reaction cannot easily be compensated for. This reflects a widespread scarcity of data on the reactivity of powders which is incompatible with their technological importance[50] and is to some extent a consequence of the preference of chemists to concentrate on systems which are well-defined from a solid-state point of view. Most of the existing data on the physical and chemical properties of powders are from the fields of powder metallurgy and ceramics , where interest has centred on the subjects of solid-solid[51,52] reactions and sintering[15].

Powdered materials certainly have many more variables which can

influence reaction rate than have monocrystalline reactants , and the decomposition of the latter is by no means straightforward. These variables include grain size , grain size distribution , packing density , porosity , total surface area and contact area between grains[50]. Porosity and contact area are of particular importance in the decomposition of a powder for the following reason. If the grains constituting a mass of powder do not decompose independently , that is , if there is co-operative behaviour , the influence of one grain on another can only be exerted by either solid-state processes at the areas of contact , or via the product gas phase in the intergranular spaces.

In the experiments to be described , finely powdered $CuSO_4$, $NiSO_4$ and $ZnSO_4$ were decomposed as 30 - 40 mg samples packed by gentle tapping in a small Pt cup suspended in a vacuum furnace. The $Fe_2(SO_4)_3$ selected for study consisted of particles each of which was an aggregate of thousands of tiny grains. These aggregates were of particular interest because of the possibility of three decomposition mechanisms : each grain may decompose independently ; each aggregate may decompose independently ; the sample mass as a whole may decompose at a macroscopic interface or interfaces.

Scanning electron micrographs were taken of all the materials and their decomposition products , and , together with microscopic examination in reflected light , provided information on the reaction morphologies. The fact that the decomposition products for $CuSO_4$, $NiSO_4$ and $Fe_2(SO_4)_3$ are of different colours from the reactants was of considerable help in locating the reaction interface by light microscopy. The correlation of this evidence with the weight loss measurements is discussed and an attempt is made to rationalise the decomposition mechanisms.

APPARATUS AND PROCEDURE

The elements of a system for studying the weight loss of a decomposable material at high temperatures in vacuum are : (1) a means of controlling and measuring high temperatures ; (11) a means of maintaining a high vacuum during decomposition ; (111) a means of monitoring continuously the sample mass. The three sections of the system used for this work are shown in figs. 19 , 20 and 21 , and some comments will be made on each in turn. First , however , a few words will be said about temperature measurement.

Temperature measurement

An excellent account of this topic is given by Margrave[53] and an indication is given in fig. 18 of the working ranges of the three thermometers most frequently encountered in high temperature studies.

Fig. 18

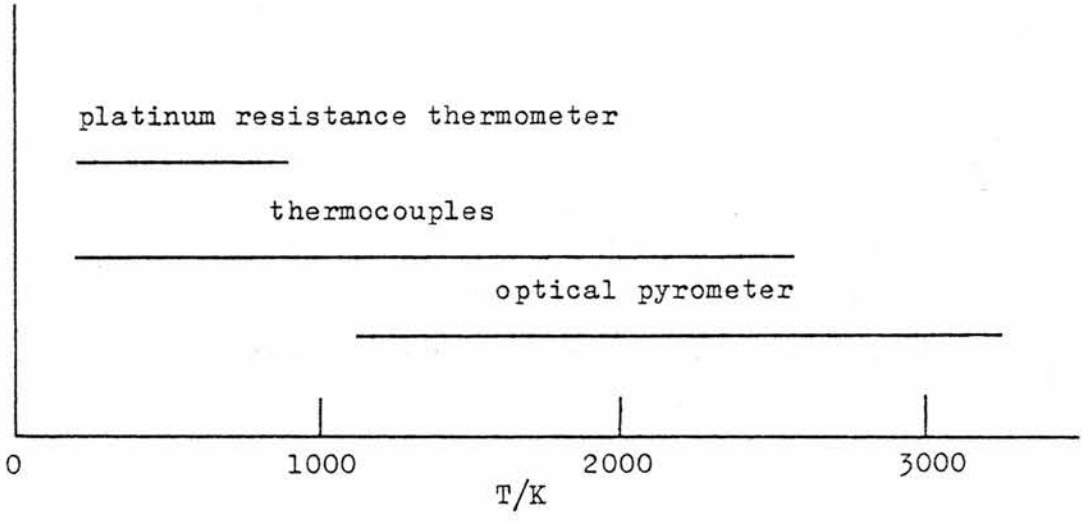

For the temperature range of this work (500-1500 K) , thermocouples are most suitable and were interpreted using the I.P.T.S. (1968) tables[54]. Cold junction temperatures were measured with a certified mercury thermometer graded in 0.1 K intervals and thermocouple e.m.f. was read from a high input resistance digital voltmeter with a resolution of 1 μV , which at 1000 K is equivalent to 0.08 K for a Pt13%Rh-Pt

thermocouple. Calibration was made against the melting points of KCl , NaCl and K_2SO_4 as listed in the JANAF tables[55]. The method of calibration is described in part two and is capable of an accuracy of $\pm$0.2 K. Pt13%Rh-Pt thermocouples were found to be superior in both accuracy and durability , particularly where SO_3 gas was present , and the one chromel-p-alumel thermocouple in the system was replaced as soon as money became available.

Temperature control

During the course of this work , money became available with which to buy a modern temperature programmer (system 2 in fig. 19). The principles of operation of this and the older programmer (system 1 in fig. 19) are essentially the same. If one wishes to maintain a temperature of , say , 1000 K at the hot zone of a tubular resistance furnace , the e.m.f. of a thermocouple situated there is compared electronically with the voltage corresponding to 1000 K for the particular thermocouple used. The difference is amplified and this so-called error signal is used to increase or diminish the power delivered to the furnace. The extension of such an isothermal control system for variable heating and cooling rates simply involves driving a potentiometer to give a voltage corresponding to that obtained when the thermocouple is heated or cooled at some constant rate. Systems 1 and 2 differ mainly in the device used to deliver power to the furnace : system 1 modifies the amplitude of the voltage sine wave at the furnace terminals , while system 2 permits only portions of the mains voltage to appear at the terminals. The sensor thermocouple (Pt13%Rh-Pt for both systems) is situated in good thermal contact with the furnace wall so that it can experience quickly the effects of a change in the delivered power and so feed back a reduced error signal. The result is that large fluctuations in temperature do not

Fig. 19. Two temperature control systems.

System 1

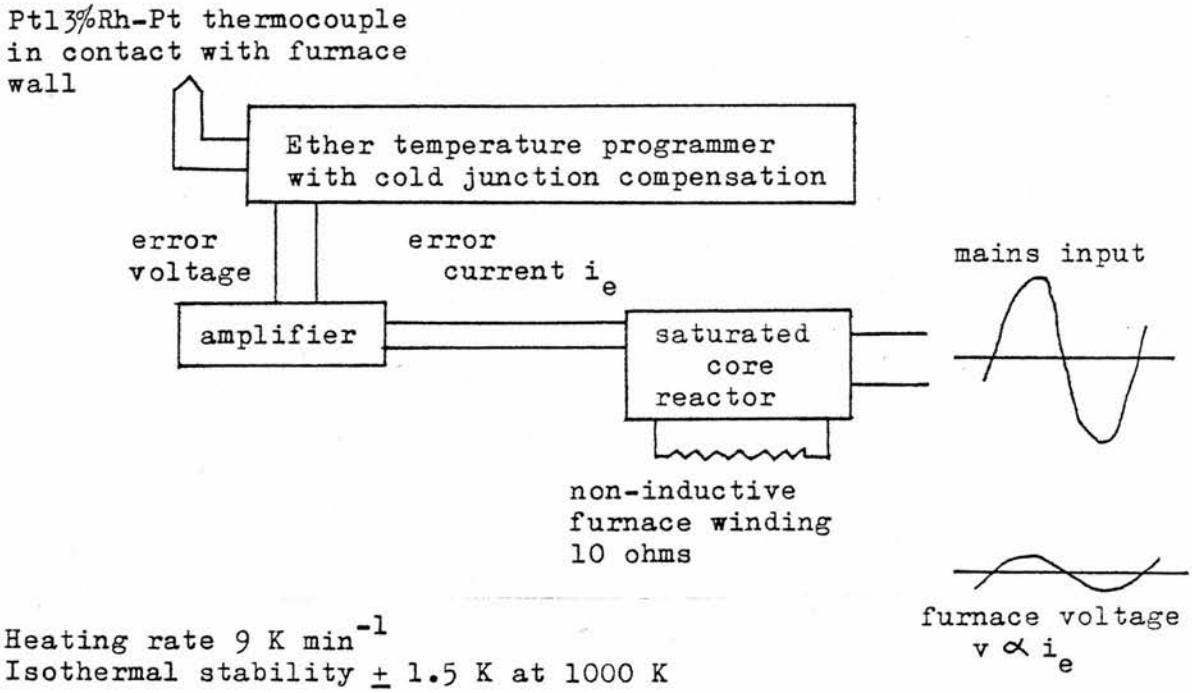

Heating rate 9 K min^{-1}
Isothermal stability $\pm$ 1.5 K at 1000 K

System 2

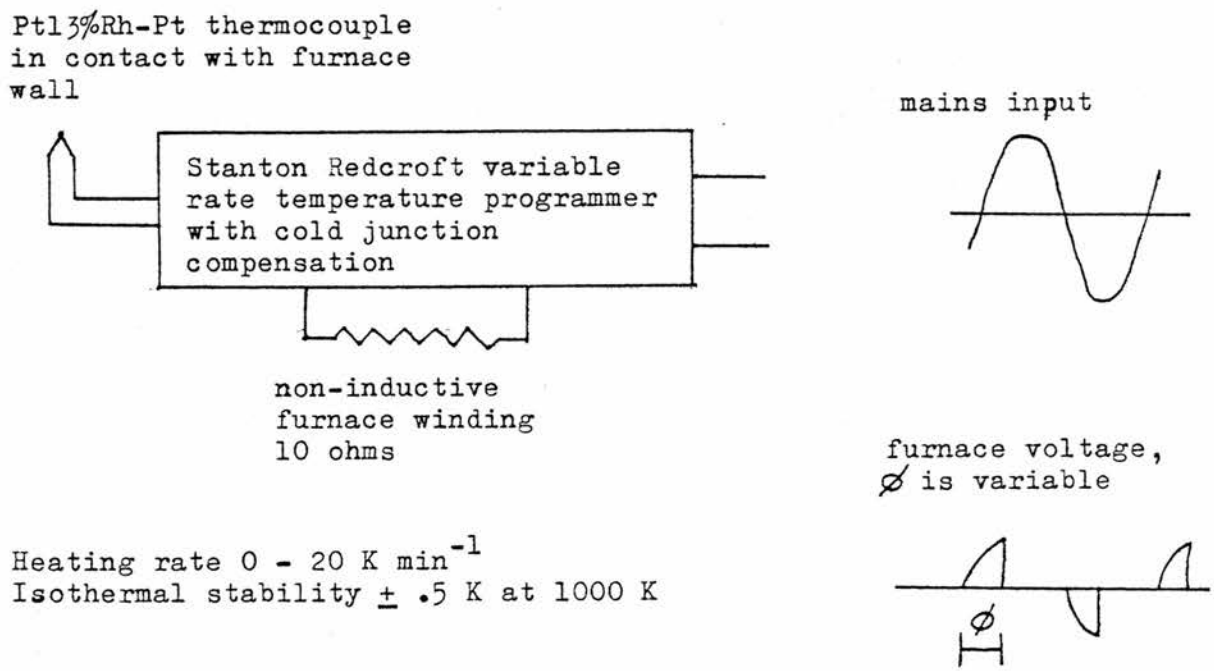

Heating rate 0 - 20 K min^{-1}
Isothermal stability $\pm$ .5 K at 1000 K

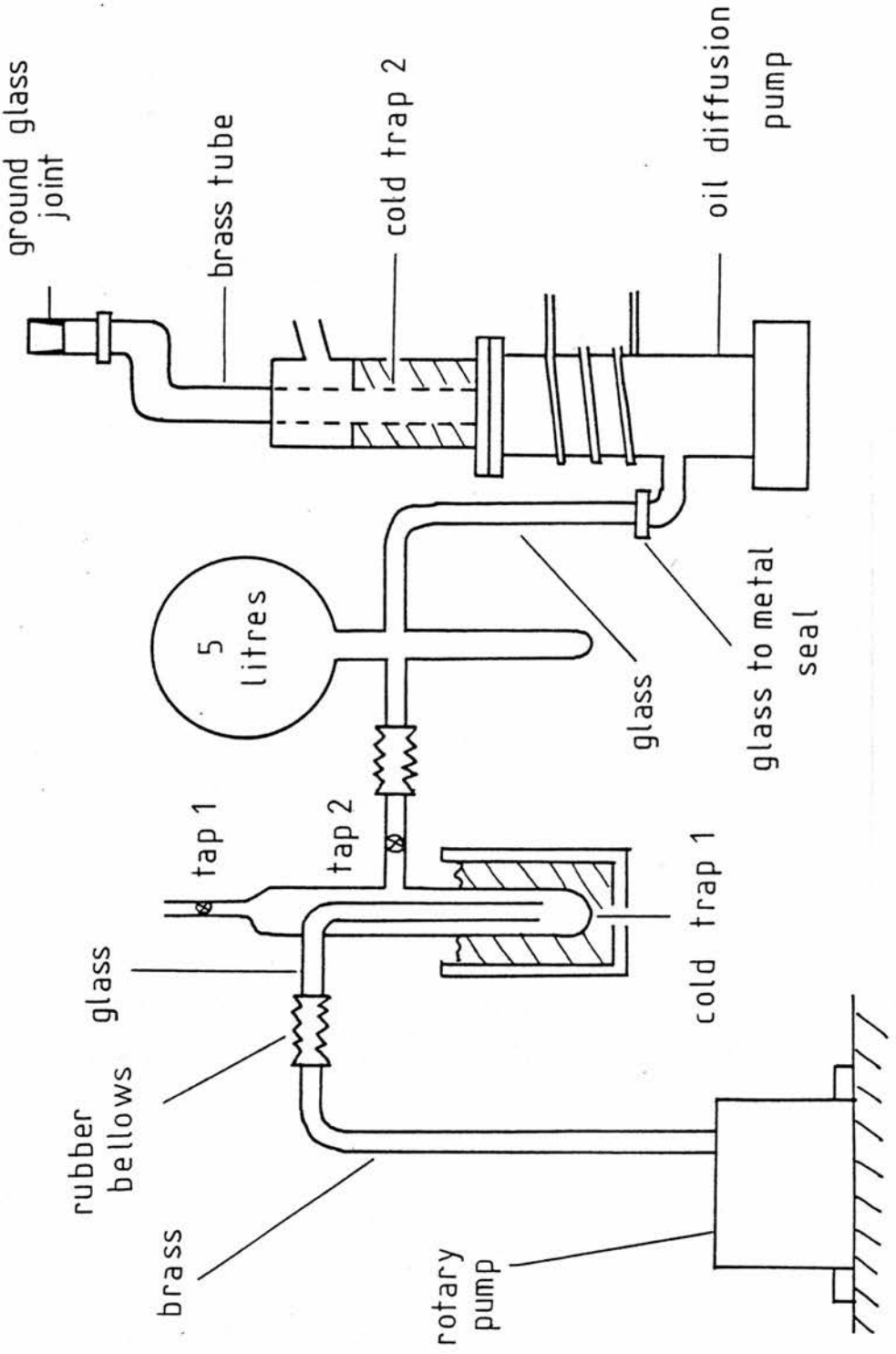

Fig. 20. Vacuum system.

occur during isothermal operation , the actual variations being $\pm$1.5 K for system 1 and $\pm$0.5 K for system 2. The cold junction of the sensor thermocouple was situated 15 cm away from the furnace at the end of a strip of asbestos board so that it could be at ambient temperature. This is important as temperature programmers are designed to compensate for changes in ambient temperature and it is assumed that the cold junction temperature equals that inside the programmer.

Vacuum system

The system used for this work is shown in fig. 20 and uses an oil diffusion pump backed by a rotary pump. Operating procedure is as follows. Taps 1 and 2 are closed , the rotary pump is switched on and tap 2 is slowly opened. The system begins to evacuate and liquid N_2 is put round trap 1. The system is left in this state for 30 min , then trap 2 is filled and the oil diffusion pump is switched on. After 15 min the pressure , as measured by a Penning gauge , begins to fall from about 10^{-2} to 10^{-5} Torr over a period of about 4 h after which tap 2 is closed , tap 1 is opened and the rotary pump is switched off. Any incondensable gases in the system (eg. air from small leaks) are now pumped into the buffer volume whose capacity was adequate to maintain a sufficiently low pressure to allow the diffusion pump to function for at least 8 h. During an actual decomposition reaction the pressure typically rose to 2×10^{-5} Torr.

Microbalance and furnace

The apparatus shown in fig. 21 consists of an upper , fixed section and a lower , movable part , which meet at a gasketed male-female joint held closed by o-rings. The upper section comprises a C.I. Electronics microbalance , a chromel-p-alumel (later replaced by Pt13%Rh-Pt) thermocouple which extends down to a point 2 mm from the

Legend for fig. 21. (Microbalance and vacuum furnace).
1. microbalance head ; 2. ground glass joint for connection to the vacuum system ; 3. glass-to-glass joint ; 4. branch to Penning gauge ; 5. counter weight ; 6. molybdenum section of the suspension wire ; 7. aluminium-to-glass joint ; 8. aluminium ; 9. cold junction for the thermocouple measuring sample temperature ; 10. this projection is bolted to a rigid frame ; 11. o-rings compress these sections together ; 12. rubber gasket ; 13. aluminium ; 14. aluminium-to-silica joint ; 15. silica tube ; 16. water-cooling jacket ; 17. cold junction for sensor thermocouple for temperature controller ; 18. asbestos stop ; 19. sensor thermocouple ; 20. sample thermocouple ; 21. Pt section of suspension wire ; 22. furnace ; 23. Pt sample cup ; 24. fixed poles on which the furnace can be lowered to expose the sample cup.

Fig. 21. Microbalance and vacuum furnace.

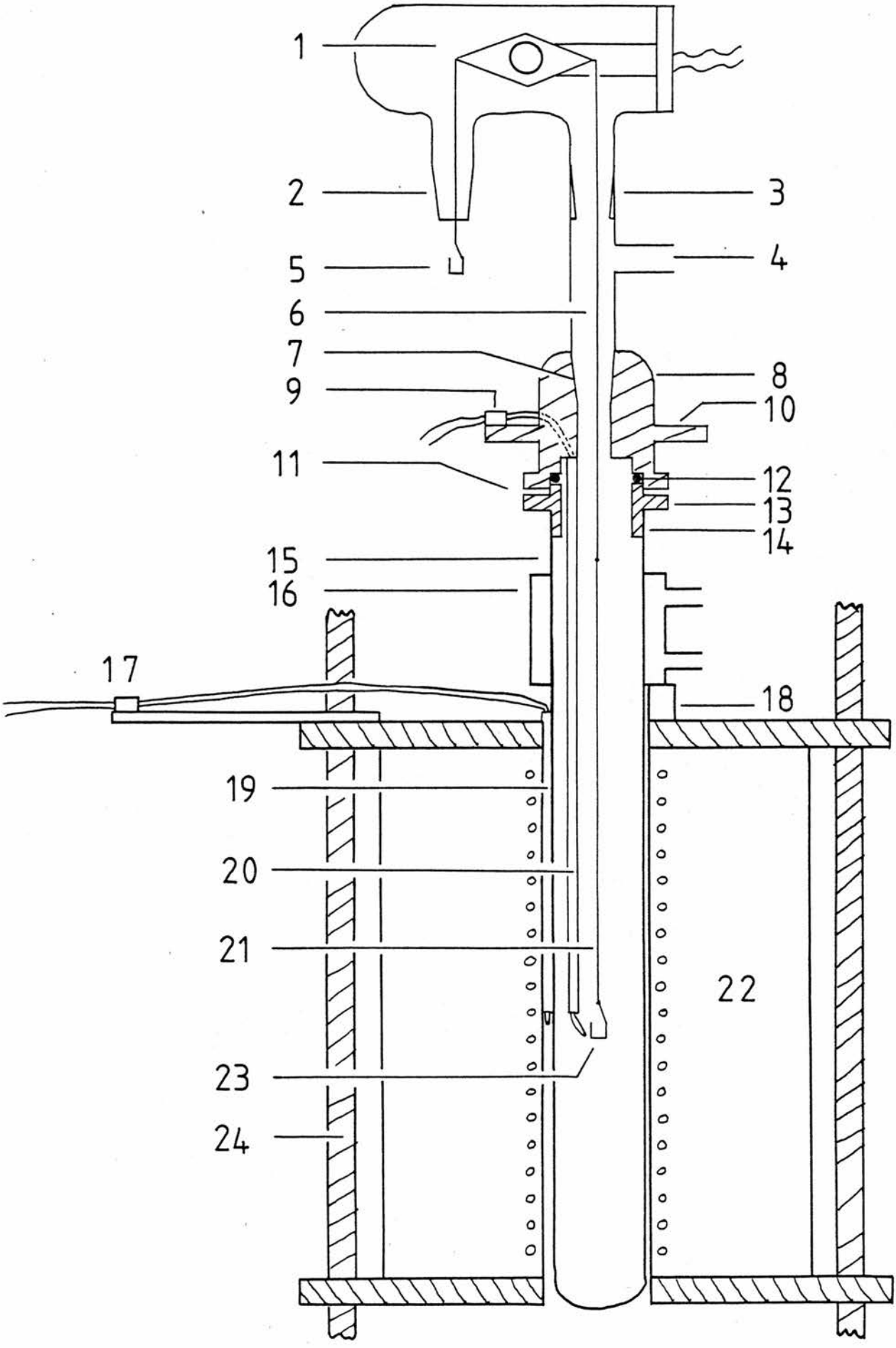

sample cup , and a T-junction which leads off to a Penning pressure gauge. The lower part consists of a 46 mm diameter silica tube with one end closed , sitting inside a tubular resistance furnace mounted on two fixed rods so that it can be lowered to expose the sample cup.

The sample to be decomposed is contained in a Pt cup of diameter 7 mm and height 7 mm , which is suspended in the hot zone of the furnace from one arm of the microbalance. Platinum was used for the lower , hot section of the suspension wire to avoid attack by the SO_3 gas emanating from the sample. In calibrating the microbalance , which has ranges 0 - 2.5 mg , 0 - 10 mg and 0 - 100 mg , it was recognised that the true mass of a sample differs from the balance reading in air due to buoyancy effects[56]. For this reason , the zero and full scale settings for each scale were adjusted with the system evacuated.

In constructing the furnace , Kanthal A wire was wound on a 260 mm long and 50 mm diameter ceramic tube , cemented in place and then packed round with asbestos powder enclosed in a thin steel cylinder and this itself was surrounded by a 180 mm diameter steel cylinder , the cavity between being filled with asbestos wool. Heat conduction upward from the furnace through the silica tube was prevented by a tight-fitting brass cooling jacket.

Procedure

Experiments were conducted as follows. The sample (30 - 60 mg) was packed into the Pt cup by gently tapping the base against a wooden bench top. The vacuum was created as described already and , when a pressure of 10^{-2} Torr was attained , the temperature programmer was switched on at a heating rate of 10 K min^{-1}. When a temperature of 650 K was reached , the system was left for 5 h to equilibrate. Next the temperature was raised to the desired value at 10 K min^{-1} and then , upon switching off the programmer , there was a further rise and fall of 7 K before the temperature stabilised at better

than ± 2 K for the remainder of the experiment. Weight loss readings were started when the temperature became steady , which was about 10 min after switching off the programmer.

To terminate the experiment , the power to the diffusion pump and furnace is switched off. If , however , the sample is to be recovered for examination , only the power to the furnace is switched off and the vacuun is maintained till the furnace has cooled (~3 h). If this precaution is not taken , air from the buffer volume or SO_3 evaporated from the cold traps may react with hot sample.

Sample-mounting for scanning electron microscopy

The instrument used was a Cambridge Stereoscan 600 for which the samples were sputter-coated with gold and mounted on 1 cm diameter stubs. It was considered most desirable to scan reactant or product material as it was packed in the Pt cup (fig. 22) but this proved possible in only one case ; the build-up of charge in the lower layers of the powder which are not completely coated tends to obliterate the image. This problem was obviated by holding a thin layer of the material on the stub using double-sided sticky tape , followed by sputter coating. It was found most convenient to withdraw surface product material by the technique shown in fig. 22(b).

High temperature chemistry of Cu^{2+}, Ni^{2+}, Zn^{2+} and Fe^{3+} sulphates.

The stoichiometries and thermodynamic functions from vapour pressure measurements for the decomposition of these sulphates are given in reviews by Stern and Weise[57] and by Kellogg[58].

$CuSO_4$ decomposes in air in two steps :

$$2CuSO_4 \rightarrow CuO.CuSO_4 + SO_3$$

$$CuO.CuSO_4 \longrightarrow 2CuO + SO_3$$

The infra-red spectra of $CuSO_4$ and $CuO.CuSO_4$ (basic sulphate) have been recorded and are characterised by bands at 960 , 1075 and

1140 cm^{-1} , and 995 , 1035 and 1140 cm^{-1} respectively [59,60].

$NiSO_4$ decomposes to NiO in a single step and its i.r. spectrum has bands at 983 , 1080 , 1155 and 1230 cm^{-1} [44].

$ZnSO_4$ decomposes in two stages :

$$3ZnSO_4 \longrightarrow ZnO.2ZnSO_4 + SO_3$$

$$ZnO.2ZnSO_4 \rightarrow 3ZnO + 2SO_3$$

This formula for the basic sulphate has been confirmed in several reports [59,61] , although Hoschek [62] proposes $ZnO.1\frac{1}{2}ZnSO_4$. A polymorphic transition in $ZnSO_4$ is reported near 1010 K in some studies [61,63,64] but is not mentioned in others [62,65]. DTA work in part two of this thesis locates this transition at 1003.5 $\pm$ 1.5 K. The i.r. spectra of $ZnSO_4$ and $ZnO.2ZnSO_4$ are characterised by bands at 990 , 1070 and 1145 cm^{-1} , and 1035 , 1170 and 1225 cm^{-1} respectively [59,60].

$Fe_2(SO_4)_3$ decomposes in a single step to Fe_2O_3 ; there is no record of the i.r. spectrum in the literature.

The above reactions are written with SO_3 as the decomposition product , but $SO_2 + \frac{1}{2}O_2$ are also possible. DTA of these four sulphates in a flowing mixture of $SO_2 + O_2$ was carried out by the author using apparatus described in part two . For all four salts , the decomposition temperature was elevated considerably when Pt foil was present to catalyse the formation of SO_3. This is taken as indicating SO_3 and not $SO_2 + O_2$ as the immediate gaseous decomposition product. There is confirmation of this conclusion for the case of $Fe_2(SO_4)_3$ from matrix isolation of its gaseous decomposition product in high vacuum [66].

The i.r. spectra referred to above were run as nujol mulls as it was found that the compression involved in compacting KBr discs results in pressure-induced transformations of the crystal structures.

Materials

(a) Fine powders. Information on these is given in table 3. Dehydrations were carried out in a muffle furnace with the hydrate (10 g) contained in a capped silica crucible. The resulting anhydrous cake was then ground to a fine powder in an agate mortar. All samples were stored over P_2O_5 in a vacuum desiccator and a single batch was used for all experiments with a particular salt. Scanning electron micrographs of the three powders were recorded and are shown in figs. 23,24 and 25. Examination with reflected light at x50 magnification using a binocular microscope revealed the outlines but not the surface texture of the induvidual grains. The $CuSO_4$ and $NiSO_4$ particles appeared to be crystalline and the $ZnSO_4$ particles were highly porous. During the course of this work X-ray powder diffraction facilities were not available. However , the infra-red spectra of the powders corresponded to those recorded by others [44,59,60].

(b) Aggregates of $Fe_2(SO_4)_3$. Fisons laboratory reagent grade $Fe_2(SO_4)_3$ was stored over P_2O_5 in a vacuum desiccator and all subsequent operations were performed as quickly as possible to minimise any hydrolysis by atmospheric moisture. The i.r. spectrum showed a very broad absorption centred at 1100 cm^{-1} but there is no spectrum cited in the literature for comparison. Microscopic examination in reflected light showed the material to be a polydisperse powder of particles each of which was an aggregate of thousands of tiny grains. The large aggregates used for this work were separated out by sieving and are shown in fig. 26. Fig. 27 shows a single aggregate and in fig. 28 the size of a grain is seen to be about 2 μm.

Packing

It has been mentioned already that samples were packed in the Pt cup by gentle tapping. Some idea of the packing density of each powder

Fig. 22. Methods of examining powders by SEM.
(a) in situ ; (b) surface layer adheres to sticky tape and this is then mounted on a stub.

TABLE 3 Fine powders

Material	Source	Preparation
$CuSO_4$	Fisons analytical grade $CuSO_4.5H_2O$.	Dehydration at 300 °C for 48 h followed by pulverisation.
$NiSO_4$	Fisons analytical grade $NiSO_4.7H_2O$.	" " 300 °C " " " " "
$ZnSO_4$	Fisons analytical grade $ZnSO_4.7H_2O$.	" " 350 °C " " " " "

TABLE 4 Free space in samples.

Material	% space
$CuSO_4$	68
$NiSO_4$	75
$ZnSO_4$	76
$Fe_2(SO_4)_3$	79

was obtained by filling the cup to the brim , recording the mass of powder and calculating the actual volume of the salt from its tabulated density[57]. The % space in the sample mass is given by

$$\% \text{ space} = \frac{V_{cup} - V_{sample}}{V_{cup}}$$

RESULTS

In the following pages data are presented for the isothermal decomposition in high vacuum of the following : (a) 40 mg samples of finely powdered $CuSO_4$; (b) 30 mg samples of finely powdered $NiSO_4$; (c) 40 mg samples of finely powdered $ZnSO_4$; (d) 60 mg samples of $Fe_2(SO_4)_3$ consisting of 100-300 μm aggregates each of which is composed of 2 μm grains.

As explained above , the immediate gaseous reaction products for all four reactions have been shown to be SO_3 and not $SO_2+\frac{1}{2}O_2$. For $NiSO_4$ and $Fe_2(SO_4)_3$ the solid products are the corresponding oxides but $ZnSO_4$ and $CuSO_4$ can yield their oxides or their basic sulphates (oxide sulphates) $ZnO.2ZnSO_4$ and $CuO.CuSO_4$. Several samples of $CuSO_4$ and $ZnSO_4$ were decomposed to an extent corresponding to complete conversion to their basic sulphates and the i.r. spectra obtained indicated clearly the reactions :

$$CuSO_4 \longrightarrow CuO + SO_3$$

$$3ZnSO_4 \longrightarrow ZnO.2ZnSO_4 + SO_3$$

Morphological evidence

The appearances of the reactants have been described above. Examination of the product phases was made using low power light microscopy and scanning electron microscopy (SEM). The following observations were made.

(a) $CuSO_4$ and $NiSO_4$ decomposed at a clearly visible , single macroscopic interface of constant area , which formed on the exposed surface of the reactant and advanced in a direction parallel to the axis of the cup.

The product layer in both cases was a powder of loosely packed oxide particles which SEM showed to be crystalline. The remaining reactant showed only slight nucleation with product in both cases.

(b) $ZnSO_4$ decomposed like $CuSO_4$ and $NiSO_4$ but there was one difference. The product layer , $ZnO.2ZnSO_4$, appeared to have sintered partially , creating a clearly visible gap between itself and the wall of the cup (fig. 41). SEM examination at x2000 showed that the sintering was not far advanced (fig. 42). This was the only sample which could be examined in situ.

(c) The decomposition of the 60 mg samples of 100-300 μm $Fe_2(SO_4)_3$ aggregates was found to occur independently for each grain in each aggregate. Samples were examined by light microscopy after decomposition was taken to extents of 5% , 20% and 90% , and in each case all aggregates were intact and , when dissected , were of uniform colouration. There were no visible interfaces within each aggregate and the grains were all of the same shade of red-brown , which was only slightly less intense at 5% than at 90%.

Weight loss measurements

The weight loss results given in tables 7, 8 and 9 , and illustrated in figs. 30,31,33,34,36 and 37, were obtained by arbitrarily setting the weight loss equal to zero at a zero of time taken as the onset of temperature stability. The weight loss prior to this was typically 3% of the reactant mass.

For reactions in which each particle of the reactant mass decomposes independently , it is the usual practice to express the weight loss data as the fractional decomposition α , and the results for $Fe_2(SO_4)_3$ are presented in this form in table 10 and figs. 43&44. $\alpha = 1$ when $t = \infty$, but in practice this is attained by boosting the temperature to force complete decomposition. $\alpha = 0$ corresponds to the original undecomposed salt , and at the onset of temperature stability α was typically 0.1.

Analysis of the plots of w or α against t suggested the rate laws

given in table 5. The temperature (T) dependencies of the rate constants, k , were all of the form $\log(k) = -(A\ K)/T + B$, where A and B are constants. The equations are :

$$\log(k_1/(\text{mg min}^{-1})) = \frac{-(1.367 \pm 0.054)\times10^4\ K}{T} + 15.94 \pm 0.69$$

$$\log(k_2/(\text{mg min}^{-1})) = \frac{-(1.360 \pm 0.108)\times10^4\ K}{T} + 13.85 \pm 1.20$$

$$\log(k_3/(\text{mg}^2\ \text{min}^{-1})) = \frac{-(1.243 \pm 0.073)\times10^4\ K}{T} + 12.69 \pm 0.81$$

$$\log(k_4/\text{min}^{-1}) = \frac{-(1.158 \pm 0.03)\times10^4\ K}{T} + 12.20 \pm 0.39$$

Accepting that the temperature dependence of the rate constants is of the form $k \propto e^{-\Delta H_a/RT}$, the activation enthalpies , ΔH_a , are compared with the standard enthalpy changes , ΔH° , in the same temperature region in table 6.

TABLE 5. Empirical rate laws.

Material	rate law	function plotted	slope	figures
$CuSO_4$	$dw/dt = k_1$	w v. t	k_1	30,31
$NiSO_4$	$dw/dt = k_2$	w v. t	k_2	33,34
$ZnSO_4$	$dw/dt = k_3 w^{-1}$	w v. $t^{\frac{1}{2}}$	$(2k_3)^{\frac{1}{2}}$	38,39
$Fe_2(SO_4)_3$	$-dr/dt = k'_4$	$1-(1-\alpha)^{\frac{1}{3}}$ v. t	k_4*	45,46

* $k_4 = k'_4/r_m$, r_m is the average radius of a grain.

TABLE 6. Comparison of ΔH_a and ΔH^o values.

Reaction	$\Delta H_a/(kJ\ mol^{-1})$	$\Delta H^o/(kJ\ mol^{-1})$
$CuSO_4 \rightarrow CuO + SO_3$	262	217
$NiSO_4 \rightarrow NiO + SO_3$	260	248
$3ZnSO_4 \rightarrow ZnO.2ZnSO_4 + SO_3$	238	225
$\frac{1}{3}Fe_2(SO_4)_3 \rightarrow \frac{1}{3}Fe_2O_3 + SO_3$	222	203

TABLE 11. Comparison of mean free paths (l) of gas molecules with the dimensions of interparticle spaces (S) in the product layer.

Material	*l/μm	S/μm
CuO	$>10^3$	<10
NiO	$>10^3$	<10
$ZnO.2ZnSO_4$	$>10^2$	<10
Fe_2O_3	$>10^2$	$<10^2$

* formula used was $kT/(P_{eq}\sqrt{2}\,\pi\,d^2)$ where d is the collision diameter.

TABLE 7 . Kinetic data for the decomposition of 40 mg samples of powdered $CuSO_4$.

time	weight loss /mg at temperatures /K					
/min	772	780	784	786	797	799
0	0.00	0.00	0.00	0.00	0.00	0.00
5	0.10	0.15	0.10	0.10	0.03	0.03
10	0.20	0.20	0.20	0.20	0.50	0.55
15	0.25	0.25	0.35	0.40	0.90	0.90
20	0.30	0.35	0.45	0.50	1.20	1.25
25	0.40	0.50	0.60	0.65	1.55	1.55
30	0.50	0.60	0.75	0.80	1.85	1.95
35	0.60	0.70	0.90	1.00	2.10	2.30
40	0.65	0.80	1.00	1.15	2.40	2.70
45	0.75	0.95	1.15	1.30	2.70	3.00
50	0.85	1.05	1.35	1.50	3.00	3.40
55	0.90	1.20	1.50	1.70	3.30	3.75
60	1.00	1.35	1.60	1.85	3.65	4.10
65	1.10	1.50	1.75	2.00	4.05	4.45
70	1.20	1.65	1.90	2.20	4.35	4.80
75	1.15	1.80	2.05	2.35	4.70	5.15
80	1.35	1.90	2.20	2.55	5.00	5.45
85	1.40	2.05	2.35	2.75	5.30	5.75
90	1.50	2.25	2.55	2.95	5.50	6.05
95	1.60	2.40	2.70	3.15	5.75	6.40
100	1.70	2.55	2.90	3.35	6.05	6.65
105	1.80	2.75	3.05	3.55	6.30	6.95
110	1.90	2.85	3.20	3.80	6.55	7.25
115	2.00	2.95	3.35	3.95	6.80	
120	2.10	3.10	3.50	4.10		
125	2.20	3.25	3.65	4.30		
130	2.30	3.40	3.80	4.45		
135	2.40	3.50	3.90	4.70		
140	2.50	3.65				

TABLE 8 . Kinetic data for the decomposition of 30 mg samples of powdered $NiSO_4$.

time	weight loss / mg at temperatures / K					
/min	875	888	897	907	918	932
0	0.00	0.00	0.00	0.00	0.00	0.00
5	0.10	0.15	0.35	0.35	0.65	1.10
10	0.15	0.30	0.65	0.60	1.05	2.30
15	0.20	0.50	0.95	0.95	1.70	3.25
20	0.30	0.65	1.35	1.25	2.20	4.10
25	0.40	0.80	1.65	1.65	2.70	4.95
30	0.50	0.95	2.00	2.05	3.30	5.80
35	0.65	1.15	2.30	2.45	3.80	6.60
40	0.75	1.30	2.60	2.90	4.35	7.45
45	0.85	1.50	2.90	3.25	4.90	8.30
50	0.95	1.65	3.20	3.55	5.35	9.10
55	1.05	1.80	3.65	3.90	5.90	
60	1.15	2.00	3.80	4.25	6.50	
65	1.25	2.15	4.15	4.55	7.05	
70	1.35	2.30	4.40	4.90	7.50	
75	1.45	2.45	4.70	5.20	7.80	
80	1.55	2.60	5.00	5.55		
85	1.65	2.70	5.30	5.90		
90	1.75	2.90	5.60	6.20		
95	1.85	3.05	5.90	6.55		
100	1.95	3.20	6.15	6.85		
105	2.00	3.35	6.40	7.15		
110	2.10	3.50	6.65	7.45		
115	2.20	3.65	6.90	7.75		
120	2.30	3.80		8.00		
125	2.40	3.90				
130						

TABLE 9 . Kinetic data for the decomposition of 40 mg samples of powdered $ZnSO_4$.

time	weight loss / mg at temperature / K							
/min	871	875	883	909	918	929	939	959
0	0.00	0.00	0.00	0.00	0.00	0.00	0.00	0.00
5	0.20	0.25	0.30	0.35	0.55	0.50	0.70	1.10
10	0.35	0.45	0.55	0.60	0.95	1.00	1.30	1.90
15	0.50	0.60	0.80	0.85	1.30	1.45	1.90	2.60
20	0.60	0.75	1.00	1.10	1.65	1.80	2.40	3.25
25	0.80	0.90	1.15	1.30	1.90	2.20	2.85	3.90
30	0.90	1.00	1.30	1.50	2.20	2.50	3.25	4.50
35	1.00	1.10	1.45	1.70	2.45	2.80	3.65	
40	1.10	1.20	1.55	1.90	2.70	3.10	4.00	
45	1.15	1.30	1.65	2.05	2.90	3.35	4.30	
50	1.25	1.40	1.75	2.20	3.10	3.60	4.70	
55	1.30	1.45	1.90	2.35	3.25	3.85	4.95	
60		1.55	1.95	2.50	3.45	4.10	5.30	
65		1.65	2.05	2.60		4.35	5.52	
70		1.70	2.10	2.70		4.65	5.85	
75			2.20	2.85		4.80	6.10	
80			2.30	3.00		5.00	6.35	
85				3.15		5.20	6.55	
90				3.25		5.30		
95				3.35		5.40		
100				3.45				

TABLE 10 . Kinetic data for the decomposition of 60 mg samples of $Fe_2(SO_4)_3$ particles each of which is an aggregate of smaller particles.

time	fraction decomposed (α) at temperature /K					
/min	777.0	778.5	786.5	787.5	795.5	806.5
0	0.100	0.110	0.110	0.145	0.145	0.090
10	0.135	0.155	0.145	0.215	0.235	0.255
20	0.175	0.205	0.195	0.275	0.315	0.410
30	0.205	0.245	0.255	0.345	0.410	0.520
40	0.235	0.295	0.305	0.410	0.490	0.645
50	0.265	0.335	0.365	0.470	0.570	0.735
60	0.305	0.380	0.430	0.540	0.645	0.815
70	0.335	0.420	0.480	0.590	0.705	0.880
80	0.365	0.460	0.530	0.645	0.755	0.920
90	0.400	0.500	0.580	0.695	0.805	0.950
100	0.430	0.530	0.635	0.735	0.855	0.960
110	0.460	0.570	0.675	0.775	0.890	
120	0.490	0.600	0.705	0.805	0.920	0.970
130	0.510	0.635	0.745	0.835	0.930	
140	0.540	0.665	0.785	0.865	0.950	0.980
150	0.570	0.695	0.815	0.900	0.960	
160	0.590	0.735	0.845	0.910	0.960	0.990
170	0.610	0.755	0.865	0.930	0.970	
180	0.645	0.785	0.900	0.940		
190		0.805	0.950	0.910		
200				0.920		

$$\text{Here } \alpha = \frac{\text{weight loss at time t}}{\text{weight loss after complete decomposition}}$$

and complete decomposition was achieved by raising the temperature to 850 K.

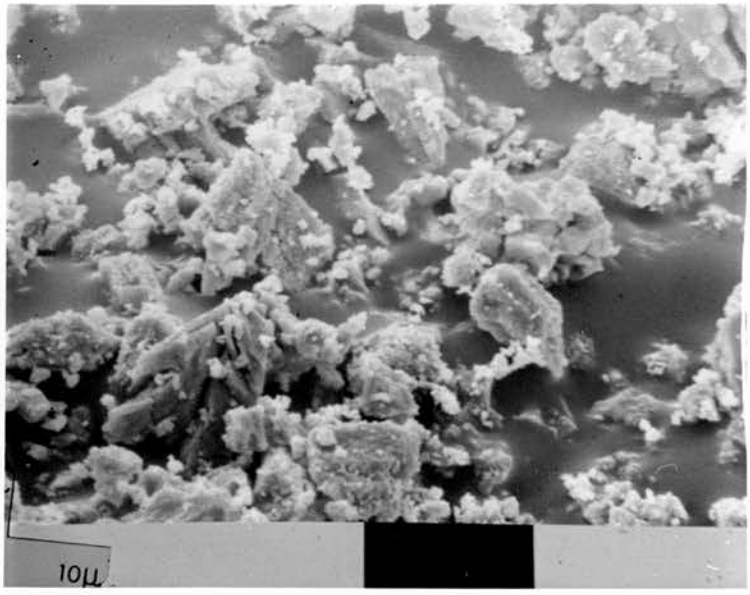

Fig. 23. Grains of powdered $CuSO_4$ dropped onto sticky tape.

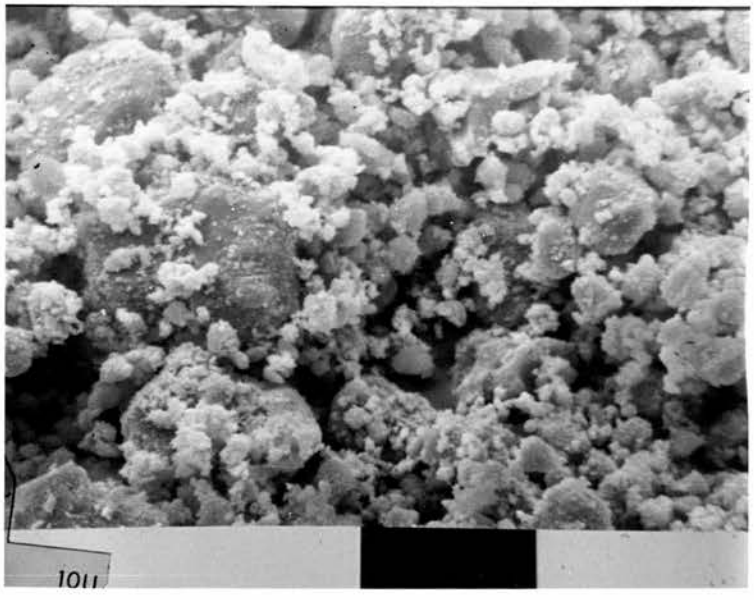

Fig. 24. Grains of powdered $NiSO_4$ dropped onto sticky tape.

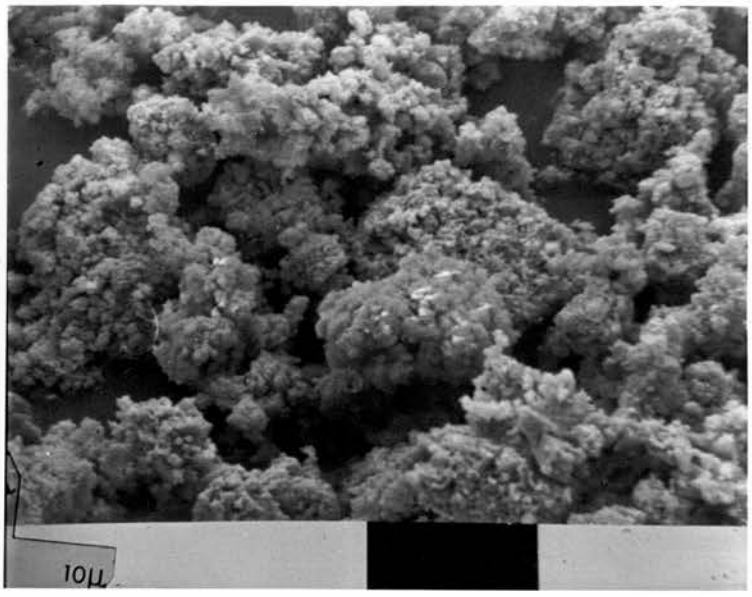

Fig. 25. Grains of powdered $ZnSO_4$ dropped onto sticky tape.

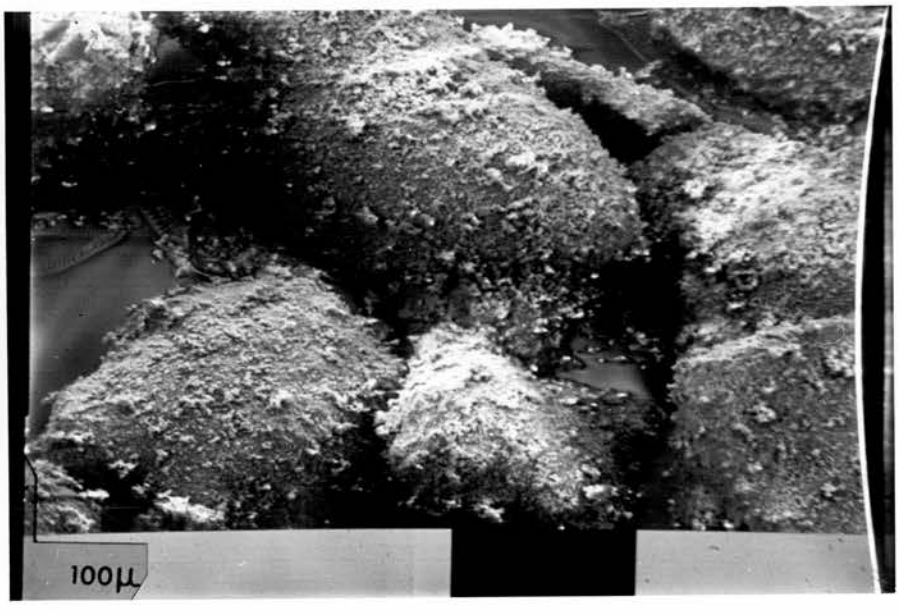

Fig. 26. Aggregates of grains of $Fe_2(SO_4)_3$.

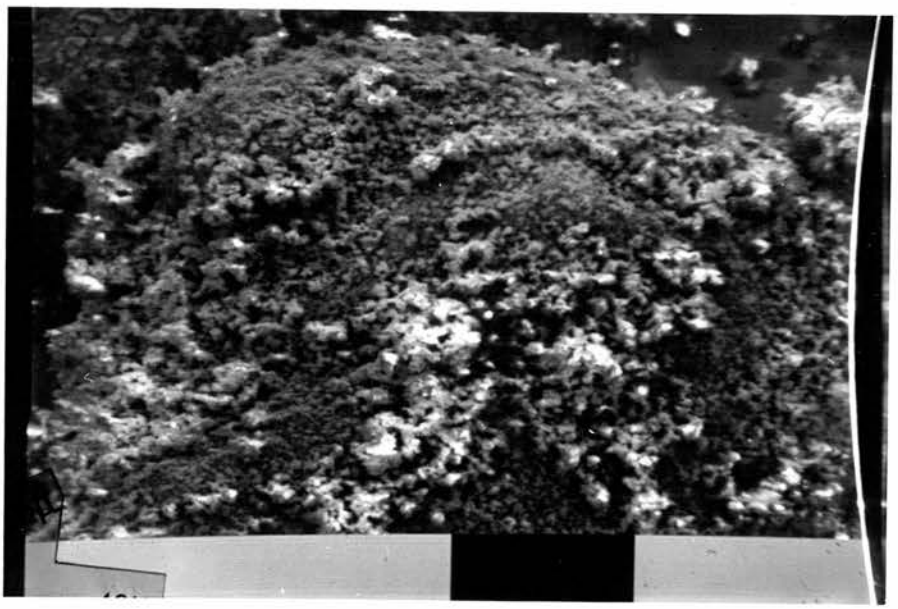

Fig. 27. A single aggregate of $Fe_2(SO_4)_3$.

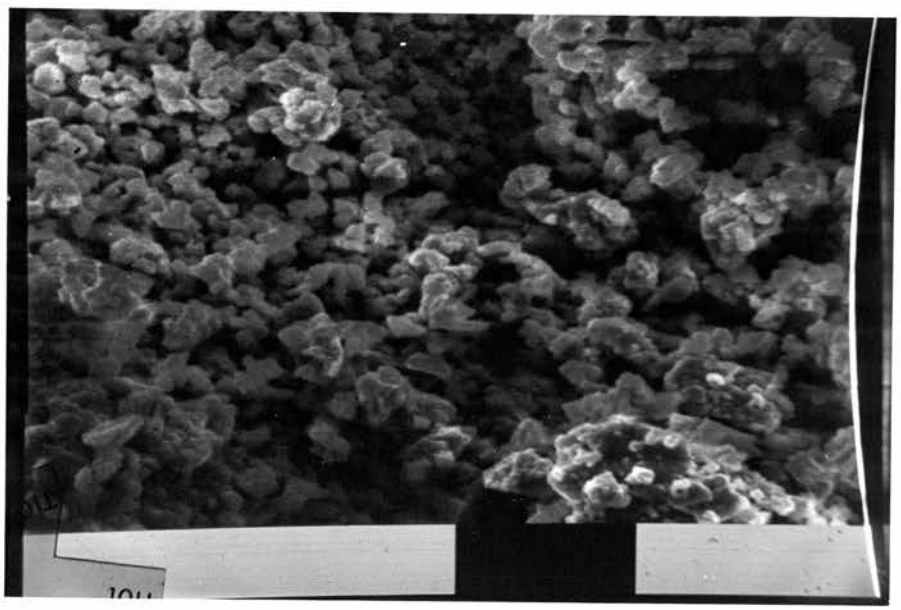

Fig. 28. The individual grains in a $Fe_2(SO_4)_3$ aggregate.

Fig. 29. Deleted.

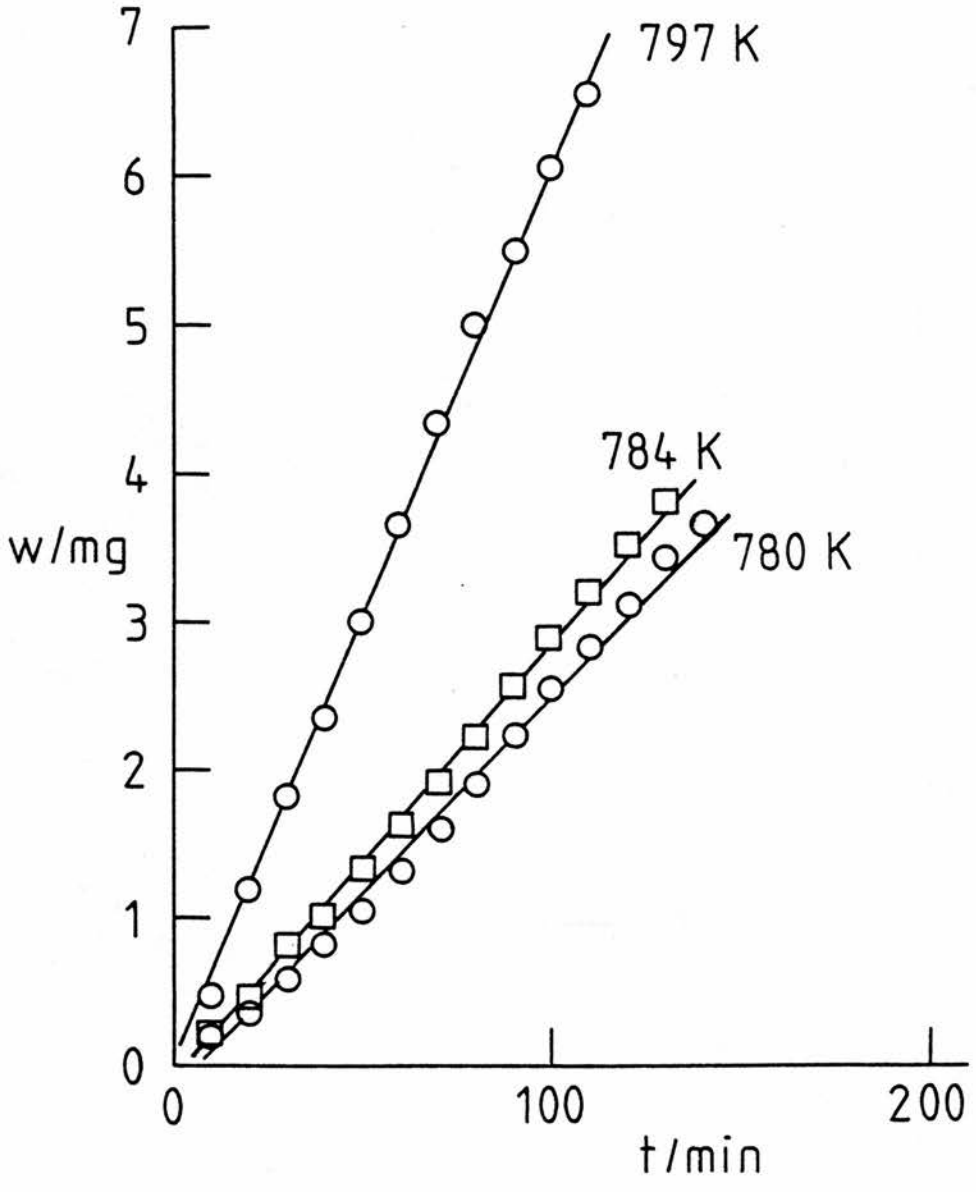

Fig. 30. Weight loss data for the decomposition of powdered $CuSO_4$.

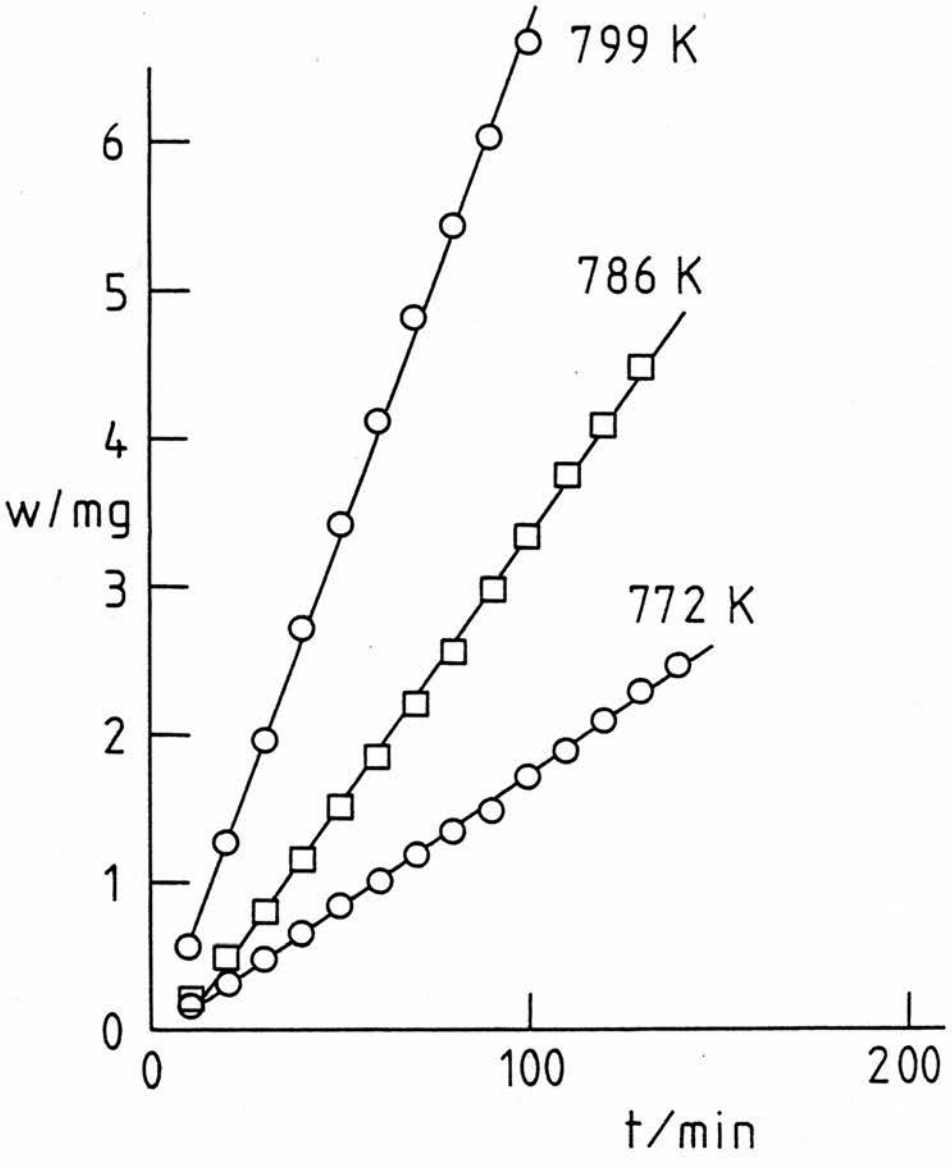

Fig. 31. Weight loss data for the decomposition of powdered $CuSO_4$.

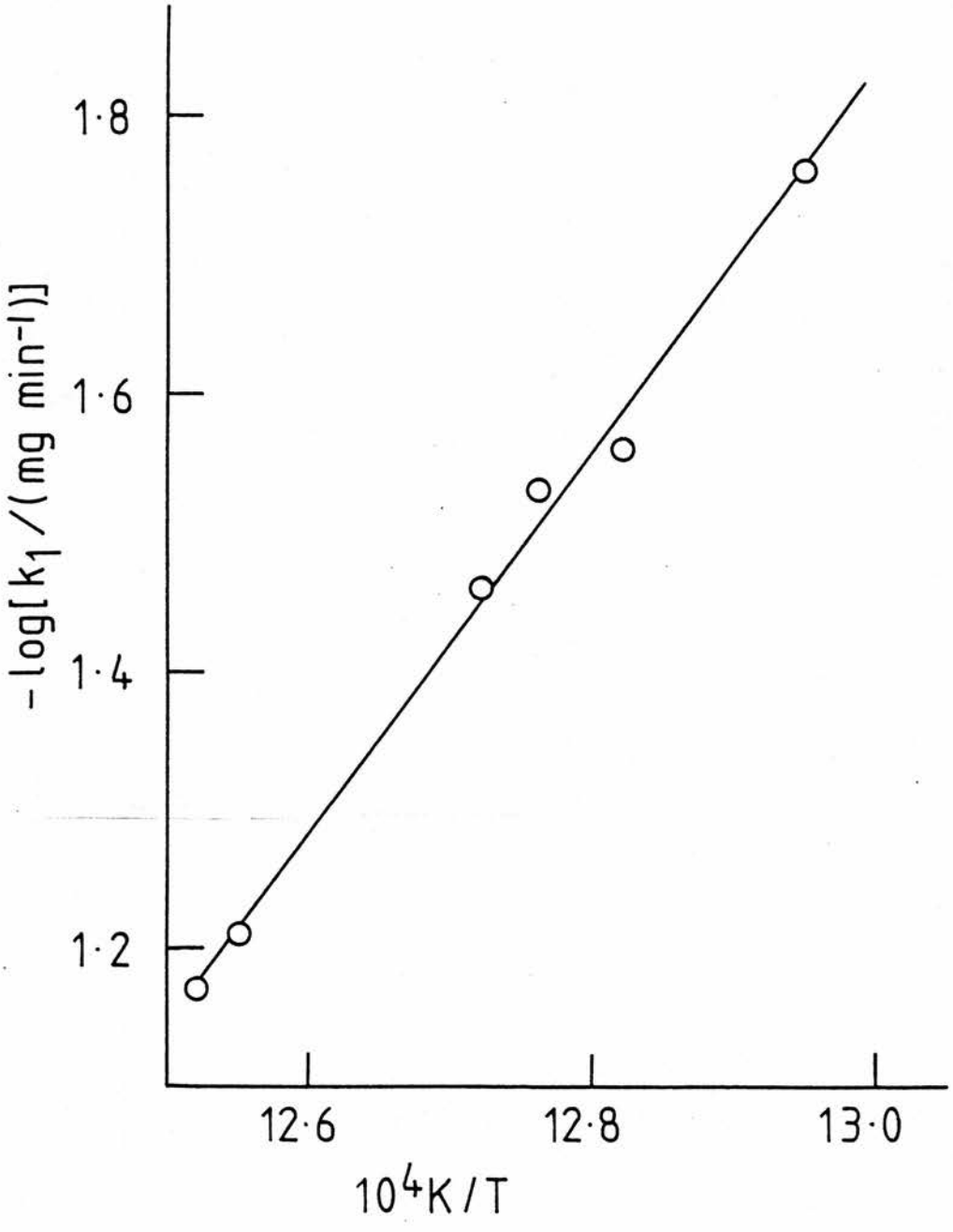

Fig. 32. The temperature dependence of the $CuSO_4$ decomposition rate constant.

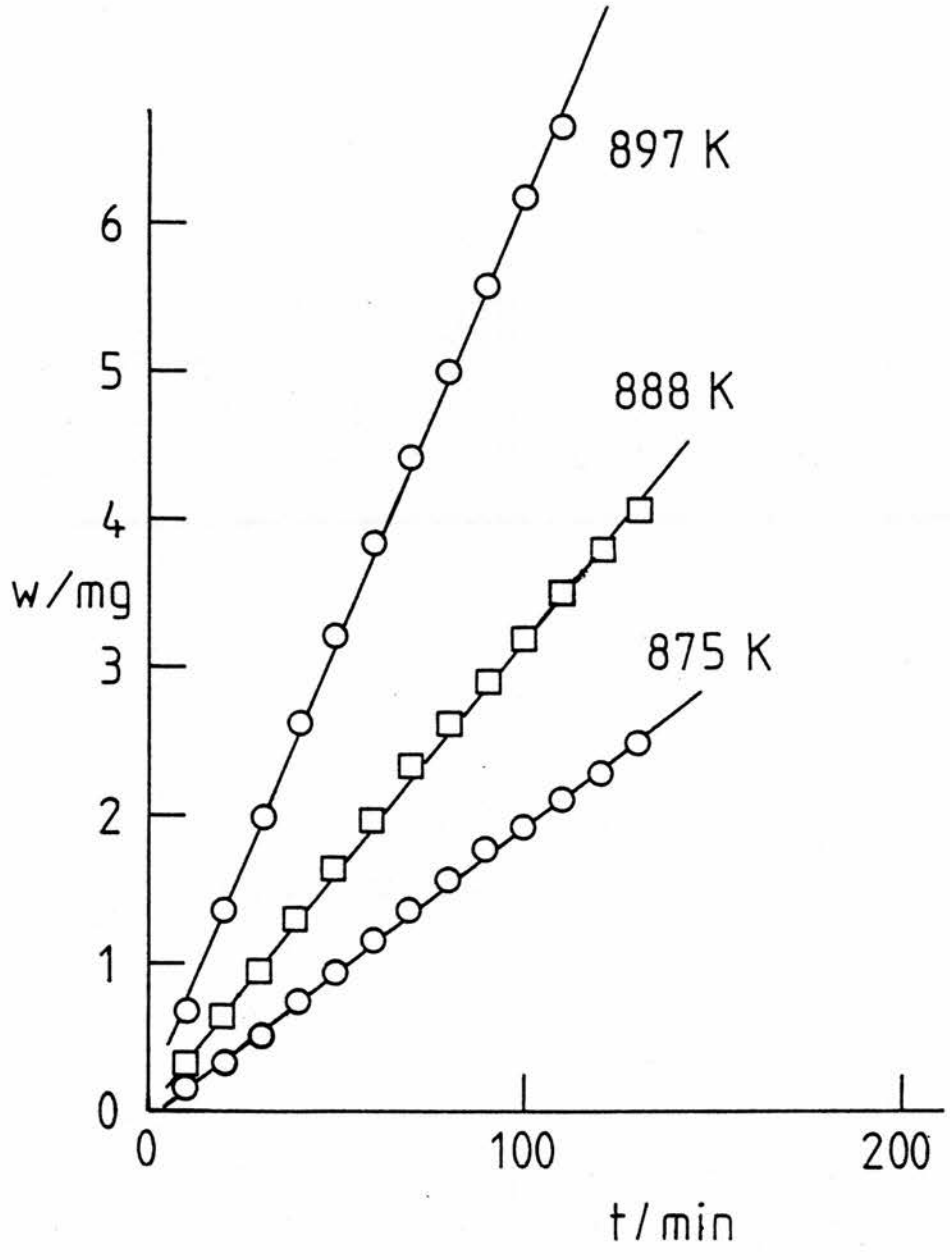

Fig. 33. Weight loss data for the decomposition of powdered $NiSO_4$.

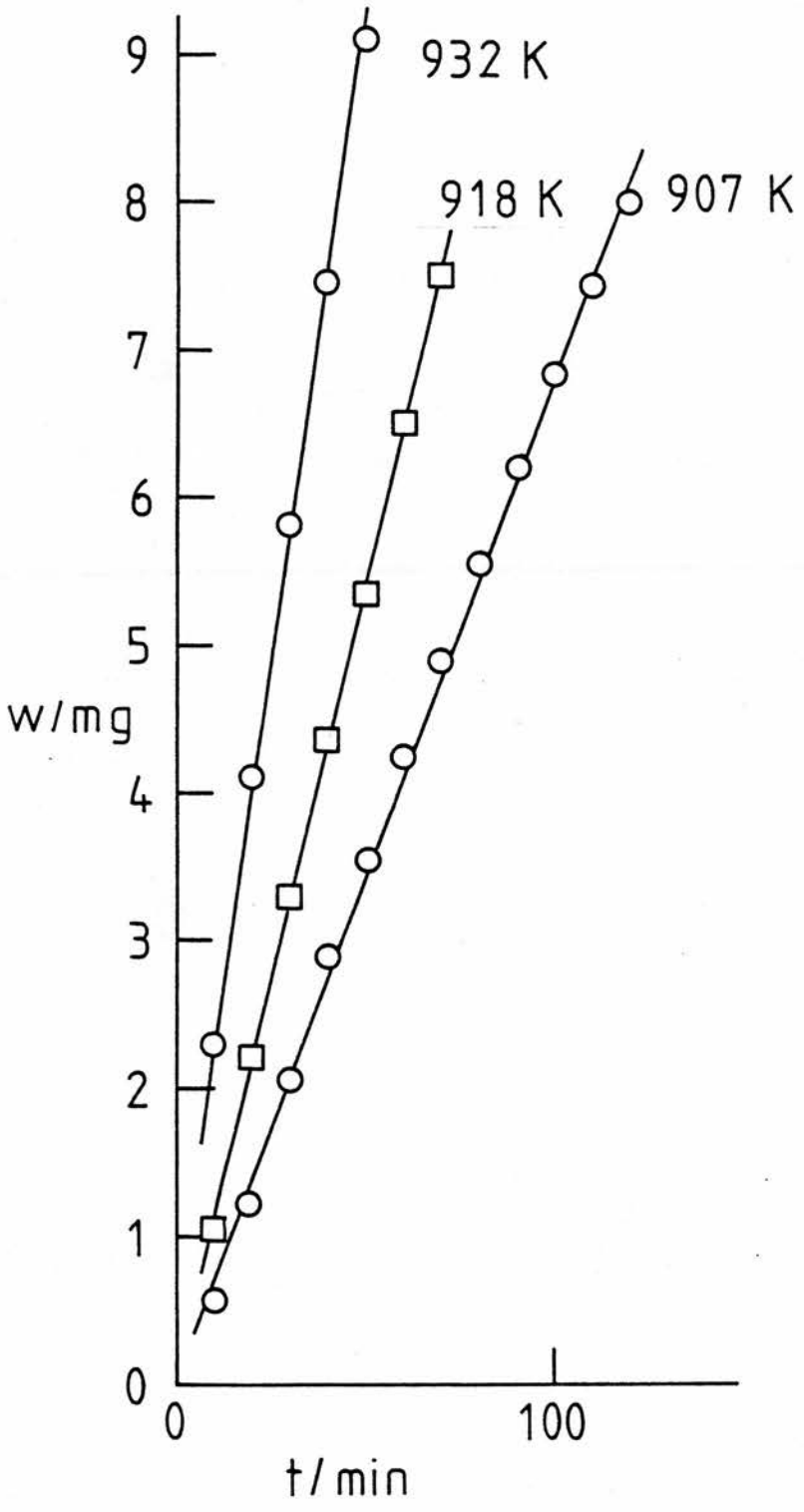

Fig. 34. Weight loss data for the decomposition of powdered $NiSO_4$.

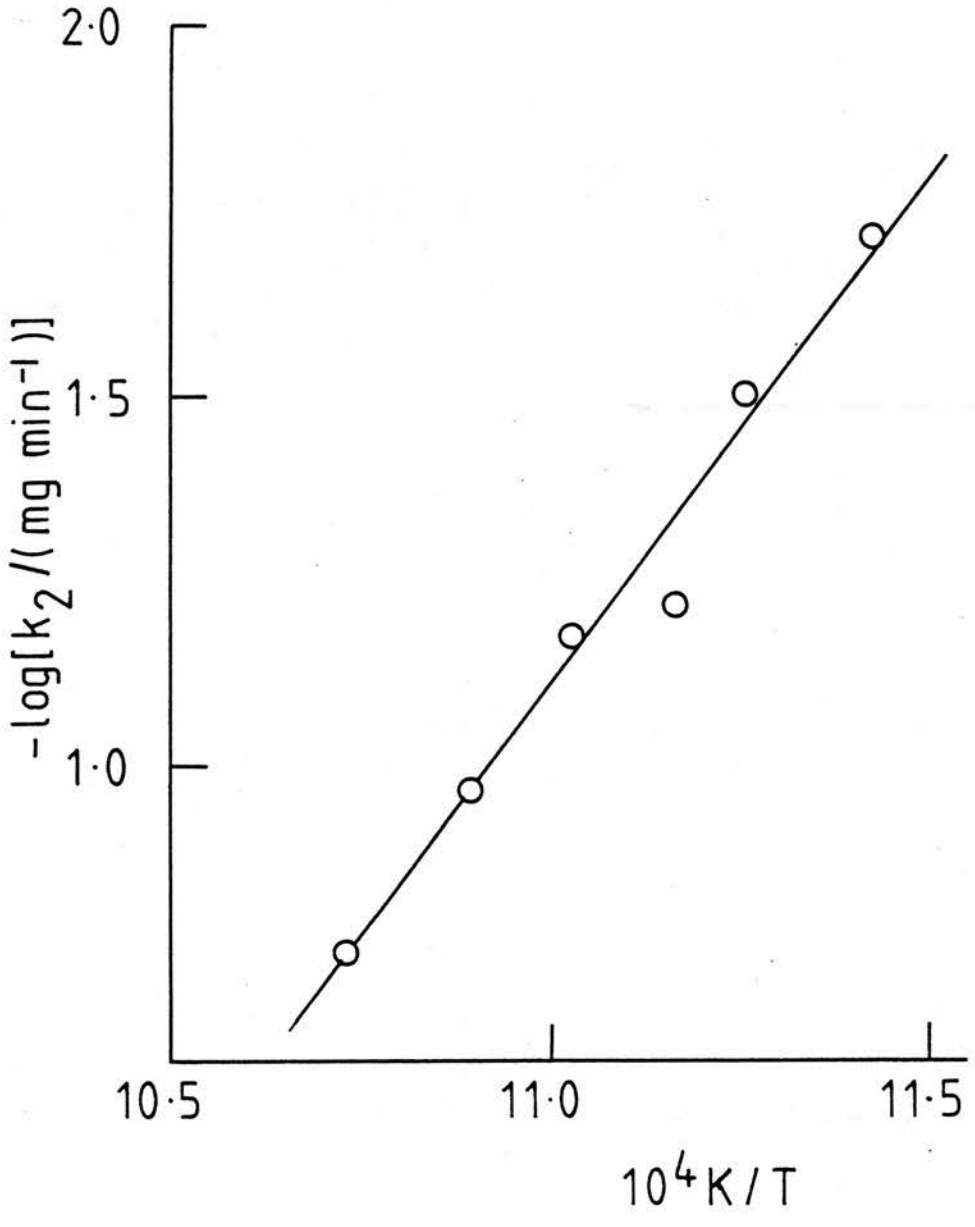

Fig. 35. The temperature dependence of the $NiSO_4$ decomposition rate constant.

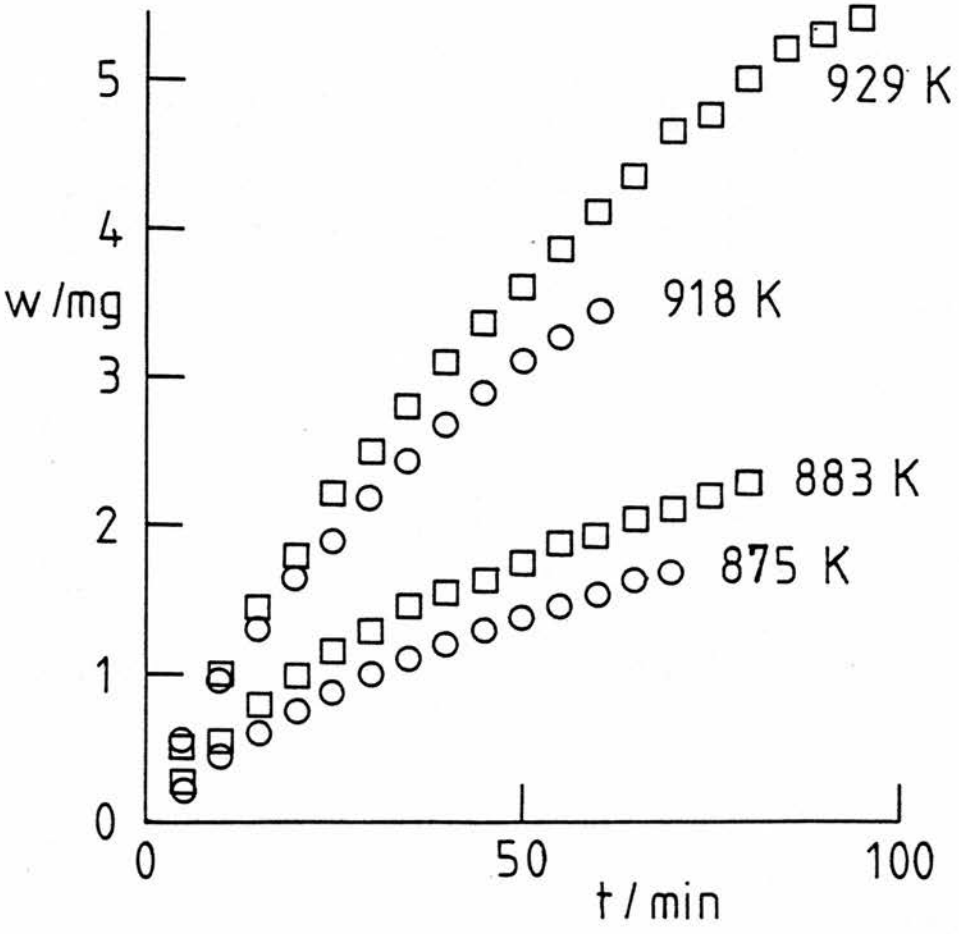

Fig. 36. Weight loss data for the decomposition of powdered $ZnSO_4$.

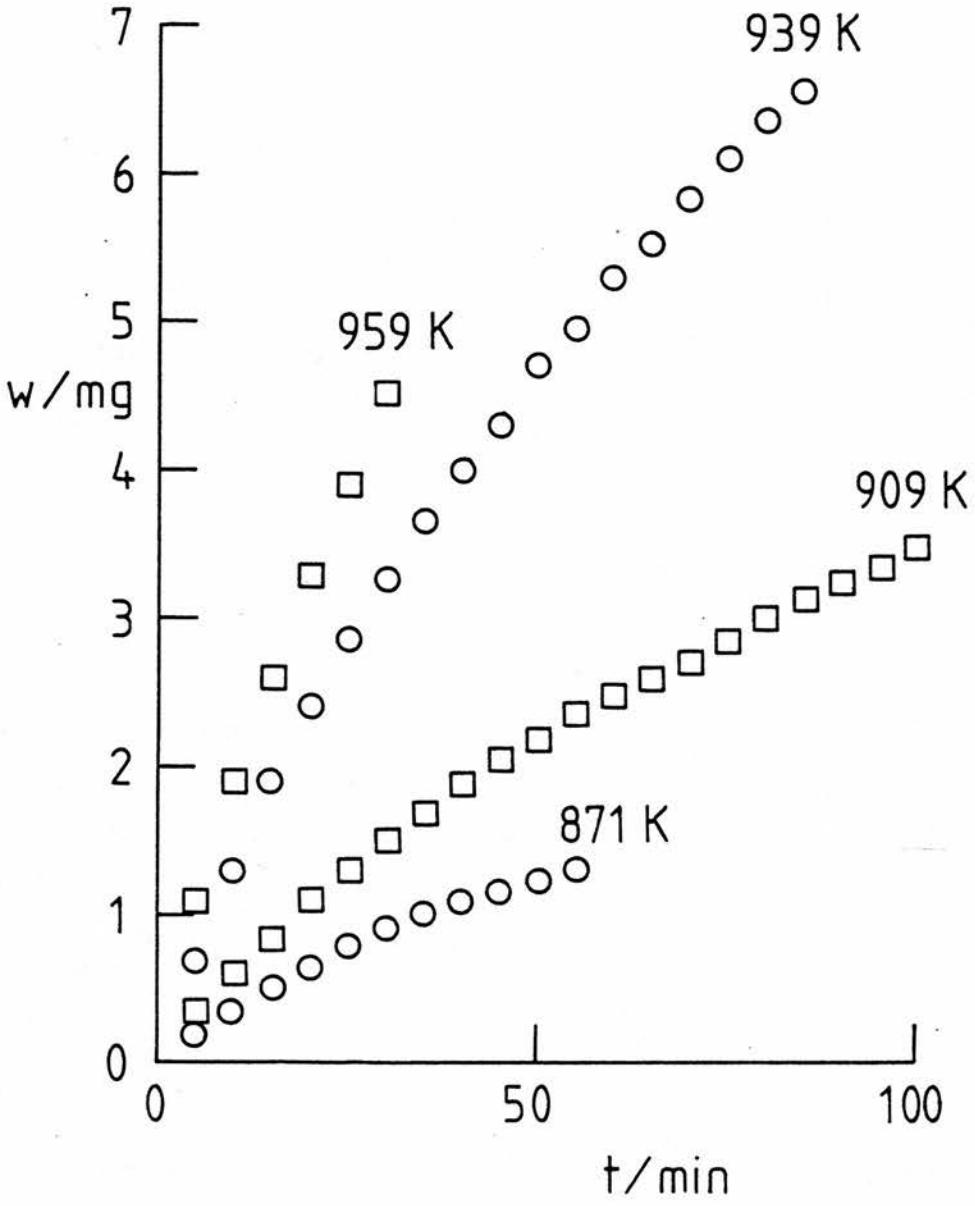

Fig. 37. Weight loss data for the decomposition of powdered $ZnSO_4$.

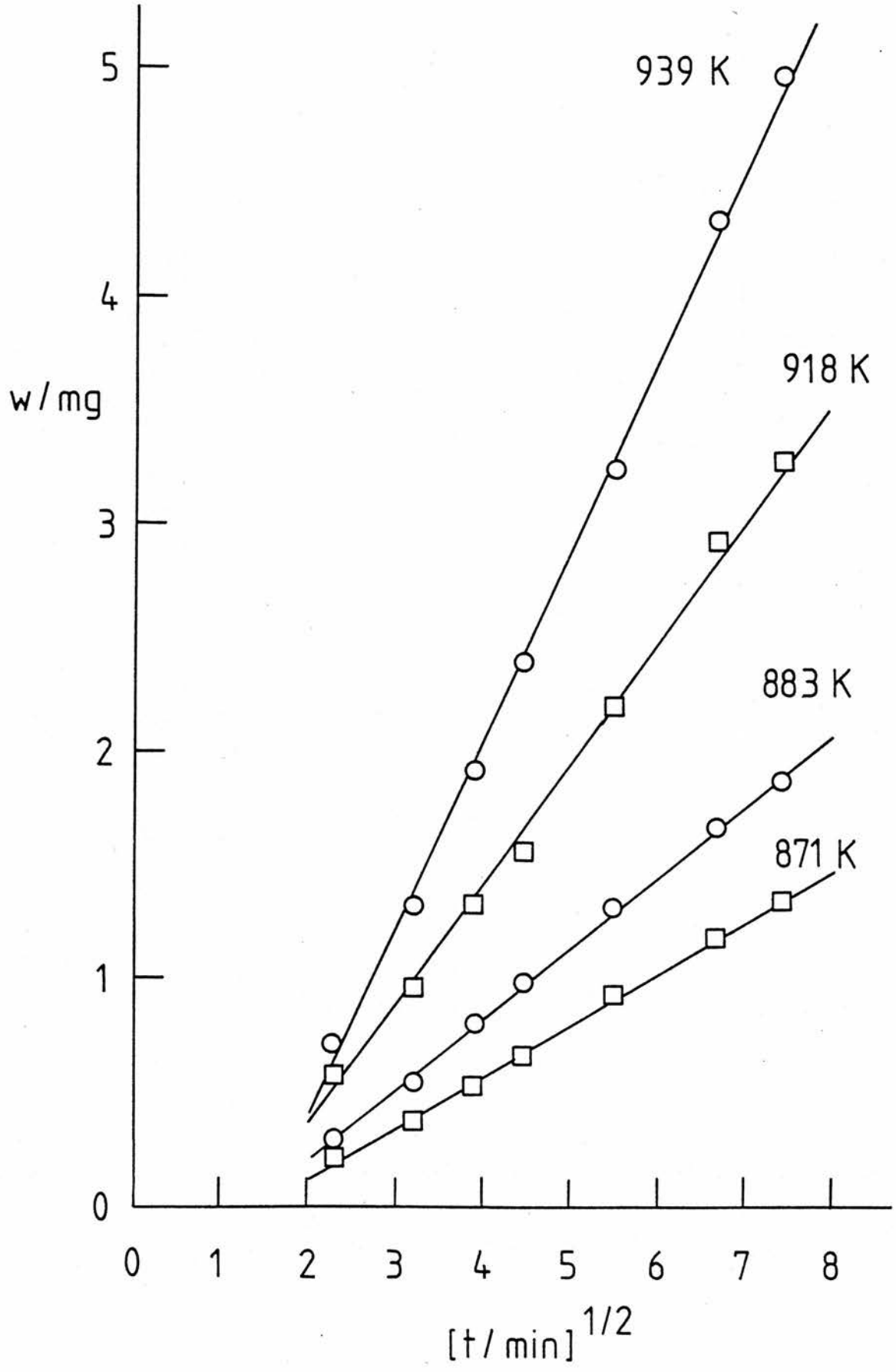

Fig. 38. The dependence of weight loss on $t^{\frac{1}{2}}$ for the decomposition of $ZnSO_4$.

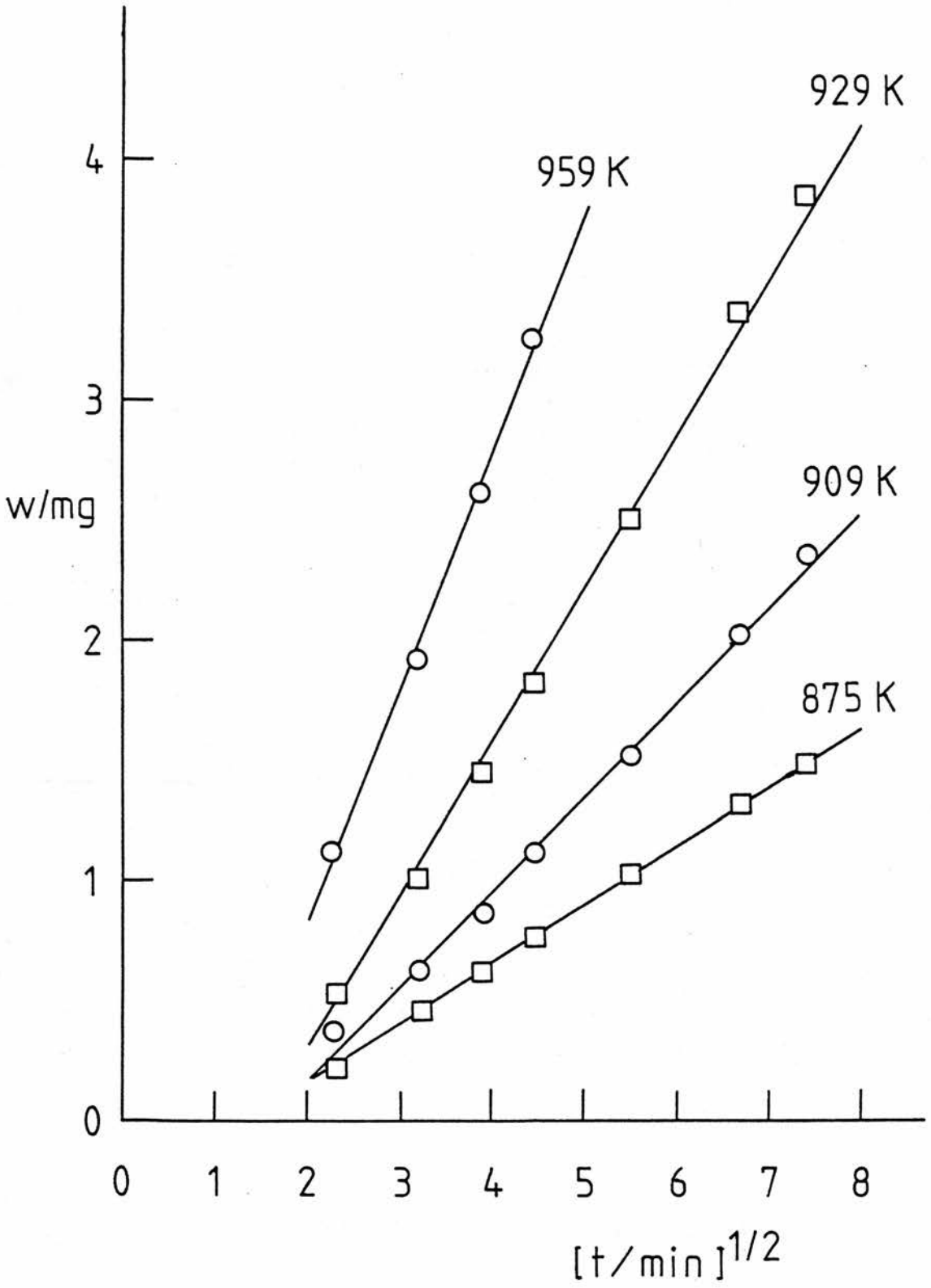

Fig. 39. The linear dependence of weight loss on $t^{\frac{1}{2}}$ for the decomposition of $ZnSO_4$.

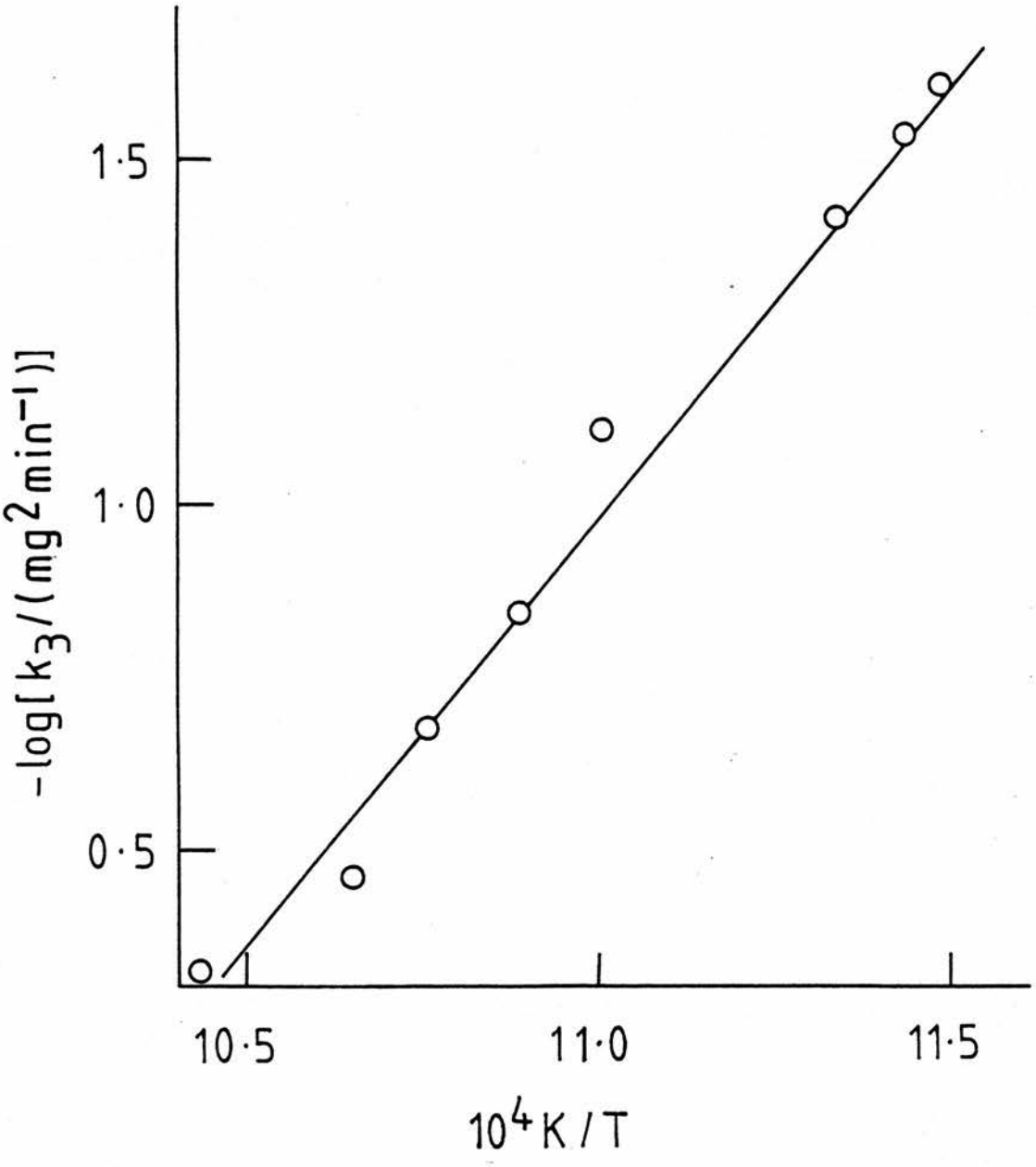

Fig. 40. The temperature dependence of the $ZnSO_4$ decomposition rate constant.

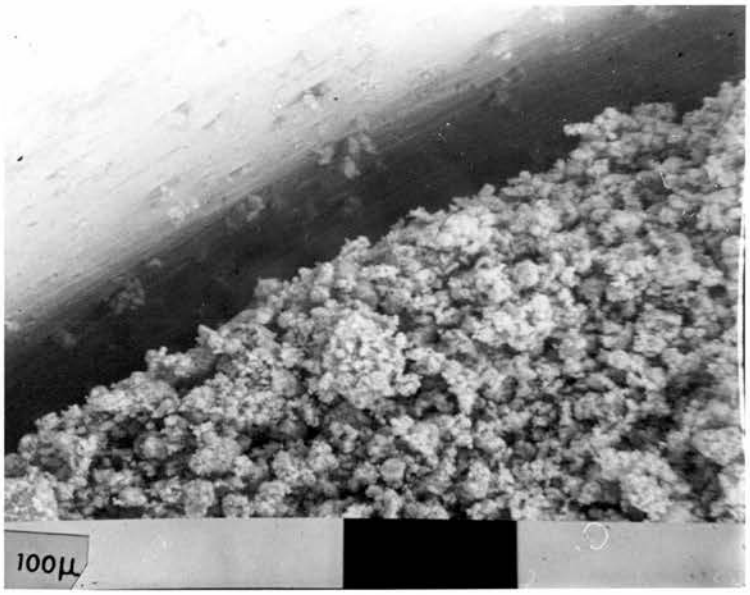

Fig. 41. The shrinkage of the product layer ($ZnO.2ZnSO_4$) has created a gap between itself and the wall of the cup.

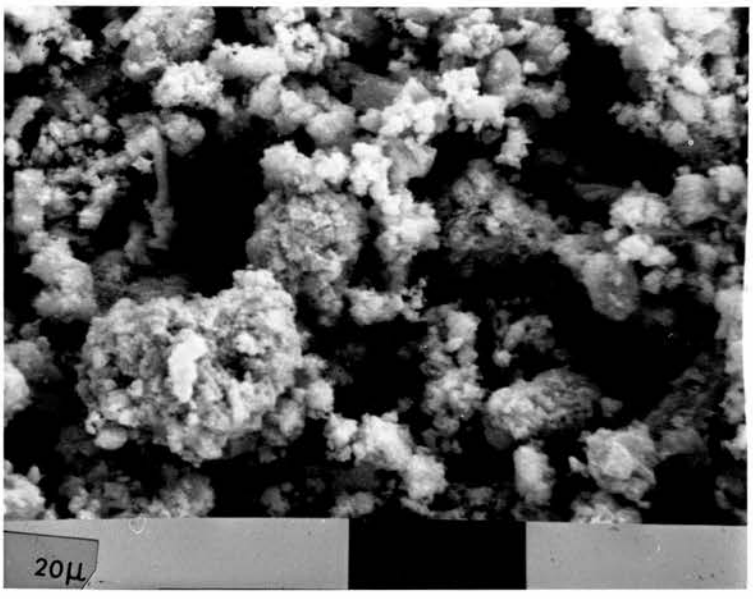

Fig. 42. Sintering , which manifests itself as above , is not at an advanced stage.

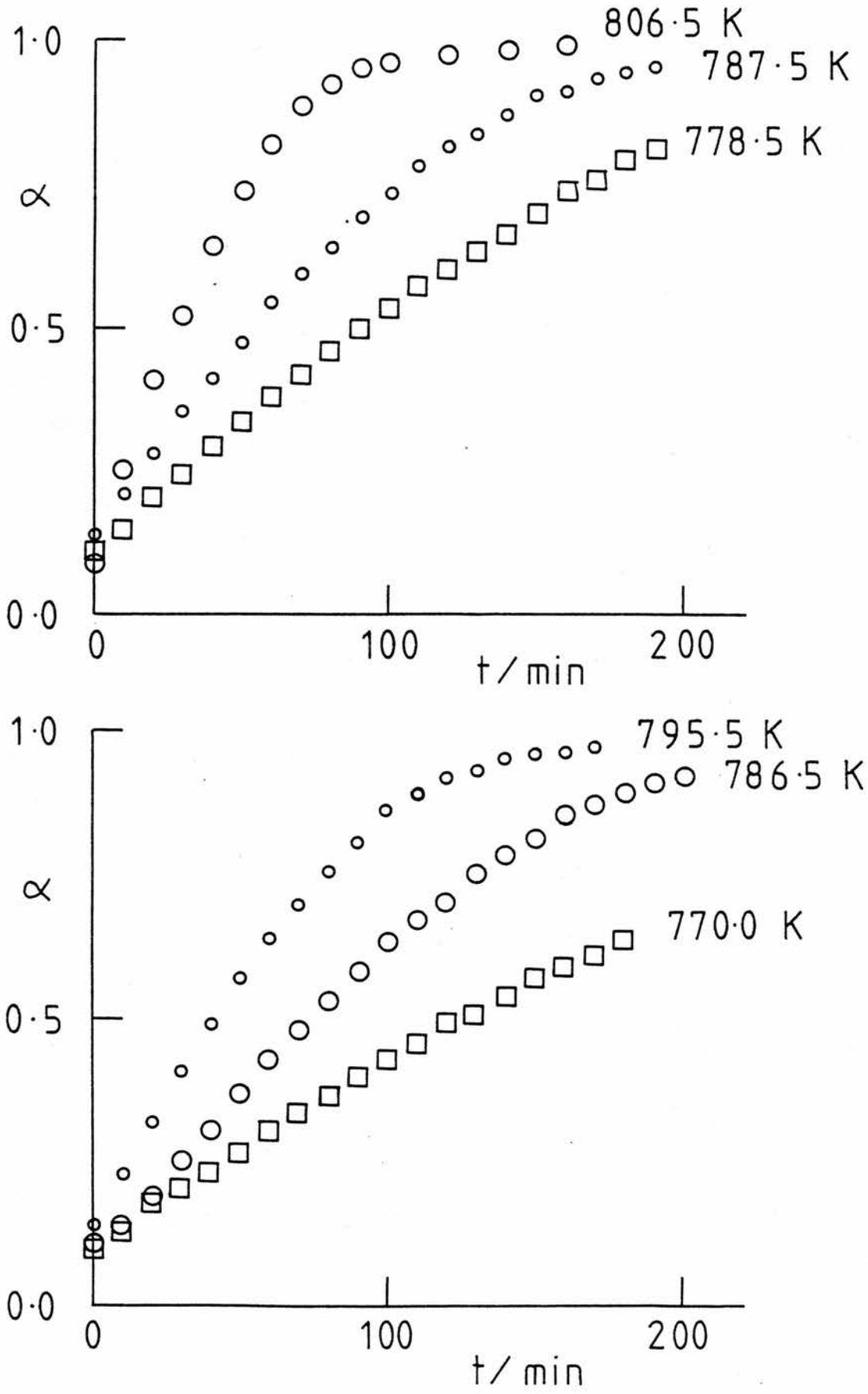

Figs. 43 and 44. The extent of decomposition ,α, of $Fe_2(SO_4)_3$ against time.

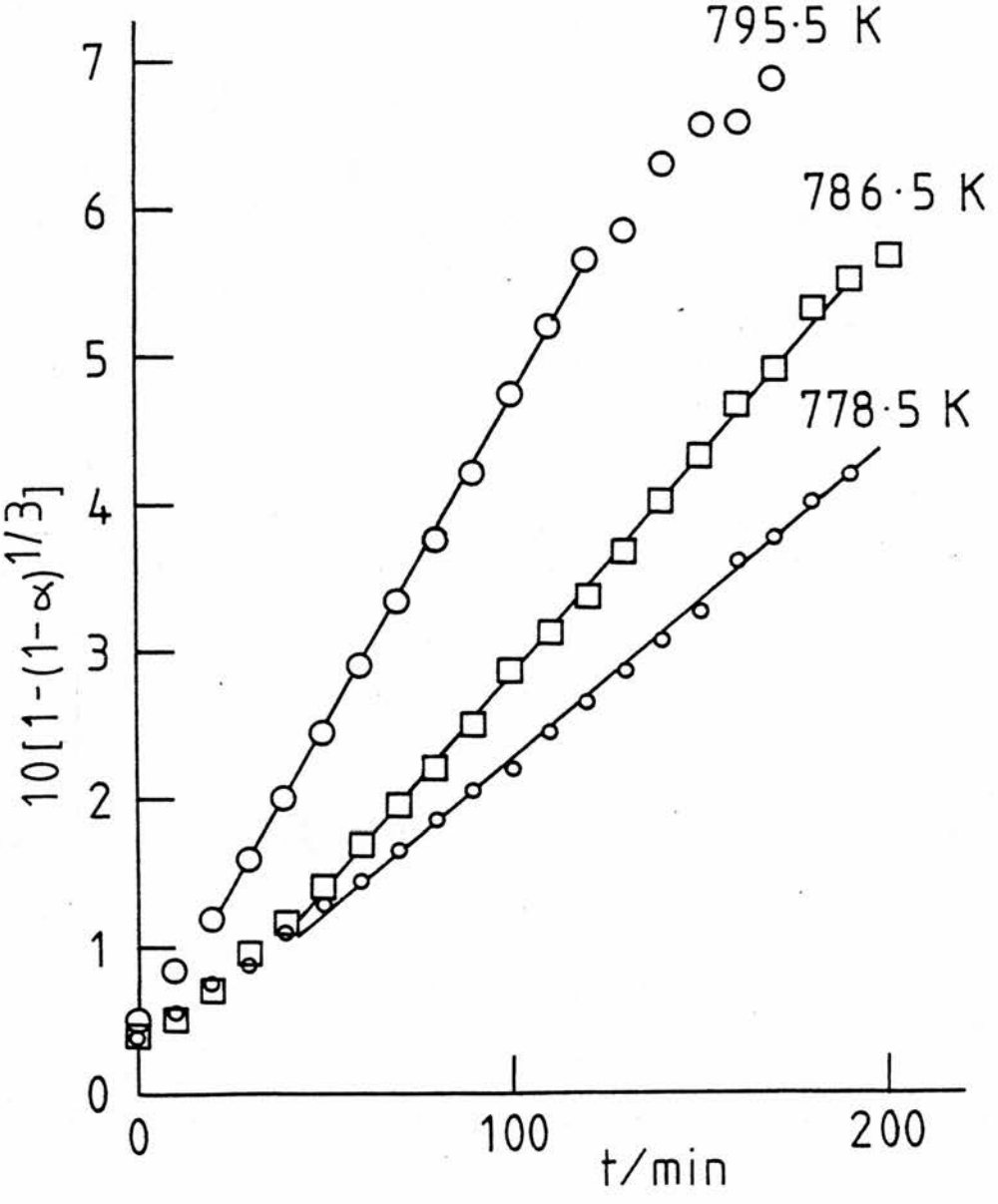

Fig. 45. The linearity of these plots suggests that $Fe_2(SO_4)_3$ decomposes by the contracting sphere mechanism.

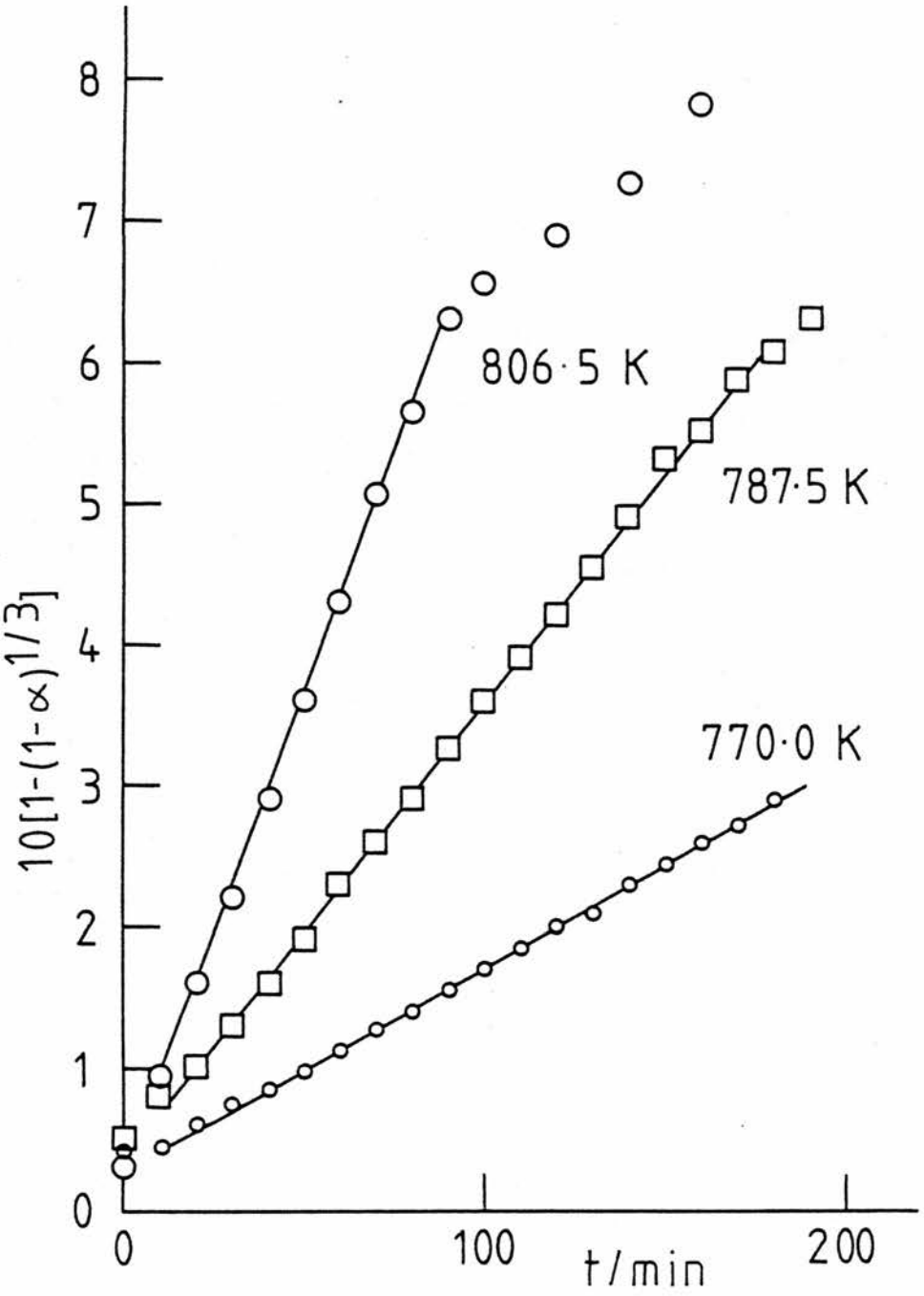

Fig. 46. The linearity of these plots suggests that $Fe_2(SO_4)_3$ decomposes by the contracting sphere mechanism.

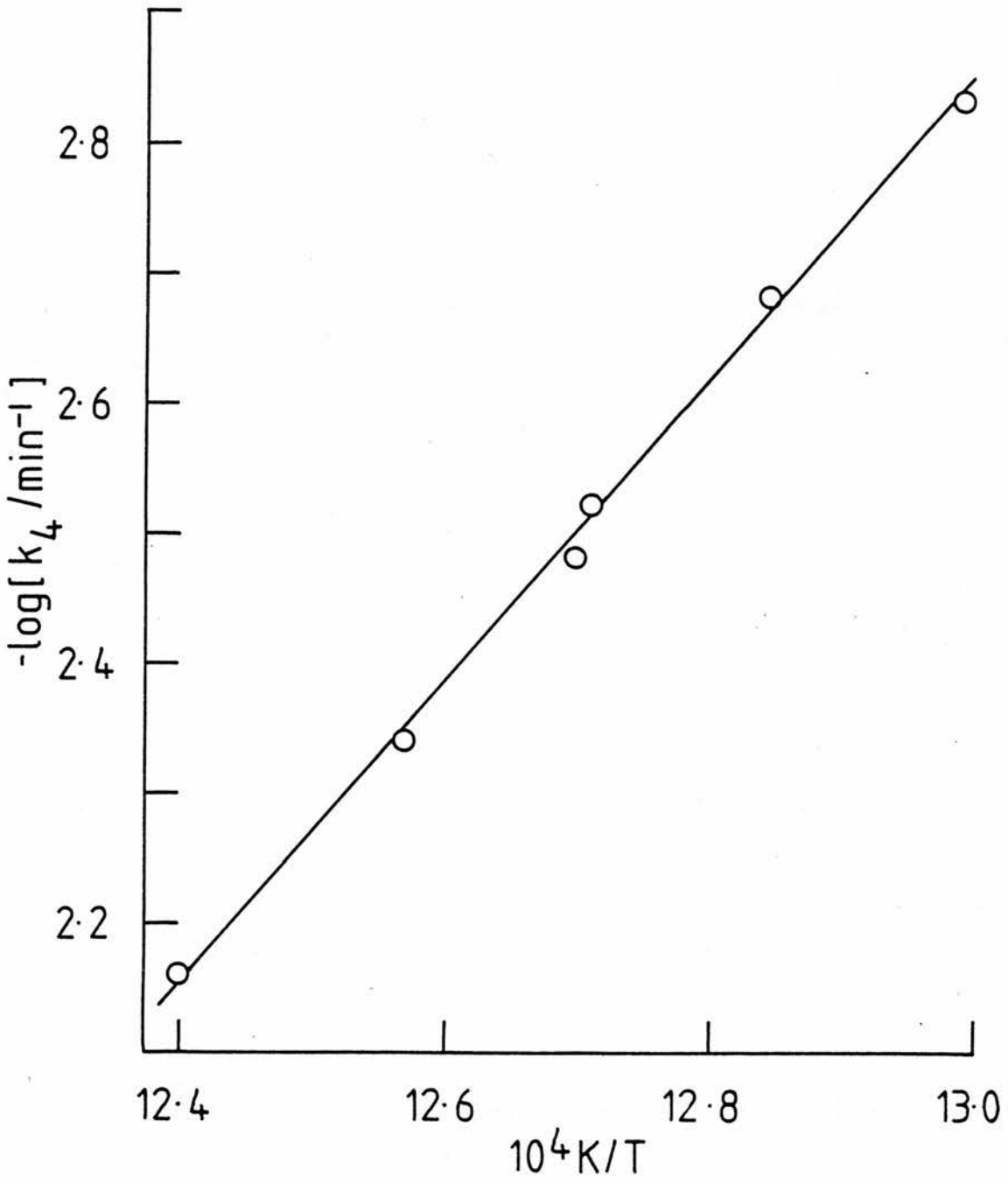

Fig. 47. The temperature dependence of the $Fe_2(SO_4)_3$ decomposition rate constant.

DISCUSSION

In this section the data presented in the preceding pages will be discussed and an attempt will be made to reconcile the different modes of decomposition encountered.

$CuSO_4$ and $NiSO_4$ decomposed at a single macroscopic interface of constant area , which formed on the exposed surface of the sample and advanced as a plane in a direction parallel to the axis of the cup. The product layer in both cases was a powder of loosely packed oxide particles. The rates of reaction conformed to the laws $dw/dt = k_1$ and $dw/dt = k_2$, indicating that the growing product layer did not influence the processes occurring at the interface. The activation enthalpies were a little larger than the corresponding standard enthalpy changes.

$ZnSO_4$ decomposed at a single macroscopic interface as did $CuSO_4$ and $NiSO_4$, but the decomposition product , $ZnO.2ZnSO_4$, appeared to have undergone sintering. Examination by SEM , however , suggested that the sintering was not far advanced. The reaction rate diminished as the reaction proceeded , that is , as the product layer grew in thickness , and the rate law was $dw/dt = k_3 w^{-1}$ (the parabolic law). The activation enthalpy was a little larger than the corresponding standard enthalpy change.

In the 100-300 μm aggregates of $Fe_2(SO_4)_3$ each 2 μm grain decomposed independently by the contracting sphere mechanism described above. Here the kinetic law is $-dr/dt = k_4'$, where dr/dt is the rate of change of the radius of the contracting spherical interface. As explained , the integrated rate law relating the fractional decomposition , α , of the whole sample to the mean radius r_m of the grains (about 2 μm in this case) and the rate constant k_4' is (eq. 19)

$$1-(1-\alpha)^{\frac{1}{3}} = (k_4'/r_m)t = k_4 t$$

where k_4 is the slope of the plots in figs.45 and 46. From figs. 45

and 46 it can be seen that the contracting sphere model holds up to $1-(1-\alpha)^{\frac{1}{3}} = 0.6$, that is , $\alpha = 0.95$. This mechanism assumes a very rapid and complete surface nucleation so that at low values of α the grains should be completely covered with oxide. This is indeed what was observed when the aggregates of these grains were broken up and examined under the light microscope at $\alpha = 0.05$. The activation enthalpy for interface advance was a little larger than the corresponding standard enthalpy of reaction.

Before attempting to reconcile these different modes of decomposition, a few words will be said about gas transport in the samples. Table 11 compares the mean free path , l , of an SO_3 molecule at the maximum possible pressure in the sample mass (i.e. the equilibrium vapour pressure) with the magnitude , S , of the interparticle spaces. In all cases , $l \gg S$, which suggests that Knudsen flow will be the predominant mode of gas transport in the product layer. This is a convenient conclusion since it permits the application of equation 13.

A model for the decomposition of packed powders will now be described , which invokes solid-state interaction of grains to account for the possibility of co-operative reaction. There are , however , difficulties associated with the model and the author's aim in presenting it is really to illustrate a possible line of attack on the problem.

Solid-state interaction mechanism

For this model it is assumed that the sample is packed into a cup as described above and that the reaction is initiated by the formation of nuclei of the product phase on the exposed surface of the sample. If these nuclei spread by very rapid two-dimensional growth on the surface of each grain in the exposed layer , these grains will almost immediately become completely covered with product. The contact of

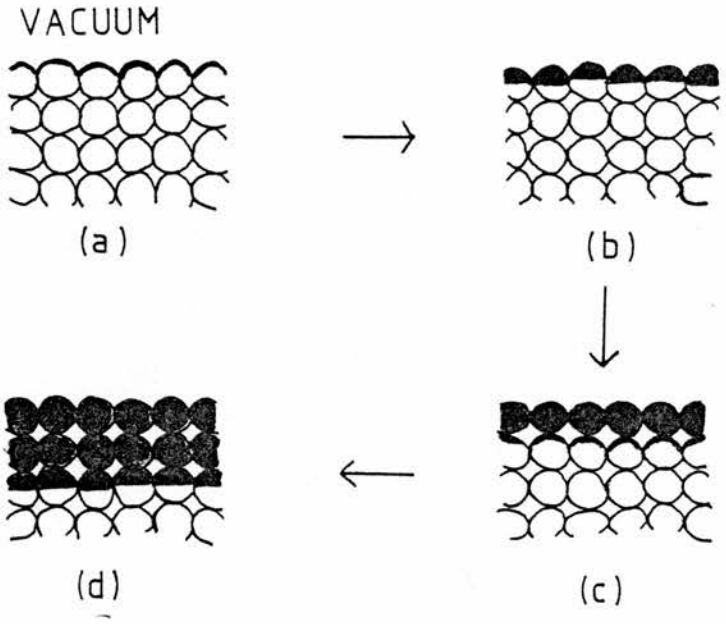

Fig. 48. The nucleation-by-contact mechanism.
(a) product forms on the exposed surface of the powder;
(b) reaction proceeds by the advance of intragranular interfaces;
(c) completely decomposed grains nucleate the reactant grains beneath; (d) the overall effect is the advance of a macroscopic interface.

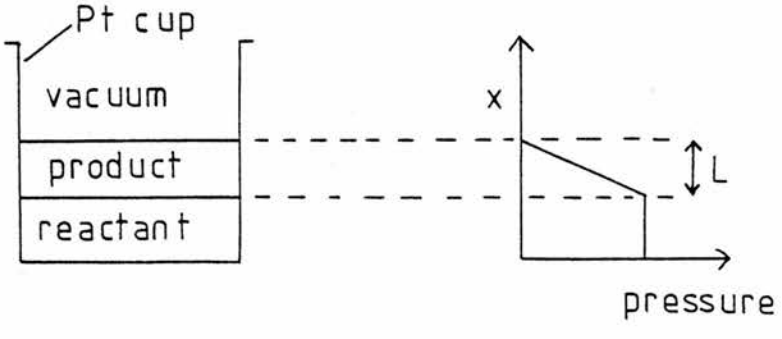

Fig. 49. The pressure variation in the sample assuming that the reactant grains decompose partially to create an equilibrium vapour pressure around themselves.

such grains with the reactant grains beneath can result in the nucleation of the latter by means of the solid-state diffusion of product ions across the grain boundaries. In this way every grain in the sample mass can very quickly become coated with a layer of product and subsequent reaction could occur by the thickening of this shell (the contracting sphere mechanism). From this point on , there is no longer any co-operative behaviour. It is , of course , possible that the reaction may be initiated by the independent nucleation of each grain ; the nucleation - by - contact mechanism is mentioned here only to suggest consistency between the behaviour of $Fe_2(SO_4)_3$ and the cases to be described.

If , instead of growing two-dimensionally , the nuclei which form on the exposed surface begin to grow three-dimensionally , the reactant grains beneath will become nucleated by the contact mechanism only when the grain above has completely decomposed. This process is represented in fig. 48 and is based on the assumption that nucleation of the reactant grains in the lower layers does not occur until contact is made with a decomposed grain. The result of this behaviour is that reaction is occurring , in effect , at a single macroscopic interface.

An SO_3 molecule leaving an intragranular interface will pass through the product layer in the grain to enter an intergranular space. To escape into the furnace the molecule must now travel through the labyrinth of spaces between the grains of product. If one assumes that the sum of the areas of the intragranular interfaces is constant during the reaction , then there will be a constant flux , J_o , of SO_3 molecules breaking away from the reactant lattice. The probability of an SO_3 molecule becoming incorporated at an intragranular interface (by reaction with oxide there) on striking it will be denoted by z.

The difficulty now in applying eq. 13 is that the path of an SO_3

molecule from the interface inside a grain to the exposed surface of the sample , as described above , is not a tube. To proceed further with this analysis , it will be assumed that an equation with the same form as eq. 13 relates the flux , J , emerging from the exterior surface of the sample , to J_o. The equation is

$$J = J_o /(1 + zCL/S)$$

where C is some constant characteristic of the texture of the product layer and S has the dimensions of intergranular spaces. Two limiting cases of this equation are : (1) $J = J_o$ when $1 \gg zCL/S$; (2) $J = J_oS/(zCL)$ when $1 \ll zCL/S$.

Case 1 implies a constant reaction flux which is unmodified by the growing product layer and is equivalent to the rate law $dw/dt = k$. This corresponds to the behaviour of $CuSO_4$ and $NiSO_4$. The inequality $1 \gg zCL/S$ means that there is no back reaction , either because no molecules are reflected back to the interface or , more realistically , because z is very small (i.e. a highly irreversible reaction).

Case 2 implies a reaction rate which is inversely proportional to the thickness , L , of the product layer. L ,however , is proportional to the weight loss , w , so that this second case is equivalent to the rate law $dw/dt = kw^{-1}$. This behaviour corresponds to the decomposition of $ZnSO_4$ and is the result of an increasing rate of back reaction. It will be recalled from the introduction that $J(P_{eq}) = J_o /z$, where $J(P_{eq})$ is the flux associated with the equilibrium pressure of SO_3 at the interface. Case 2 can now be written $J = J(P_{eq})S/(CL)$ and comparison with $dw/dt = kw^{-1}$ shows that $J(P_{eq}) \propto k$. This result has the following consequence for the temperature dependence of k. From the kinetic theory of gases[29],

$$J(P_{eq}) \propto P_{eq}/T^{\frac{1}{2}}$$

$$\therefore \log(k) = \log(J(P_{eq})) + C_1 = \log(P_{eq}) - \tfrac{1}{2}\log(T) + C_2$$

where the C's are constants. From thermodynamics[29],

$$\log(P_{eq}) = -\Delta H^{o}/(2.303RT) + C_3$$

$$\therefore \log(k) = -\Delta H^{o}/(2.303RT) - \tfrac{1}{2}\log(T) + C_4$$

The variation in $\frac{1}{2}\log(T)$ was typically 0.015 compared to a variation in log(k) of 0.6 in this work , so that the former can be ignored. The conclusion is that the temperature dependence of k should yield ΔH^{o} for the reaction , that is , $\Delta H_a = \Delta H^{o}$. In fact , ΔH_a exceeds ΔH^{o} by 5% for the decomposition of $ZnSO_4$.

(It is interesting to note that , given an equilibrium vapour pressure at the reaction interface ($P_i = P_{eq}$) , the value of ΔH_a when there is Poiseuille flow through the product layer is twice ΔH^{o}. This result is derived as follows. From eq. 15

$$J \propto P_i^{2}/L$$

$$\therefore \text{rate} = dw/dt \propto P_i^{2}/L \propto P_i^{2}/w \quad \text{and}$$

comparison with $dw/dt = kw^{-1}$ shows that $k \propto P_i^{2}$ and

$$\log(k) = \log(P_i^{2}) + C_5 = \frac{-2\Delta H^{o}}{2.303RT} + C_6 \ .$$

This highlights the importance of establishing the nature of gas transport through the product layer.)

The most unsatisfactory point in the above treatment of reaction at a macroscopic interface concerns the assumption that nucleation occurs on the exposed surface and not in the bulk of the sample. The grains in the bulk of the sample mass differ from those at the surface in two possible ways. First , the grains in the lower layers make contact with other grains in all directions. However , it is difficult to see why this slightly greater intergranular contact should suppress nucleation or decomposition. Second , the bulk grains may decompose partially to create a local pressure of SO_3 which will suppress further net decomposition if it does not leak away quickly. From the free

volume data (table 4) it can be calculated that less than 10^{-3} % of the sample mass need decompose to establish an equilibrium pressure , assuming no leakage. If the reaction is near equilibrium in the reactant layer , it would certainly explain the absence of significant decomposition there because SO_3 will then be lost mainly from its uppermost part. However , this implies a pressure profile of the kind shown in fig. 49 , with J given by $J(P_{eq})CS/L$; a constant flux is not possible.

It was decided to test the hypothesis of nucleation by contact and this was done by intimately mixing samples of $CuSO_4$ and $NiSO_4$ with their respective oxides (5%). The resulting samples decomposed at rates not significantly different from the uncontaminated salts and visual examination showed that the product in the reactant layer did not initiate reaction there. This would seem to outrule the kind of solid-state interaction suggested above.

It would seem then , that intergranular interaction cannot be explained by a solid-state mechanism nor by a local pressure of product gas. Other even more speculative theories were explored ; for example , the possibility that the diminishing rate is the consequence of self-cooling , the possibility that rate is controlled by the desorption of product gas from the exterior surface of the sample , etc.. All were more inconsistent with the data than the mechanism given above.

CONCLUSION

It is possible to obtain well-defined rate data for the decomposition of packed and aggregated powders. The decomposition may occur independently for each grain or the mass of powder may behave like a continuous porous solid and decompose at a single macroscopic interface. This latter behaviour implies intergranular interaction via the gas phase or by solid-state processes (eg. diffusion, heat conduction) at the areas of contact. However , no completely satisfactory rationalisation of the data could be made on the basis of these ideas. The outstanding problem is that of coupling fluxes of heat and matter in a system of complicated and changing geometry.

Despite failing to account for co-operative behaviour , the author feels that the rate data and its correlation with reaction morphology are an interesting contribution to the body of facts on the reactivity of powders.

PHASE DIAGRAMS : THEORY AND PRACTICE

INTRODUCTION

The following brief account of solid-state phase diagrams is in two sections. The first deals with the thermodynamic relations which dictate the shape of a diagram and the second describes the techniques most frequently used in phase diagram determination.

The principal applications of solid-state phase diagrams are in understanding and manipulating the properties of materials , and detailed accounts of their technological uses are given in a series of monographs edited by Alper[67] and a recent publication from the Chemical Society[68]. In materials development , however , phase diagrams are only a starting point. Of equal importance is the exploitation of the kinetics of phase changes to produce metastable states and particular microstructures[69,70]. Although outside the subject of equilibrium thermodynamics , kinetic effects dictate which technique is most suitable for studying a particular system.

THE THERMODYNAMIC BASIS OF PHASE DIAGRAMS

This section aims to provide a brief account of the relationship between thermochemistry and phase diagrams with particular reference to recent work in this field. First , the thermodynamic equations underlying isobaric unary and binary diagrams will be derived , then their use in constructing phase diagrams from thermochemical data will be described. The notation used is that prescribed by McGlashan[71,72] and is explained in appendix 1.

Thermodynamic equations underlying phase diagrams

For a closed system at constant temperature and pressure , the equilibrium state corresponds to a minimum in the free energy G. For a unary (single component) system which undergoes the following sequence of changes on heating

$$A_\alpha \longrightarrow A_\beta \longrightarrow A_l \quad (\alpha, \beta = \text{polymorphs} ; l = \text{liquid}),$$

the transition temperatures can be shown to be a consequence of the temperature dependences of the free energies of the α , β and l phases. In fig. 50(a) the stable phase at any temperature T is that for which $\Delta^{\phi}_{\alpha}G^{*}_{A}(T)$ is most negative , where $\phi = \alpha$, β or l . When $\Delta^{\phi}_{\varepsilon}G^{*}_{A}(T) = 0$, phases ε and ϕ are in equilibrium and $T = T^{\varepsilon+\phi}$, the $\varepsilon \rightarrow \phi$ transition temperature. The choice of ${}^{\alpha}G^{*}_{A}(T)$ as the zero line in fig. 50(a) was arbitrary ; any phase could have been used as the reference state. There will be a discontinuity in the enthalpy (and entropy) at the $\alpha \rightarrow \beta$ transition point given by

$$\Delta^{\beta}_{\alpha}H^{*}_{A}(T^{\alpha+\beta}) = -T^{\alpha+\beta}\left(d\Delta^{\beta}_{\alpha}G^{*}_{A}(T)/dT\right)_{T^{\alpha+\beta}}$$

as shown in fig. 50(b). The extension of $\Delta^{\alpha}_{\alpha}G^{*}_{A}(T)$ beyond $T^{\alpha+\beta}$ represents the superheating of phase α . Similarly , the extension of $\Delta^{\beta}_{\alpha}G^{*}_{A}(T)$ below $T^{\alpha+\beta}$ represents the supercooling of phase β .

To complete this analysis , the calculation of the differences

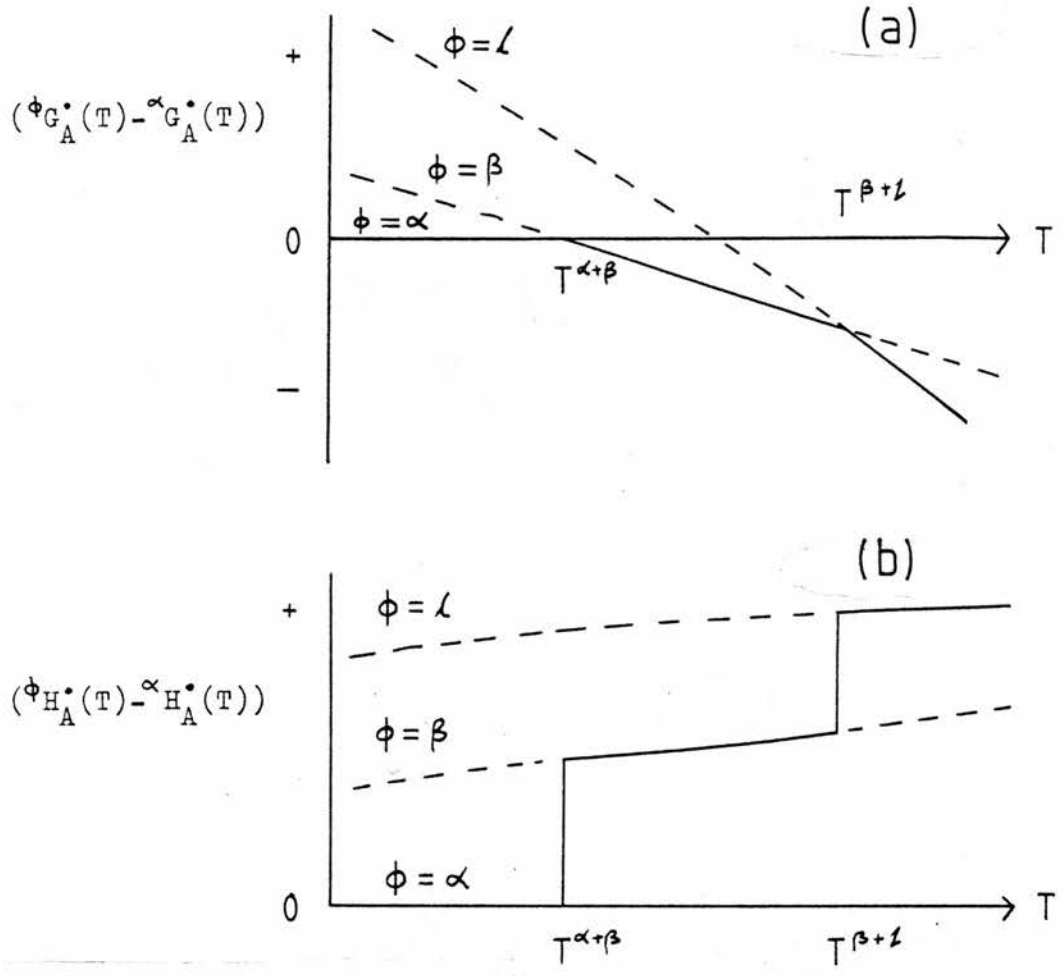

Fig. 50. (a) the equilibrium form of A at any T is that with the lowest free energy; (b) at the phase transition temperatures the enthalpy changes discontinuously.

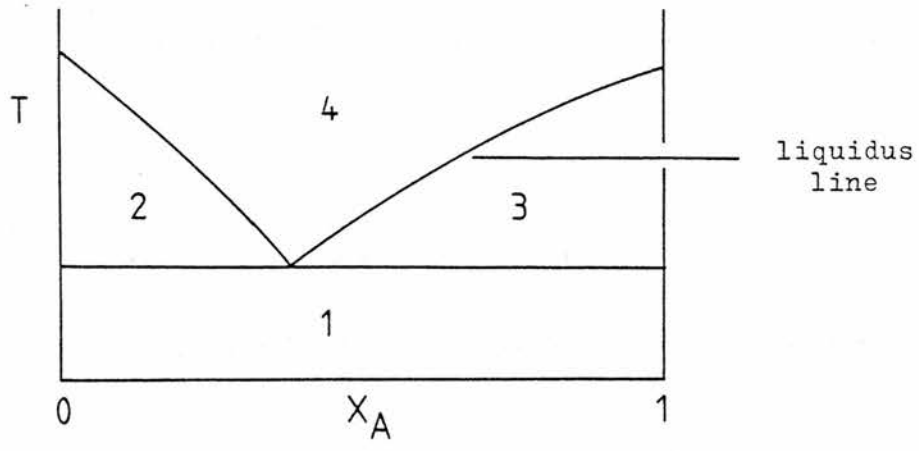

Fig. 51. A eutectic system B-A. 1= solid A + solid B
2= solid B + liquid , 3= solid A + liquid , 4= liquid.

$\Delta^{\phi}_{\varepsilon}G^{*}_{A}(T)$ will be described , where ε and ϕ can coexist at $T^{\varepsilon+\phi}$.
The appropriate equation is

$$\Delta^{\phi}_{\varepsilon}G^{*}_{A}(T) = \Delta^{\phi}_{\varepsilon}H^{*}_{A}(T) - T\Delta^{\phi}_{\varepsilon}S^{*}_{A}(T)$$

and the enthalpy and entropy differences can be calculated from the following data : ${}^{\varepsilon}C^{*}_{p,A}(T)$, ${}^{\phi}C^{*}_{p,A}(T)$, $\Delta^{\phi}_{\varepsilon}H^{*}_{A}(T^{\varepsilon+\phi})$ and $T^{\varepsilon+\phi}$; all of which can be measured by calorimetry[73]. Applying Hess's law gives the following equation

$$\Delta^{\phi}_{\varepsilon}G^{*}_{A}(T) = \left\{\Delta^{\phi}_{\varepsilon}H^{*}_{A}(T^{\varepsilon+\phi}) + \int_{T^{\varepsilon+\phi}}^{T}\Delta^{\phi}_{\varepsilon}C^{*}_{p,A}(T)dT \right.$$
$$\left. -T\left(\Delta^{\phi}_{\varepsilon}H^{*}_{A}(T^{\varepsilon+\phi})/T^{\varepsilon+\phi} + \int_{T^{\varepsilon+\phi}}^{T}(\Delta^{\phi}_{\varepsilon}C^{*}_{p,A}(T)/T)dT\right)\right\} \qquad (20)$$

The simplest binary phase diagram is that illustrated in fig. 51 , which involves a liquid and two completely immiscible solids A and B. The molar free energy of the liquid phase is given by

$${}^{l}G_{m}(T,X) = X\,{}^{l}G^{*}_{A}(T) + (1-X)\,{}^{l}G^{*}_{B}(T) + \Delta_{mix}{}^{l}G^{ideal}_{m}(T,X) + {}^{l}G^{E}_{m}(T,X) \qquad (21)$$

where X is the mole fraction of component A , $\Delta_{mix}{}^{l}G^{ideal}_{m}$ is the ideal molar free energy of mixing and ${}^{l}G^{E}_{m}$ is the molar excess free energy of the solution. For atomic components

$$\Delta_{mix}{}^{l}G^{ideal}_{m}(T,X) = RT(X\ln X + (1-X)\ln(1-X))$$

but for salts the dissociation into ions must be taken into account[74]. The chemical potentials of atomic components A and B in the liquid phase are

$$^{l}G_A(T,X) = {}^{l}G_A^*(T) + RT\ln({}^{l}a_A(T,X))$$

$$^{l}G_B(T,X) = {}^{l}G_B^*(T) + RT\ln({}^{l}a_B(T,X))$$

where $^{l}a_A = X\,{}^{l}\gamma_A(T,X)$ and $^{l}a_B = (1-X)\,{}^{l}\gamma_B(T,X)$. The molar excess free energy is related to the activity coefficients by

$$^{l}G_m^E(T,X) = RT(X\ln({}^{l}\gamma_A(T,X)) + (1-X)\ln({}^{l}\gamma_B(T,X)))$$

Identical equations to the above , with superscripts l replaced by s , apply to a solid solution.

In fig. 51 the intersection of an isotherm T with the right hand liquidus line gives the composition (mole fraction of A) of the liquid which is in equilibrium with pure solid A in the right hand two-phase region. If this composition is C_l , then

$$^{l}G_A(T,C_l) = {}^{s}G_A^*(T)$$

$$\therefore\ \Delta_s^{l}G_A^*(T) + RT\ln(C_l\,{}^{l}\gamma_A(T,C_l)) = 0 \qquad (22)$$

When there is complete miscibility of solids A and B , the phase diagram may look like fig. 52(a). Here the intersections of an isotherm T with the liquidus and solidus lines give the compositions of the liquid and solid solution in equilibrium in the two-phase region. If these compositions are C_l and C_s , then

$$^{l}G_A(T,C_l) = {}^{s}G_A(T,C_s)$$

$$^{l}G_B(T,C_l) = {}^{s}G_B(T,C_s)$$

It follows that

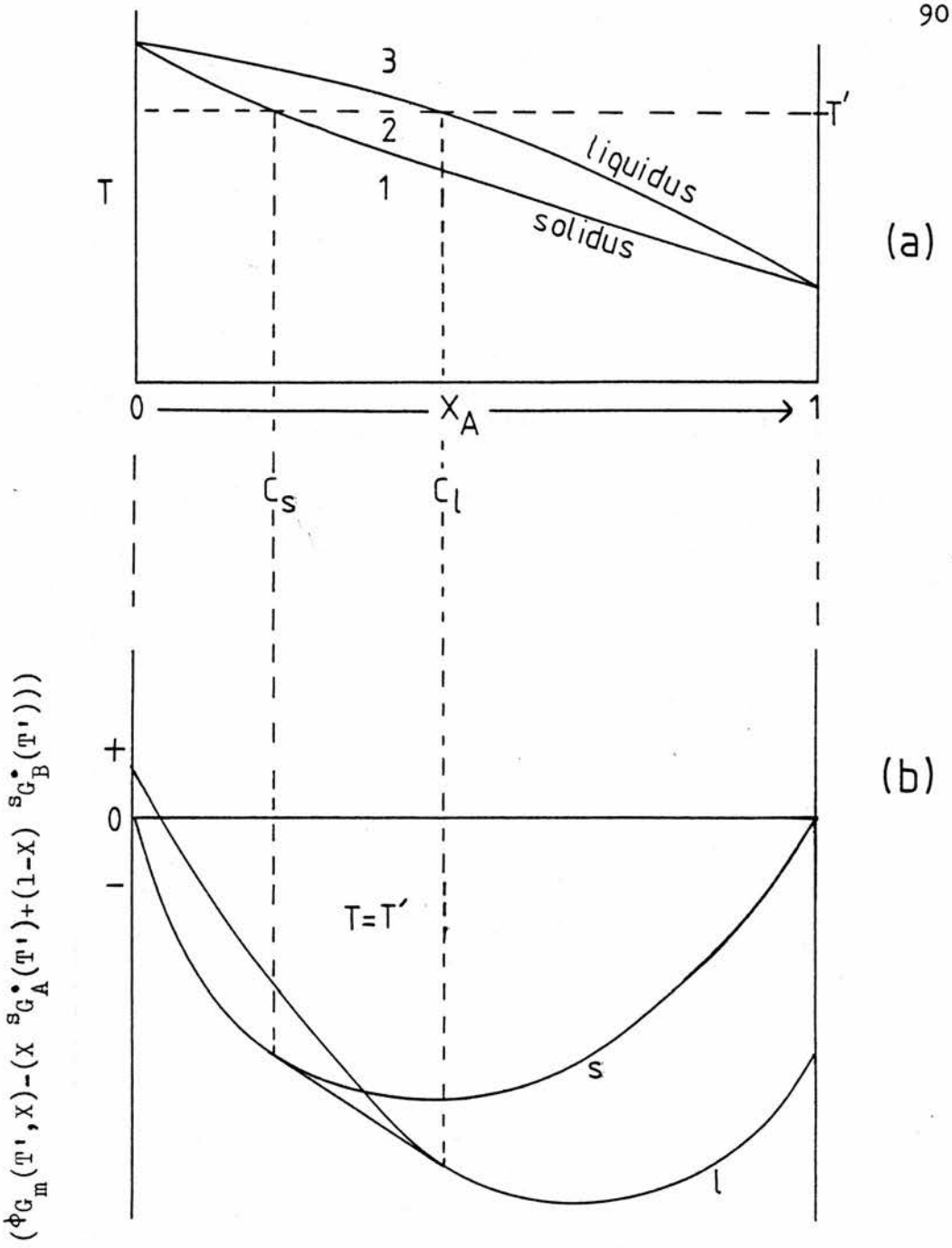

Fig. 52. (a) phase diagram for the system B-A. 1 = solid solution , 2 = solid solution + liquid , 3 = liquid.
(b) free energy of solid solution (s) and liquid (l) as functions of X along isotherm T'. From X = C_s to C_l , the coexistence of s and l gives the minimum free energy.

$$\Delta^{l}_{s}G^{*}_{A}(T) + RT(\ln(C_{l}\,{}^{l}\gamma_{A}(T,C_{l})) - \ln(C_{s}\,{}^{s}\gamma_{A}(T,C_{s}))) = 0 \qquad (23)$$

$$\Delta^{l}_{s}G^{*}_{B}(T) + RT(\ln((1-C_{l})\,{}^{l}\gamma_{B}(T,C_{l})) - \ln((1-C_{s})\,{}^{s}\gamma_{B}(T,C_{s}))) = 0 \qquad (24)$$

Eqs. 23 and 24 apply equally to the case of partially miscible solids in equilibrium with liquid.

The relationship between the phase diagram in fig. 52(a) and the integral free energies of the solution phases is illustrated in fig. 52(b) for the isotherm T'. At each composition X on the isotherm , the equilibrium phase or combination of phases is that for which the free energy of the system is a minimum. The free energy of a two-phase region is represented by the common tangent to the free energy curves of the two phases.

To calculate the curves in fig. 52(b) the excess free energies of the solid solution and liquid must be available as analytical functions. In the regions in which the system exists as a solid solution or liquid,these functions can be calculated via the activity coefficients which are obtainable from e.m.f. and vapour pressure measurements[75]. Extrapolation of the excess functions to wider ranges of T and X depends on the degree of non-ideality of the solutions. In the regular solution approximation , for example , $S^{E}_{m} = 0$ and $H^{E}_{m} = X(1-X)q_{o}$, where q_{o} is a temperature-independent constant[6]. In the subregular approximation , $S^{E}_{m} = 0$ and $H^{E}_{m} = X(1-X)(q_{o} + q_{1}X)$[76]. The quasi-chemical description of solutions gives G^{E}_{m} as a power series in $X(X-1)/T$ [6]. More will be said further on about the mathematical representation of excess functions.

The computer calculation of phase diagrams

It is possible to obtain an approximation of a phase diagram if the following data are available : (1) $\Delta^{\phi}_{\alpha}G^{*}_{i}(T)$ for all phases ϕ of each component i ; (11) ${}^{\phi}G^{E}_{m}(T,X)$ for all possible solution

phases ϕ . The sources of these data were mentioned above.

One approach to calculating the phase diagram involves computing the integral free energy of each phase or combination of phases at each coordinate in the diagram and noting which gives a minimum value there. The phase boundaries become apparent to the eye when the results are plotted by assigning a symbol (eg. 1 for liquid , a for solid + liquid) to each of the suitably spaced coordinates (X,T).

The other approach consists in finding the values of composition of the solution phases in equilibrium at each value of T by solving equations like 22-24. Both techniques involve enormous amounts of arithmetic and a digital computer must be used. Although the possibility of such calculations has been known since 1908 [77] , it is only with the availability of computers that complicated equilibria have been approached by these techniques. Indeed , the recent interest shown in this field , almost exclusively by metallurgists , has led to the appearance of a new journal , 'CALPHAD' [78] , devoted to the calculation of phase diagrams.

Two studies are worth mentioning as they typify this kind of research.

Kaufman and Bernstein[79,80] have calculated the phase diagrams for all the binary systems formed among the refractory metals (W , Mo , Hf , Ta , etc.) by solving equations of type 22-24. The principal difficulties encountered in this work were in deciding what were the possible solid solution phases and in obtaining the required thermochemical data. The most common structures of pure metals and alloys are cubic-closest packed (ccp) , hexagonal-closest packed (hcp) , body-centred cubic (bcc) and face-centred cubic (fcc). While a metal may be stable as bcc at 1 atm up to its melting point ,

it may exist as ccp at higher pressures and may form ccp solid solutions with another metal at 1 atm. $\Delta^{ccp}_{bcc}G^{*}_{A}(T)$ must then be obtained from high pressure studies or it can be estimated by using equations 22-24 in conjunction with a phase diagram in which component A forms a ccp solid solution with some other component. To a first approximation activity coefficients can be taken as unity. The thermodynamic functions for the solution phases among the refractory metals have not been determined experimentally and semi-empirical methods had to be used to calculate regular solution interaction parameters. While there are disparities of several hundreds of kelvins between computed phase diagrams and the few which have been determined experimentally , the former contain the essential features of the latter in almost every case. In view of the complexity of the problems to be overcome , this work by Kaufman and Bernstein is a very impressive manipulation of thermodynamic data.

The computation of phase diagrams for inorganic systems[81-83] has advanced along similar lines but has of necessity been limited to the few systems for which the required thermochemical data is available. The study by Lin et al. of the binary and ternary systems formed among LiCl , NaCl , KCl , $MgCl_2$, $CaCl_2$ and $SrCl_2$ [84] deserves mention. The objectives of this work were : (1) to obtain in mathematical form the thermodynamic excess functions for all the binary solution phases by a critical analysis of the measured binary phase diagrams and the published binary thermodynamic data ; (11) to apply interpolation procedures to estimate the thermodynamic properties of the 20 ternary systems for use in calculating the ternary phase diagrams.

As an example , consider the application of eqs. 23-24 to the calculation of the activity coefficients of NaCl and KCl in a solid solution. The component activities in the liquid solution ,

determined by e.m.f. measurements , were fitted to suitable analytical equations ; $\Delta^{\gamma}_{s}G^{*}_{NaCl}(T)$ and $\Delta^{\gamma}_{s}G^{*}_{KCl}(T)$ were obtained from calorimetric data using eq. 20 ; the compositions of the liquid and solid solutions coexisting at any T in the two-phase region were taken from the binary phase diagram ; all these data are substituted into eqs. 23-24 which can then be solved at each T to give the component activities in the solid solution. Mathematical analysis is performed on the results to represent the excess functions as analytical equations in T and X. It has been argued by Bale and Pelton[85] that Legendre polynomials are often superior to power series for such representations and are much more amenable to computer storage and manipulation. The validity of the derived analytical equations is checked by using them to regenerate the binary diagram.

Armed with thermodynamic data in analytical form for the three binary systems of a ternary system , the excess functions of the latter are then estimated using equations derived by Toop[86] and Kohler[87] , assuming the ternary solutions to be regular. Isothermal sections of the ternary phase diagram were then calculated by minimising the integral free energy at each composition coordinate. The good agreement with the 8 experimentally determined diagrams justifies confidence in the other 12 computer predictions.

Such studies are one stage removed from experimental determinations and , with a few exceptions , should be regarded as a last resort for situations in which time or money is limiting. However , such situations often arise in the development of new materials and to facilitate the application of these methods as research aids , various workers have made available their programmes[68].

EXPERIMENTAL TECHNIQUES FOR DETERMINING PHASE DIAGRAMS[88,89]

Techniques for mapping phase diagrams for solid-state systems fall into two categories. The first comprises those methods which detect the evolution or absorption of heat which accompanies the appearance of a new phase and such methods will be loosely described as 'calorimetric'. The second category consists of techniques which identify the phases present in the system at equilibrium at each point in the phase diagram and will be called 'direct' methods. Before describing these , however , a few words must be said about the kinetics of phase changes.

For solid-state systems kinetic effects can prove to be a major obstacle in the determination of the equilibrium phase diagram. Some liquid solutions do not crystallise readily when cooled but form glasses[90]. This behaviour in silicate melts forms the basis of glass technology and occurs in many other systems. For example , Tl_2SO_4 forms liquids with $NiSO_4$, $ZnSO_4$ or $CuSO_4$ which give glasses when cooled at rates as low as a few kelvins per minute[91]. At the other extreme some liquid alloys require cooling rates of 10^6 K s^{-1} to avoid crystallisation[69].

The kinetics of phase transformations are comparable to those discussed in part one for decomposition reactions[92,93]. Solidification of a liquid , for example , is initiated by the appearance of nuclei of the solid phase either in the bulk of the liquid (homogeneous nucleation) or at its area of contact with its container or dissolved solid impurities (heterogeneous nucleation). Subsequent growth of these nuclei is an interfacial process in which heat transfer effects are crucially important , accounting for such phenomena as dendritic (branched) crystal growth. Similar processes occur in polymorphic transitions and in the decomposition of a

single solid solution to two solid solutions , though this latter process is complicated by diffusion of matter.

Calorimetric Methods

As mentioned in the introduction , melting and transitions between polymorphs are characterised by a discontinuity in enthalpy , and the heat absorption or evolution at the transition temperature provides an indication of the appearance of the new phase. Although calorimetry has already been referred to as a source of data for the computer calculation of phase diagrams , the direct determination of binary and higher phase diagrams by calorimetry has no advantages over the much simpler technique of differential thermal analysis (DTA).

The principles of DTA were described in part one and the technique has been the subject of many reviews[46,47]. DTA is recognised as a standard method for the determination of phase diagrams and this application has been reviewed by Gutt and Majumandar[94]. The way in which a temperature-composition phase diagram is derived from DTA curves is illustrated in fig. 53. Curve 1 has peaks corresponding to the changes $A_\gamma \longrightarrow A_\beta \longrightarrow A_\alpha$ which occur on cooling along isopleth 1. In curve 2 the single peak arises from the solidification of liquid to give the intermediate compound C. The single peak in curve 4 is due to the complete conversion of liquid of eutectic composition to solid C + a solid solution of C in B at the eutectic temperature. These processes are characterised by well-defined peaks on cooling or heating.

The interpretation of curves 3 and 5 is a little more complicated. When the liquid at 3 is cooled below the liquidus temperature , solid C gradually begins to crystallise out. The associated rate of heat evolution is small and the change in ΔT corresponding to the liquidus line arises mainly from the change in the steady-state

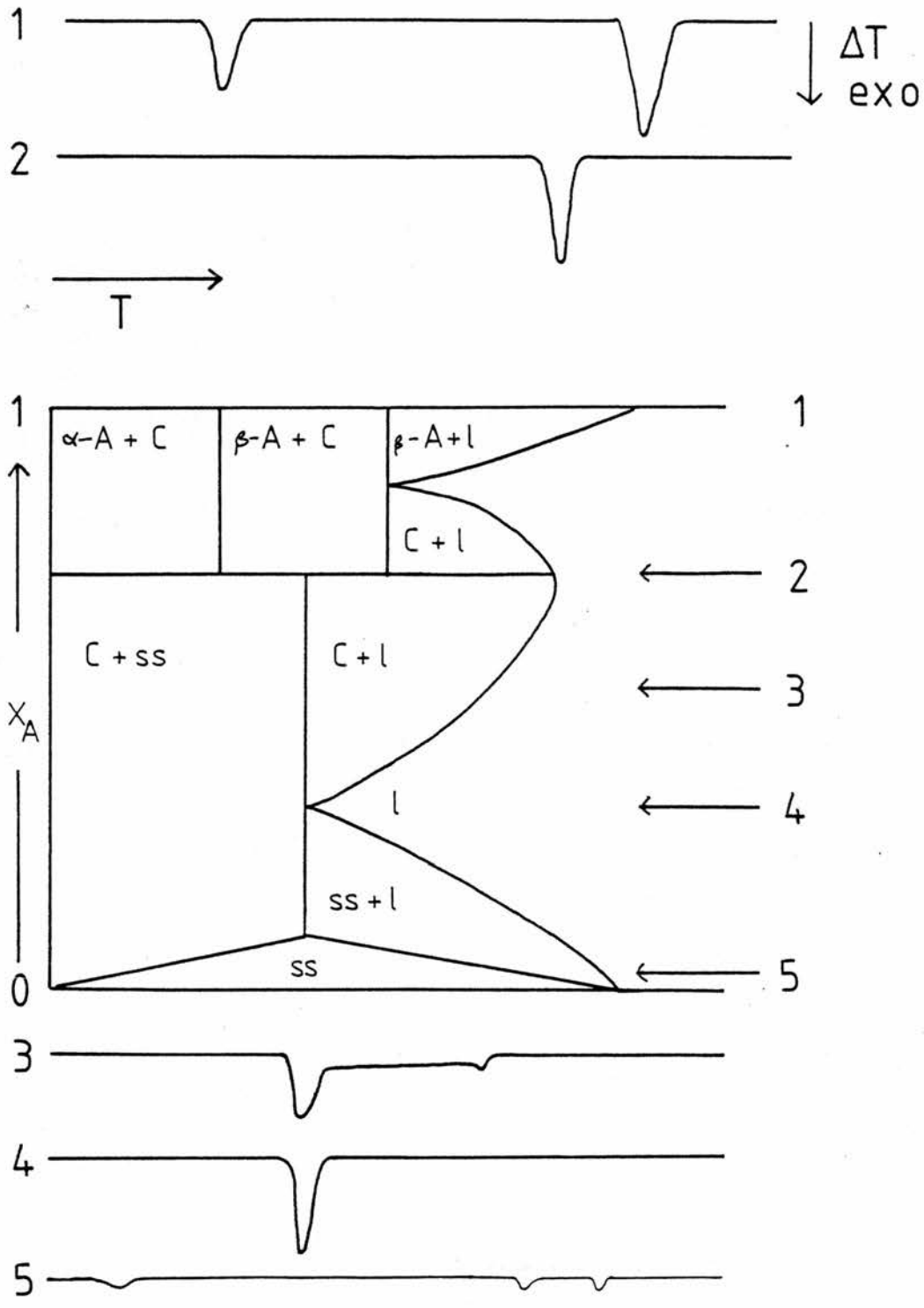

Fig. 53. DTA graphs expected on cooling various compositions of liquid in the system A-B. ss is a solid solution of compound C in B.

heat flow conditions. When the eutectic temperature is reached , the remaining liquid has the eutectic composition and undergoes a sudden solidification. The interpretation of curve 5 is similar but here a solid solution of C in B gradually crystallises out until no liquid remains. The solid solution cools to a point at which pure C begins to precipitate out gradually.

DTA is carried out at heating/cooling rates of between 5 and 10 K min^{-1} , and the results are markedly influenced by the kinetics of the processes being studied. The temperature at which a transition is detected on heating generally exceeds that at which the reverse process occurs on cooling , although many melting points are precisely reversible. The origins of this hysteresis are the superheating and supercooling required to drive the process at a measurable rate[93]. Some degree of supercooling on lowering the temperature of liquid to below the liquidus temperature can give rise to a sudden burst of crystallisation which is very clearly detectable by DTA. In some cases there is no detectable heat effect on crossing the liquidus line on heating , particularly if the heating rate is low.

The choice of the feature of a DTA curve used to locate a transformation temperature is a disputed point[94]. The onset of the phase change is not easily recognised and the general practice is to record the sample temperature at the peak in ΔT. Although this latter need not correspond to any particular stage of the process , it is more reproducible than any other feature. While a plateau in sample temperature is a necessary criterion of reversibility at the transition point , it is recognised that the heating and cooling peak temperatures set the limits within which the transition is reversible.

It is implicit in phase diagrams that the pressure during determination was 1 atm. Several designs of apparatus are described in the literature for DTA studies at pressures up to 5×10^4 atm [95,96]. In this way , P-T diagrams have been obtained for many unary systems[94,97]. Such data are used , for example , in high pressure synthesis of new materials[98] , studies of lattice stability[79] and analysis of processes occurring in the earth's core[99].

No mention has been made of the use of DTA for calorimetric determinations of enthalpies of transition but the attractiveness of such an application has led to the development of specialised instruments called 'differential scanning calorimeters'. Differential scanning calorimetry (DSC) is making an increasing contribution to thermochemistry and is the subject of a recent review[100].

Direct Methods

(a) Hot-stage microscopy.[70,101-104]

This technique permits the direct visual examination , with transmitted or reflected light , of a small specimen contained in a little resistance furnace. A cooling jacket round this furnace prevents the conduction of heat to the body of the microscope , which focuses on the sample from a distance of up to 10 cm. Instruments capable of operation up to 1700 ^{o}C are available. In phase studies it is possible to observe the formation of liquid at the solidus temperature , the formation of crystals at the liquidus temperature , and even the change in crystal structure during a polymorphic transition.

Examination in crossed polars can be particularly informative as it can distinguish isotropic and anisotropic substances[105]. The former class , comprising liquids , glasses and crystals of the cubic system , appear dark in all orientations when examined with crossed

polars. Anisotropic substances , which include crystals of the non-cubic systems , exhibit a maximum brightness each 90° of revolution. In this way , for example , anisotropic crystals in a liquid or in a glass matrix stand out as bright specks against a dark background.

(b) High temperature X-ray diffraction[106,107].

This technique can record the powder diffraction pattern of a sample held at a high temperature and so permits the identification of high temperature forms of solids. For unquenchable polymorphs this technique provides the only means of recording structural data.

(c) Quenching[108].

An attractive alternative to the application of techniques (a) and (b) is to cool the hot sample so rapidly that it cannot rearrange to the low temperature state. The high temperature structures and phases are said to be 'frozen-in' or 'quenched' and are amenable to study by room temperature microscopy and X-ray diffraction. High temperature polymorphs may be obtained virtually uncontaminated by the low temperature form but many polymorphs reconvert rapidly at room temperature and can only be studied at high temperatures.

A sample quenched from a region in which solid and liquid coexist at equilibrium will , ideally , give crystals in a glass matrix. One technique for locating a liquidus line involves holding a particular composition at a particular temperature for a sufficient time for equilibrium to be established , following which the sample is quenched. Experiments at various temperatures for a particular composition should reveal a temperature above which microscopy detects no crystals in the resulting glass. This indicates that the liquidus line has been crossed. Other variations of this method for locating liquidus lines are described in the literature[107].

The quenching technique used is dictated by the system being studied. For sluggish transitions and liquids which readily vitrify , the sample can simply be dropped into a liquid. For water soluble materials an organic liquid may be used and removed under vacuum. Small samples have a lower heat capacity and cool more quickly. At the same time , however , the high surface area to volume ratio can result in unpredictable crystallisation due to heterogeneous nucleation at the surface of the sample. A variation of this method consists in packaging the sample in a Pt envelope which is dropped into Hg liquid.

Heat transfer with these quenching methods tends to occur through a layer of vaporised liquid. This intermediate layer is eliminated by the technique called 'splat-cooling'. The hot sample is dropped onto a large , smooth Cu or brass block and another block is immediately placed on top. Heat transfer to the blocks is very rapid , particularly from liquids. A version of this technique for viscous (unpourable) liquids has been designed by the author and is described further on. Other methods are used for more extreme quenching rates , some involving a sudden blast of cold gas.

Two less frequently used direct methods of limited applicability are worth mentioning. For subsolidus equilibria , phase boundaries can be identified by noting any discontinuities in plots of electrical conductivity against temperature[89]. The dimensional changes which accompany a polymorphic transition in a single crystal and glass transitions can be detected and quantified by dilatometry[89].

Complications

To conclude this section on experimental methods , something must be said about the complication of chemical decomposition[94]. The use of the DTA apparatus illustrated in fig. 15 , in which the

sample cup is open to a flowing inert atmosphere , is limited to those systems which do not decompose or evaporate. Decomposition accounts , for example , for the limited temperature range in which many sulphate systems have to be studied[107]; solidus temperatures for almost all of the systems formed among the transition metal sulphates have never been determined.

This complication can be obviated by encapsulating the sample in a sealed Pt or silica tube to create a closed system. This method has been used by Rowe et al. to obtain the phase diagram for the system K_2SO_4- $MgSO_4$ [109].

Alternatively , for non-volatile decomposable substances , the stable temperature range can be extended by up to 300 K by the presence of an atmosphere of the product gas. This is the method used in this work to study a polymorphic transition in $ZnSO_4$ and the system Ag_2SO_4- $BeSO_4$.

(The thermodynamic basis of this effect suggested to Dewing and Richardson[110] a method for determining the vapour pressures of decomposable sulphates by DTA. The method involves noting the temperature at which the sample begins to decompose on heating in a flowing atmosphere of SO_2 , O_2 and N_2 , the composition of which (corrected for SO_3 formation) sets the value of $K_p = P_{SO_2} P_{O_2}^{\frac{1}{2}}$. The decomposition temperature should be related to K_p by the equation $\Delta G^o(T) = -RT\ln K_p$ where $\Delta G^o(T)$ is the standard change in the Gibbs function for the reaction $MSO_4 \rightarrow MO + SO_2 + \frac{1}{2}O_2$. The onset of the reverse reaction on cooling the oxide should occur at the decomposition temperature and this provides the criterion of reversibility. While reversibility was not fully investigated by Dewing and Richardson , their study of the reaction $MgSO_4 \longrightarrow MgO + SO_2 + \frac{1}{2}O_2$ was repeated by the author and the following

observation was made. For a fixed value of K_p , the onset of decomposition exceeds the onset temperature of recombination by up to 25 K. The consequence was that two distinct equations for $\Delta G^{\circ}(T)$ were obtained from the heating and cooling results respectively. A reliable determination of $\Delta G^{\circ}(T)$ has recently been made for this reaction[111] and the function lies between the limits set by the DTA results. This suggests that DTA can set the limits within which a reaction is reversible but is incapable of giving accurate thermodynamic data. This verdict confirms the work of Gal et al. on various carbonate decomposition reactions[112].

This aspect of DTA is not considered further in part two but a typical DTA graph and the vapour pressure results for the equilibrium $MgSO_4 \rightleftharpoons MgO + SO_3$ are given in appendix 2.)

ORIGINAL PHASE STUDIES

OF

SULPHATE SYSTEMS

APPARATUS FOR DTA STUDIES

The elements of a system for differential thermal analysis in a flowing atmosphere of SO_2 , O_2 and N_2 are the following : (1) apparatus for controlling the flowrates of the three gases ; (2) a differential thermocouple and some arrangement for holding the sample and a reference material ; (3) a means of measuring T and ΔT ; (4) a furnace which can be heated or cooled at constant rates (usually 5 K min^{-1}). These parts will now be described.

Gas flow apparatus

British Oxygen Company research grade SO_2 , O_2 and N_2 were used. The system to be described is capable of mixing the three gases , each having a flowrate in the range 10^{-1}-10^{2} ml min^{-1}. Before reaching the confluence point , each of the three gases passes through five devices.

The first is a pressure regulator which reduces the very high cylinder pressure to a manageable value ($\sim$1.5 atm). For SO_2 a special regulator with a stainless steel diaphragm is necessary and teflon tubing is preferable for those sections of the flow system in which there is a high pressure of this gas. The second unit is a tube of activated molecular sieve which serves to dry the gas. This precaution avoids any reactions involving water vapour at high temperatures. The third device is a flow regulator. Commercial needle valve and home-made capillary types were used. The fourth device is a 100 mm length of 1 mm internal diameter capillary tube. The purpose of this is to ensure a high linear velocity of flow which will prevent any SO_2 diffusing downstream into the O_2 or N_2 pressure regulators where it may cause corrosion. The fifth part is a two-way tap which can redirect the flow to a soap-film flowmeter. Such meters have long been used by chromatographers and are readily made from the graduated tube of a burette.

The reaction $SO_2 + \frac{1}{2}O_2 \rightarrow SO_3$ was catalysed in the vicinity of the sample by a 10 cm^2 strip of Pt foil. The equilibrium pressures of SO_2 , O_2 and SO_3 were calculated from the composition of the uncatalysed mixture by assuming a constant pressure reaction and using the following equation[58] for the temperature dependence of

$$K_p = P_{SO_2} P_{O_2}^{\frac{1}{2}} / P_{SO_3}$$

$$\log(K_p/atm^{\frac{1}{2}}) = 8.8557 - 5465.5\ K/T - 1.2157 \log(T/K)$$

Temperature measurement and differential thermocouples

The circuit used in this work for measuring sample temperature and ΔT is shown in fig. 54 , where metal A = Pt13%Rh , B = Pt and C = steel. With wires B joined at the cold junction , the voltages between the C wires are

$$V_1 = V(T_1) - V(T_c)$$
$$V_2 = V(T_2) - V(T_c)$$
$$\Delta V = V_1 - V_2$$

where the V(T) are given in thermocouple tables. T_1 and $\Delta T = T_1 - T_2$ are then calculated from the measured values of V_1 , ΔV and the cold junction temperature T_c. V_1 and ΔV were fed alternately each 5 s by manual operation of the switching box to a high input resistance digital voltmeter , which has a resolution of 1 μV ($\equiv$ 0.08 K).

The three differential thermocouple arrangements used in this work are shown in fig. 55. Of these , (a) is the apparatus used by Dewing and Richardson in their study of the decomposition of $MgSO_4$ in SO_3 atmospheres. The sample is pasted onto one junction of the thermocouple and the other is left exposed and placed close to the first. The actual sample mass required is only a few mg and the time for complete decomposition is less than with the conventional arrangement. For the same reason , however , the extent of self-cooling is less and well-defined peaks can only be obtained at higher heating

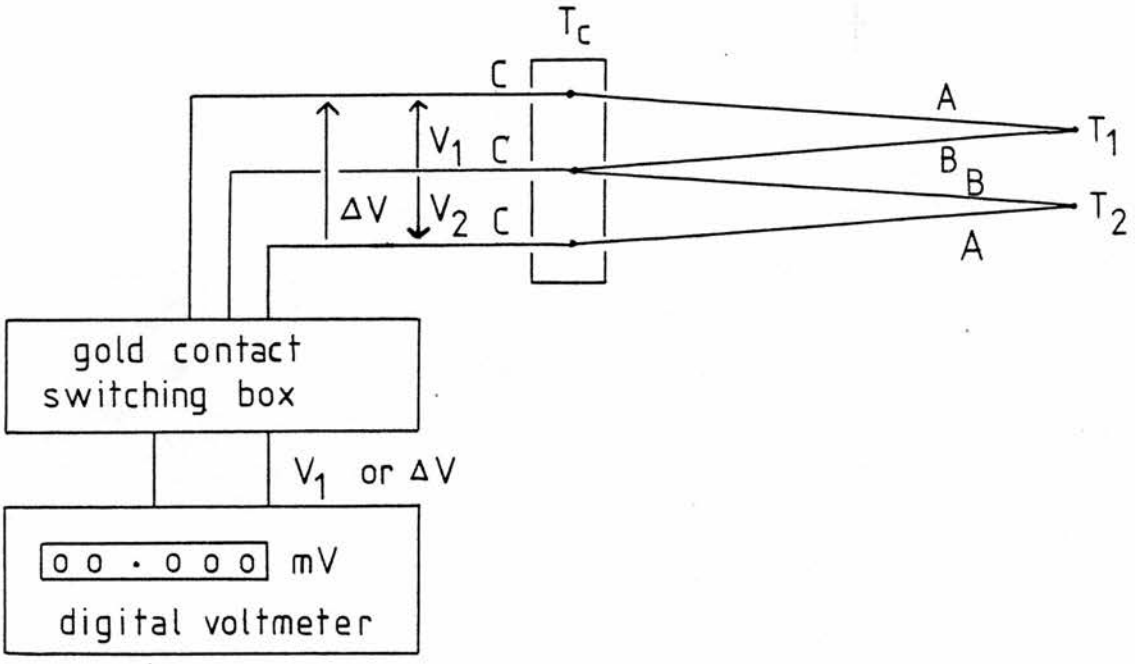

Fig. 54. Temperature measurement circuit for DTA. T_1 is the sample temperature and T_2 that of the reference substance. T_c is the cold junction temperature. A = Pt13%Rh , B = Pt , C = steel.

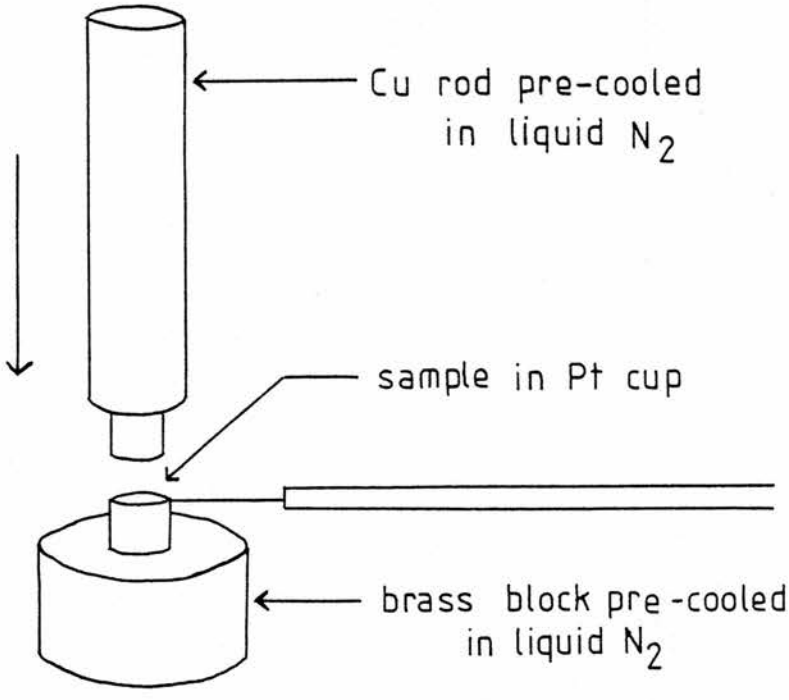

Fig. 56. Apparatus for splat-cooling viscous (unpourable) liquids.

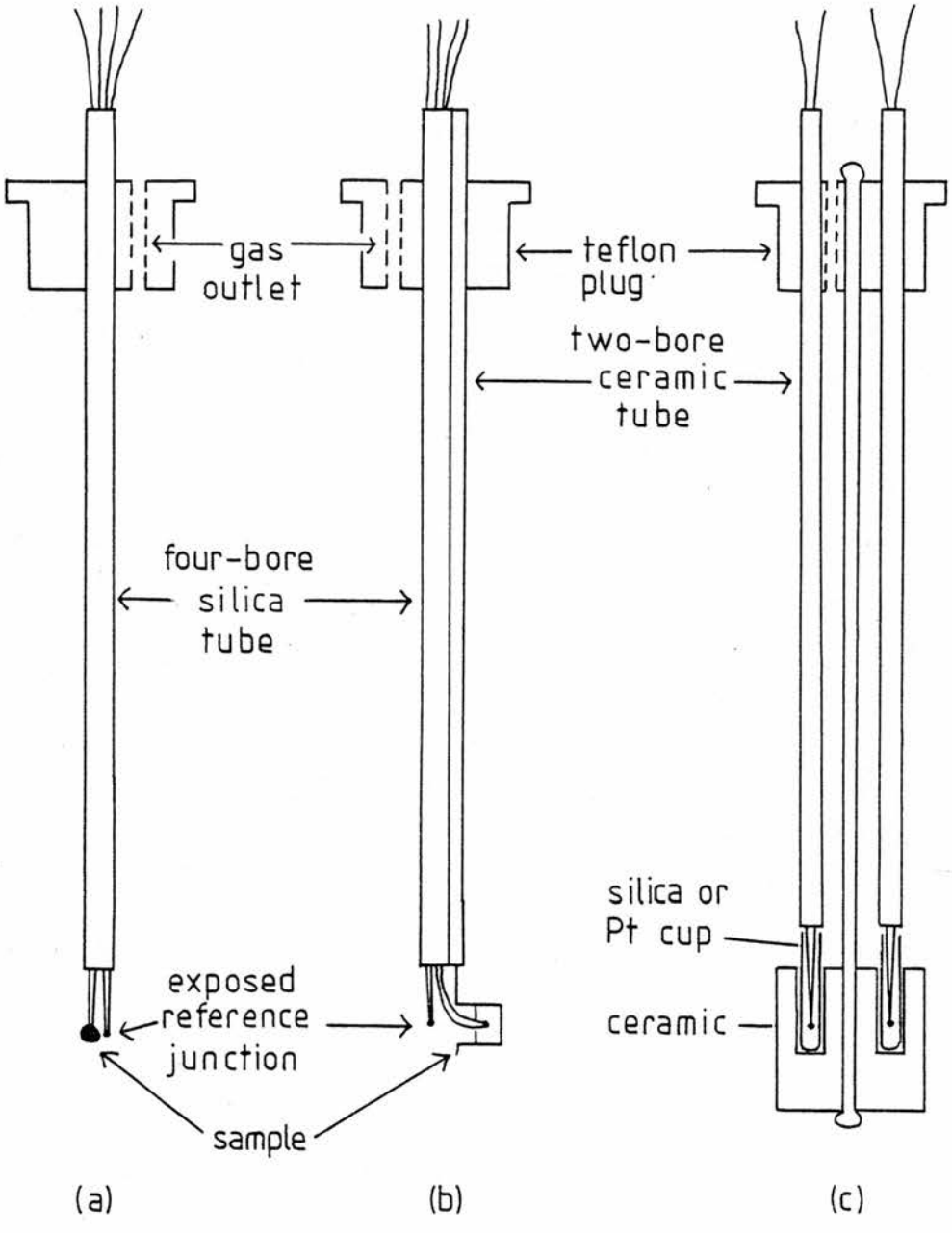

Fig. 55. Differential thermocouple arrangements used in this work.

rates. In the apparatus shown in fig. 55(b) , one thermocouple junction dips into the sample which is contained in a 7 mm diameter Pt cup , while the other junction is left exposed and placed near the first. The arrangement was found to be particularly sensitive and ΔT showed very little drift. The apparatus illustrated in fig. 55(c) is the conventional DTA arrangement in which the sample and reference materials are contained in 3 mm diameter Pt or silica cups which fit snugly into a cylindrical ceramic block. The arrangement in fig. 55(b) was used to calibrate thermocouples by obtaining plots of sample temperature at heating rates of 5 K min^{-1} for the melting of analytical grade KCl , NaCl and K_2SO_4. A plateau persists in the sample temperature for up to two minutes during which the variation is within $\pm$0.2 K. Thermocouple voltages were interpreted using the I.P.T.S. 1968[54] tables and the melting points were taken from the JANAF[55] tables.

Furnace

The furnace used for this work was constructed like that illustrated in fig. 21 by winding Kanthal A wire on a ceramic tube of length 26 cm and diameter 3 cm , and was designed to stand vertically or horizontally. The sensor thermocouple for the temperature programmer (system 1 or 2 in fig. 19) was embedded in the body of the furnace with its junction in contact with an area of the ceramic tube exposed between the windings. The cold junction was situated at the end of a 20 cm strip of asbestos board leading away from the furnace. A ceramic work tube of length 36 cm and diameter 2 cm was held in place inside the furnace by bindings of asbestos rope. All operations were carried out in a fume cupboard.

Quenching techniques

Two methods were employed : a 7 mm diameter Pt cup containing the sample was withdrawn rapidly from the furnace and either plunged into

CCl_4 or splat-cooled by inserting a Cu rod pre-cooled in liquid N_2 (fig. 56). In both cases , quenching was achieved in under 4 s and the sample was removed for examination in normal and polarised light. A specially flattened drill bit was particularly useful for removing glass as it produced suitably thin , transparent flakes.

Presentation of DTA results

Those journals which regularly publish DTA work request their contributors to present their results according to the Reports of the Nomenclature Committee of the International Confederation for Thermal Analysis (ICTA)[113,114] , and these are the conventions followed by the author. These include the use of the degree Celsius (^{o}C) , which is not recommended by IUPAC. A downward deflection in ΔT corresponds to an endothermic process and an upward deflection indicates an exothermic change.

STUDY 1. THE REVERSIBILITY OF THE $\alpha \longrightarrow \beta$ TRANSITION OF $ZnSO_4$.

A high temperature polymorphic transition of $ZnSO_4$ has been detected by several workers[61,63,64,115], but the temperature remains uncertain. The DTA graphs recorded by Nam[63] show a peak at 750 °C on both heating and cooling , while the vapour pressure plot of Ingraham and Kellogg shows a change of slope at 734 °C , from which the $\alpha \longrightarrow \beta$ enthalpy change is calculated as 20.1 kJ mol^{-1}. At least two studies contain no evidence of a transition[62,65].

The major obstacle in a DTA study in the transition temperature region is a two-step decomposition of $ZnSO_4$ ($\rightarrow ZnO.2ZnSO_4 \longrightarrow ZnO$) , for which reported values vary from 680 °C to 850 °C . In this work , a flowing atmosphere of SO_3 suppresses the decomposition with the result that the sulphate is thermodynamically stable up to 850 °C. The consequent extension of the temperature range in which the β form is chemically stable allows for a systematic study of the reverse transition.

EXPERIMENTAL

Sample preparation

Fisons analytical grade $ZnSO_4.7H_2O$ was dehydrated at 380 °C for 48 h , desiccated under vacuum for 48 h and ground to a fine powder. $MgSO_4$, prepared from Fisons analytical grade $MgSO_4.7H_2O$, was chosen as the reference material because it is thermally inert in the temperature range and atmosphere involved.

Apparatus

Differential thermocouple (c) in fig. 55 was used with 60 mg samples held in silica cups and in conjunction with temperature control system 2 in fig. 19. A $SO_2 + O_2$ mixture was passed through the furnace using the flow apparatus described and the formation of SO_3 was catalysed by a strip of Pt foil ; the absence of a catalyst

resulted in little suppression of the decomposition.

The DTA graphs illustrating the two-step decomposition of $ZnSO_4$ were obtained using apparatus (a) in fig. 55.

RESULTS

The principal purpose of this study was to examine the reversibility of the $\alpha \longrightarrow \beta$ transition of $ZnSO_4$, and DTA graphs were obtained at four heating/cooling rates. These are presented in figs. 57-60 and table 12 gives T_{onset} , the sample temperature associated with deviation from a constant heating/cooling rate , and T_{peak} , the sample temperature at a peak in ΔT. As mentioned already , the choice of the feature of a DTA graph used to locate a transition temperature is a disputed point. A plateau in sample temperature is a requirement of the phase rule if two polymorphs are in equilibrium with each other. The plateaux in the cooling curves are the most conspicuous feature of the results and on this evidence the $\alpha \rightleftharpoons \beta$ transition temperature is 730.5 $\pm$ 1.0 ^{o}C. Slight supercooling was encountered in only one case (fig. 58). Attempts to quench the β form by plunging it into CCl_4 were unsuccessful , suggesting that it reconverted rapidly at room temperature.

The small disparity of the above result with that of Ingraham and Kellogg could be a consequence of the difference in purity between the analytical grade salt used for this work and their reagent grade material. This effect has been investigated by Rao et al. for the transition of K_2SO_4 [116]. The brevity of Nam's paper makes comparison difficult and the values given by Fredrich and Blicke[64] (740 ^{o}C) and Shargorodskii[115] (735 ^{o}C) were obtained for heating only.

TABLE 12. DTA results for the $\alpha \rightleftharpoons \beta$ transition of $ZnSO_4$.

Heating rate /°C min^{-1}	Cooling rate /°C min^{-1}	T_{onset}/°C	T_{peak}/°C
4	-	747.0	750.0
-	4	731.5^p	731.5
6	-	749.0	751.5
-	6	731.5^p	730.5
8	-	748.0	751.5
-	9	729.5^p	728.5
15	-	749.0	752.0
-	14	730.0^p	728.5

p Plateau in sample temperature.

It was found that the decomposition of $ZnSO_4$ in an atmosphere of $SO_2 + O_2$ was markedly influenced by the presence of a Pt catalyst. The DTA graph obtained in the absence of a catalyst is given in fig. 61 and in it the three endothermic processes (transition followed by two-step decomposition) are very poorly resolved. In contrast , fig. 62 shows the result obtained when the formation of SO_3 was catalysed by the Pt foil. Here the $\alpha \longrightarrow \beta$ transition precedes the onset of the first stage of the decomposition by 100 °C and this latter is clearly resolved from the second stage. The decomposition of $CuSO_4$, $NiSO_4$ and $Fe_2(SO_4)_3$ were found to be similarly influenced by the presence of SO_3 and this suggests that the reaction sequence for the establishment of equilibrium in these cases is

$$MSO_4 \rightleftharpoons MO + SO_3 \rightleftharpoons MO + (1-X)SO_3 + XSO_2 + \tfrac{1}{2}XO_2$$

That is , $SO_2 + \frac{1}{2}O_2$ do not combine directly with MO to give the sulphate and consequently do not significantly suppress the decomposition. This is the evidence for the assertion in part one that these four metal sulphates decompose by the release of SO_3 and not $SO_2 + \frac{1}{2}O_2$. As mentioned before , for the case of $Fe_2(SO_4)_3$ this mechanism has been confirmed by workers using a matrix isolation technique[66].

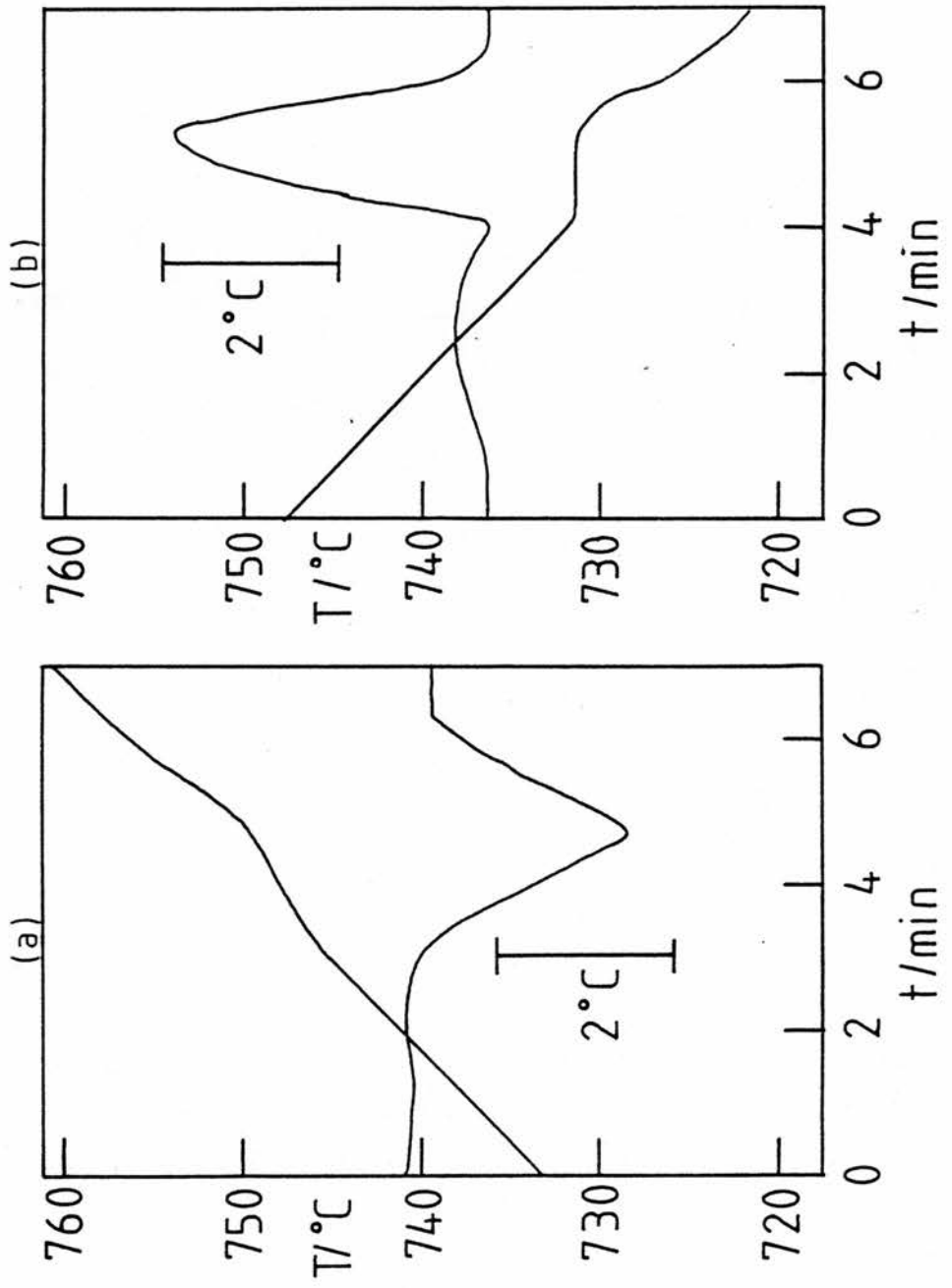

Fig. 57. DTA curves of the $ZnSO_4$ $\alpha \rightarrow \beta$ transition.
(a) heating rate $4\,^{\circ}C\ min^{-1}$; (b) cooling rate $4\,^{\circ}C\ min^{-1}$.

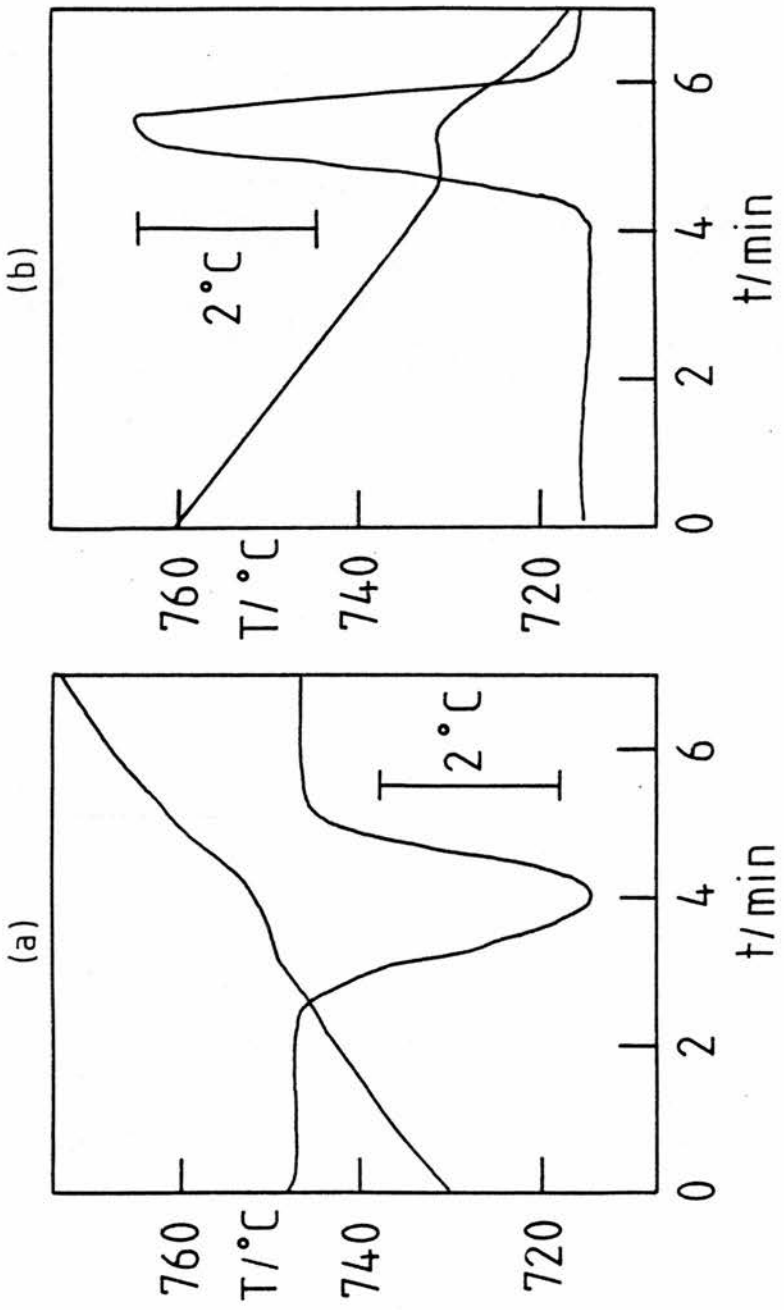

Fig. 58. DTA curves of the $ZnSO_4$ $\alpha \rightleftarrows \beta$ transition.
(a) heating rate 6 $^{o}C\ min^{-1}$; (b) cooling rate 6 $^{o}C\ min^{-1}$.

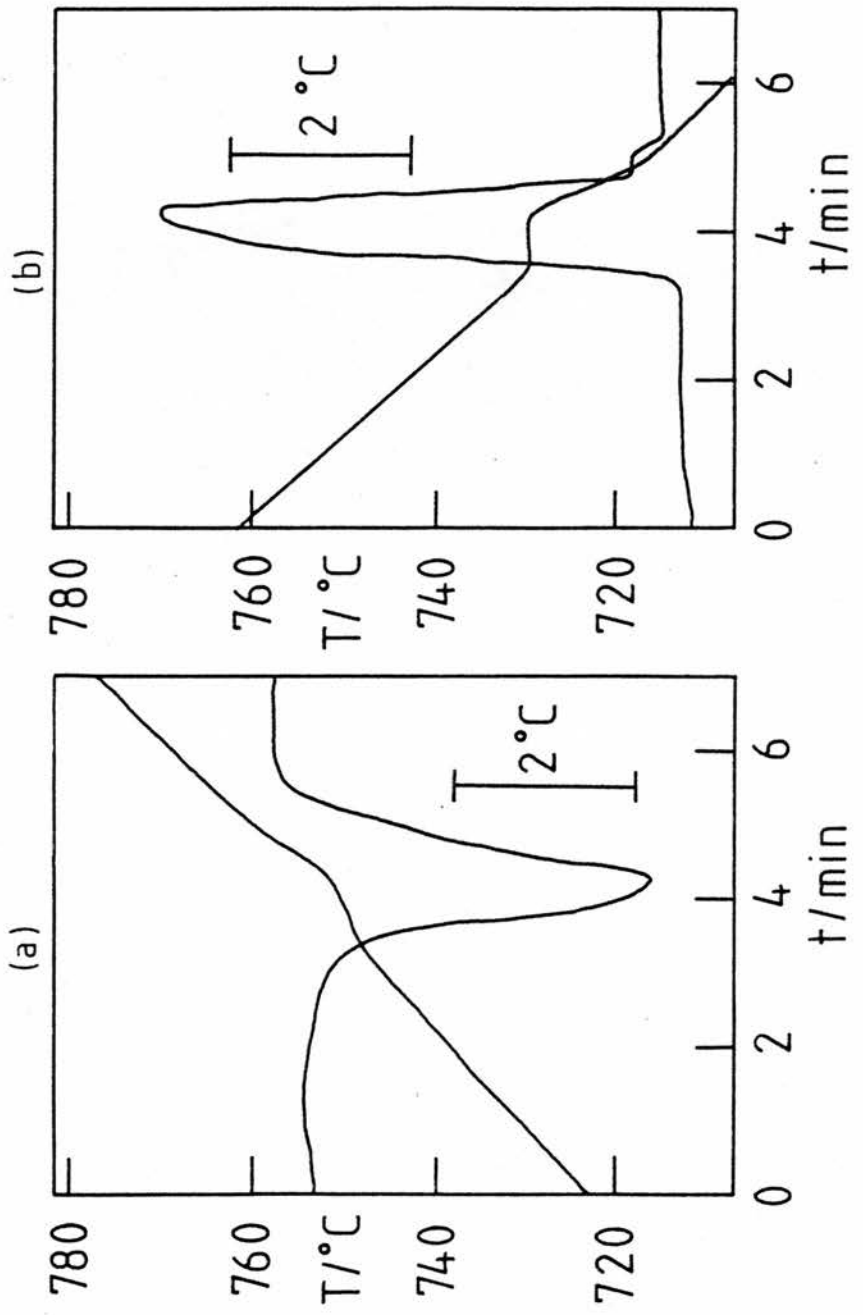

Fig. 59. DTA curves of $ZnSO_4$ $\alpha \rightarrow \beta$ transition.
(a) heating rate 9 $^{o}C\ min^{-1}$; (b) cooling rate 8 $^{o}C\ min^{-1}$.

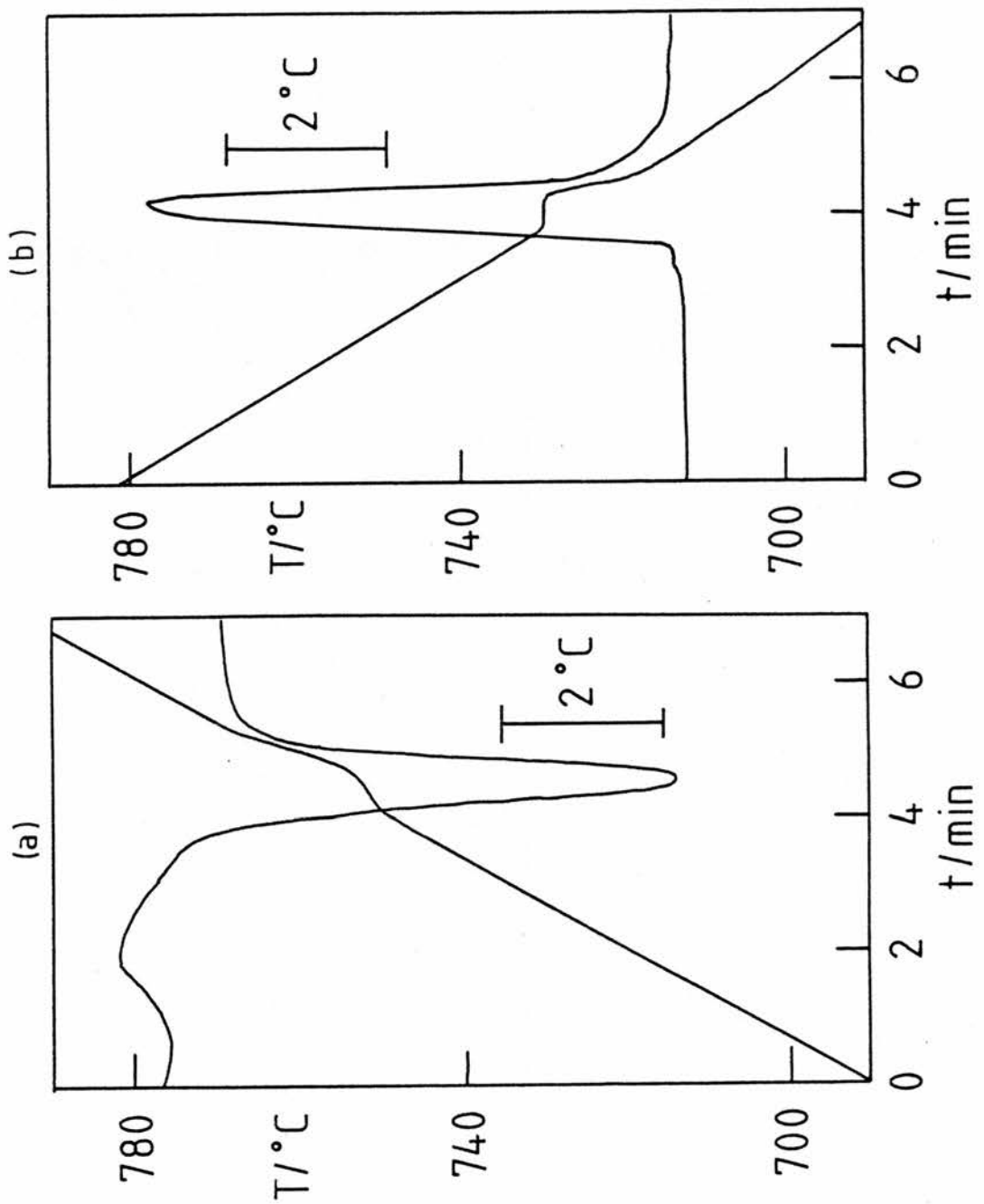

Fig. 60. DTA curves of the $ZnSO_4$ $\alpha \rightarrow \beta$ transition.
(a) heating rate 15 $^{o}C\ min^{-1}$; (b) cooling rate 14 $^{o}C\ min^{-1}$.

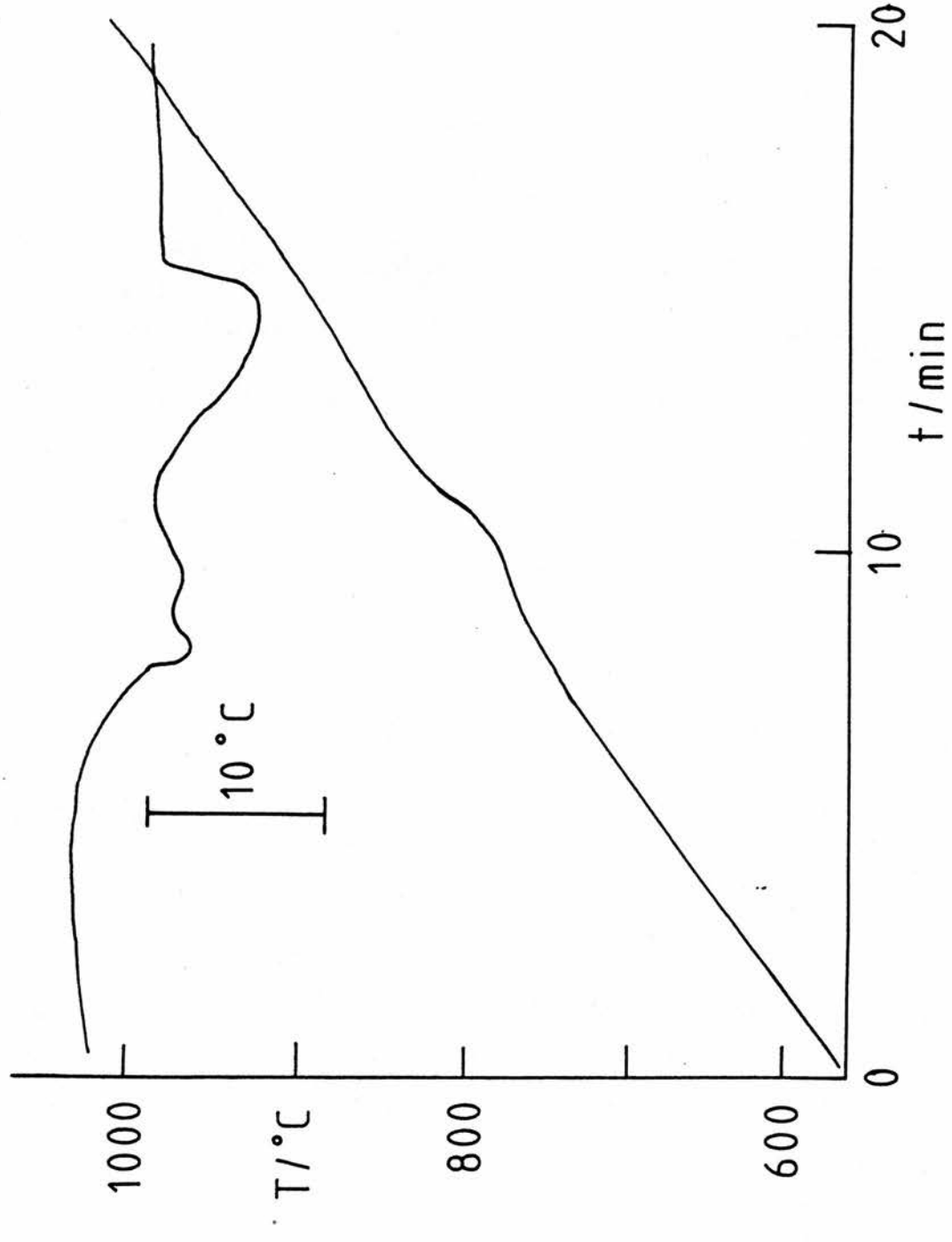

Fig. 61. DTA of $ZnSO_4$ in an uncatalysed SO_2+O_2 mixture. Compare with fig. 62.

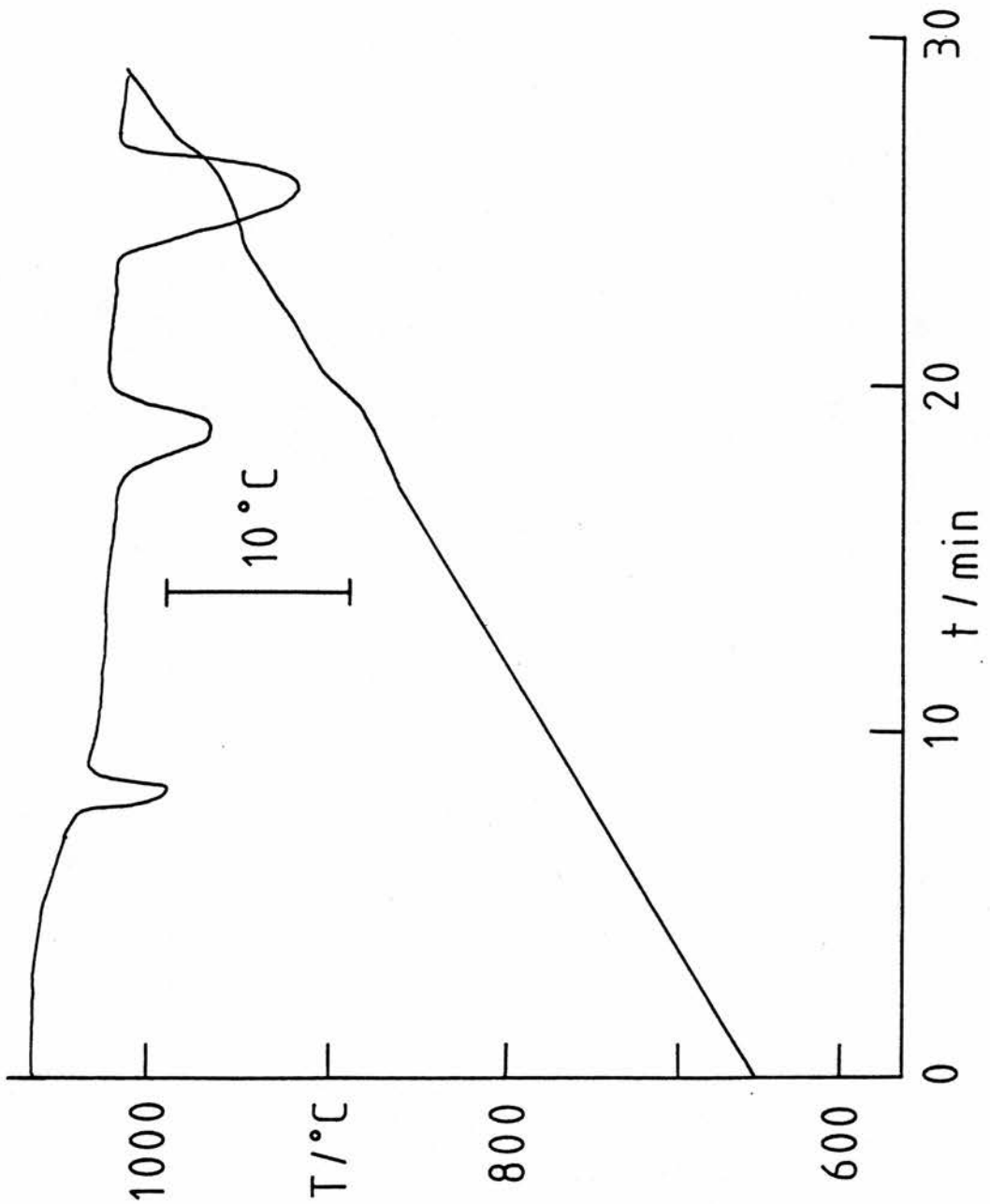

Fig. 62. DTA of $ZnSO_4$ in a catalysed SO_2+O_2 mixture. Peaks corresponding to the three stages α-$ZnSO_4 \rightarrow \beta$-$ZnSO_4 \longrightarrow ZnO.2ZnSO_4 \longrightarrow ZnO$ are clearly resolved.

STUDY 2. THE SYSTEM Ag_2SO_4-$BeSO_4$

The previously undetermined phase diagram for the system Ag_2SO_4-$BeSO_4$ was studied by DTA and quenching techniques using a flowing atmosphere of SO_3 to suppress decomposition.

There have been several studies of the $\alpha \longrightarrow \beta$ transition of Ag_2SO_4 with values of $T^{\alpha+\beta}$ ranging from 412 °C to 430 °C[57,58,118,119]. High temperature X-ray diffraction has shown the α and β forms to be orthorhombic and Na_2SO_4(1) type respectively[119]. Recorded values for the melting point range from 643 °C to 660 °C[57,58,118,119].

$BeSO_4$ obtained by dehydrating the tetrahydrate may show either poorly resolved transitions[58] or none at all[57] and decomposes above 650 °C. DTA of $BeSO_4$ held at 400 °C for 60 h , however , reveals two well-defined peaks , starting at 588 °C ($\alpha \longrightarrow \beta$) and 639 °C ($\beta \longrightarrow \gamma$) on heating[120]. On cooling , the latter peak resolves into two , separated by 4 °C , indicating the presence of a fourth polymorph (δ) existing over a narrow temperature range. The structures of the other three phases have been determined by Bosik et al.[121] as tetragonal (α) , orthorhombic (β) and cubic (γ). High temperature X-ray diffraction was employed.

EXPERIMENTAL

Materials

BDH analytical grade Ag_2SO_4 (99%) and reagent grade $BeSO_4.4H_2O$ (98%) were used. $BeSO_4$ was obtained by dehydration of the tetrahydrate at 300 °C for 24 h and was stored over P_2O_5 in a vacuum desiccator. Mixtures were prepared by grinding together the salts under CCl_4 in an agate mortar for 5 min and removing the solvent under vacuum.

Apparatus

Differential thermocouple arrangement (b) in fig. 55 with

300 mg samples was found most suitable for this work and was used in conjunction with temperature control system 2 in fig. 19. Heating/cooling rates of 5 $^{o}C\ min^{-1}$ facilitated resolution of consecutive changes while giving reasonably large peaks. The quenching techniques used were as described above and samples were examined by microscopy. There was also some access to powder X-ray diffraction facilities.

RESULTS

A transition is characterised here by its DTA peak temperature.

The $\alpha \longrightarrow \beta$ transition of Ag_2SO_4 occurred at 425 $\pm$ 3 ^{o}C on heating all compositions in the range 0-97 mol% $BeSO_4$ and was followed by the eutectic transition at 441 $\pm$ 2 ^{o}C. Only at compositions of $>$ 20 mol% $BeSO_4$ were these two peaks resolved (figs. 65(a) and 66(a)). On cooling compositions of $<$ 35 mol% $BeSO_4$, the eutectic transition was detected only as a shoulder on the Ag_2SO_4 $\beta \longrightarrow \alpha$ peak , and this latter showed increasing supercooling as the mol% of $BeSO_4$ decreased (fig. 65(b)). For example , pure Ag_2SO_4 , which melted reversibly at 661 $\pm$ 1 ^{o}C , cooled to 392 ^{o}C before transforming and raising its temperature to 420 ^{o}C (figs. 63(a) and (b)). The $\beta \longrightarrow \alpha$ transition for the unmelted salt shows considerably less supercooling (fig. 64). On cooling compositions with $>$ 35 mol% $BeSO_4$, the eutectic and Ag_2SO_4 $\beta \longrightarrow \alpha$ peaks were completely resolved and occurred at 421 $\pm$ 4 ^{o}C and 395 $\pm$ 7 ^{o}C (fig. 66(d)).

The $BeSO_4$ $\alpha \longrightarrow \beta$ and $\beta \longrightarrow \gamma$ transitions were detected at 609 $\pm$ 2 ^{o}C and 646 $\pm$ 1 ^{o}C on heating in the composition range 48-97 mol% $BeSO_4$ (fig. 66(b)). On cooling , peaks occurred at 587 $\pm$ 2 ^{o}C and 636 $\pm$ 2 ^{o}C , and there was an additional peak at 640 $\pm$ 2 ^{o}C which became gradually undetectable at $>$ 80 mol% $BeSO_4$

(fig. 66(c)). Pure $BeSO_4$ showed no transitions on heating or cooling and decomposed above 800 °C. X-ray powder diffraction showed that the recrystallisation of $BeSO_4$ from a 98 mol% mixture above the eutectic temperature is accompanied by an irreversible change from a metastable to the stable (tetragonal) structure (fig. 67).

In the composition range 0-25 mol% $BeSO_4$, the liquidus line was detected as a small exothermic effect on cooling but not on heating (fig. 65(b)) and extrapolation gave a eutectic composition of 30 mol% $BeSO_4$ (fig. 68). The other liquidus line was detected neither on heating nor cooling , despite varying the heating/cooling rate from 5 to 15 °C min^{-1} and increasing the sample mass up to 600 mg. The disappearance of the $BeSO_4$ transitions near 50 mol% , however , allowed parts of this liquidus line to be estimated. Many samples were held for up to 20 h in the vicinity of the estimated liquidus line and were quenched by the methods described. While melts 25 °C above and below the line gave , respectively , glass and $BeSO_4$ crystals in a glass matrix , crystallisation was not reproducible near the line. Crystallisation in the vicinity of the other (detected) liquidus line was similarly irreproducible.

The phase diagram presented in fig. 68 is constructed from points obtained on heating , except for the left hand liquidus line.

Further comments

(a) In the absence of the flowing mixture of $SO_2 + O_2$, samples developed a dark colouration and lost weight significantly above 600 °C.

(b) The peak temperatures on successive heating/cooling cycles

with the same sample were identical within experimental error. This indicates good homogenisation of the component powders after grinding in the agate mortar.

(c) The extra peak which appears on cooling in the $BeSO_4$ + liquid region of the diagram and which can be attributed to the exsistence of a fourth polymorph (δ) , is absent on heating probably because of superheating of the β form. The absence of this extra peak on cooling compositions with > 80 mol% $BeSO_4$ may be related to the incomplete recrystallisation of the metastable form as there is proportionally more solid to be recrystallised. The DTA results presented here are in close agreement with those obtained for $BeSO_4$ recrystallised by prolonged heating[120]. To characterise further the recrystallisation , a 98 mol% mixture was held above the eutectic temperature for 1 h , quenched and examined by SEM. The electron micrographs of this and the original (unmelted) mixture are compared in fig. 69 , which shows the kind of increase in crystal size expected during recrystallisation. This evidence substantiates the X-ray diffraction results.

(d) Many attempts were made to quench the polymorphs of both components but only room temperature forms were detected.

(e) The failure of DTA to detect the right hand liquidus line is probably a consequence of the smallness of the heat evolution when solid $BeSO_4$ forms. As mentioned above , some degree of supercooling greatly facilitates the detection of a liquidus point and this would appear to be absent here. At the outset of this work the plan was to refine the DTA results by a series of quenching experiments which would locate exactly the liquidus lines. The erratic crystallisation of the melts on rapid cooling , however , thwarted the application of this technique. On quenching large samples

(600 mg) by plunging into CCl_4 , there was usually extensive crystallisation in the bulk ; with smaller samples (50 mg) and with the splat method , cooling is certainly more rapid but , as mentioned earlier , heterogeneous nucleation is more likely. Irregularities on the surface of the Pt cup may account for unpredictable crystallisation. The difficulty in interpreting the quenching results in the vicinity of the estimated liquidus line can be appreciated from fig. 70. This shows a quenched sample which is essentially glass with very few crystalline regions. A re-run of the experiment , however , resulted in pure glass.

CONCLUSION

The phase diagram presented in fig. 68 is , like most high temperature diagrams , an approximation whose accuracy is determined by the limitations imposed by kinetics on the techniques at hand. As mentioned before , observations of kinetic effects are an important aspect of any such study and some attempt has been made to understand these using the techniques available. It has been established , for example , that the melts do not readily form glass and that small additions of Ag_2SO_4 hasten the recrystallisation of amorphous $BeSO_4$.

It is difficult to suggest a technique which could take the investigation further. It is the author's experience that molten sulphates (including this system) attack silica and this would complicate the application of hot-stage microscopy. A more extreme quenching method could probably solve the problem.

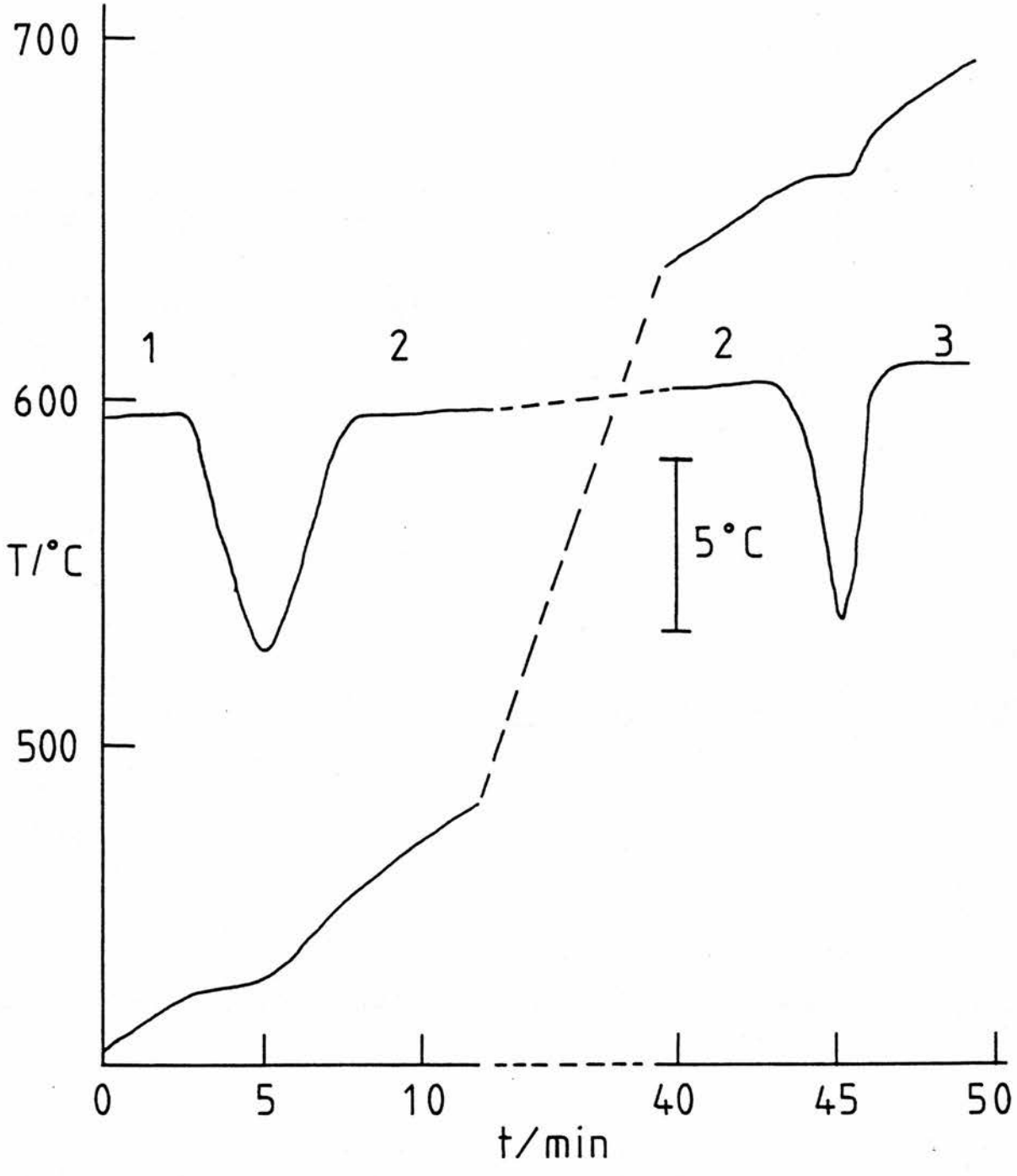

Fig. 63(a). DTA curves of Ag_2SO_4. 1 = α-Ag_2SO_4 ; 2 = β-Ag_2SO_4 ; 3 = ι-Ag_2SO_4. There was a plateau in sample temperature during melting.

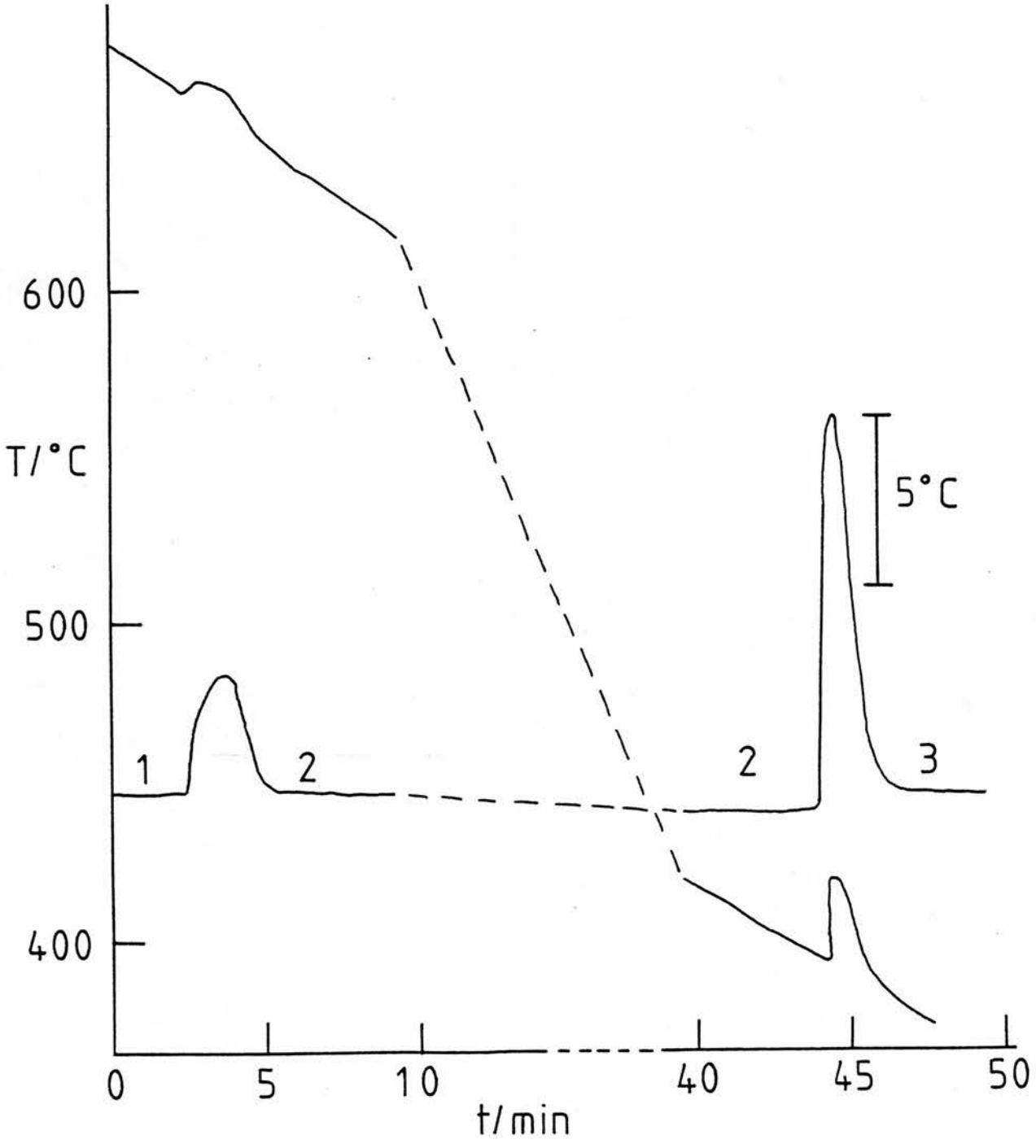

Fig. 63(b). DTA curves of Ag_2SO_4. 1 = γ-Ag_2SO_4 ; 2 = β -Ag_2SO_4 ; 3 = α -Ag_2SO_4. The $\beta \rightarrow \alpha$ transition shows considerable supercooling.

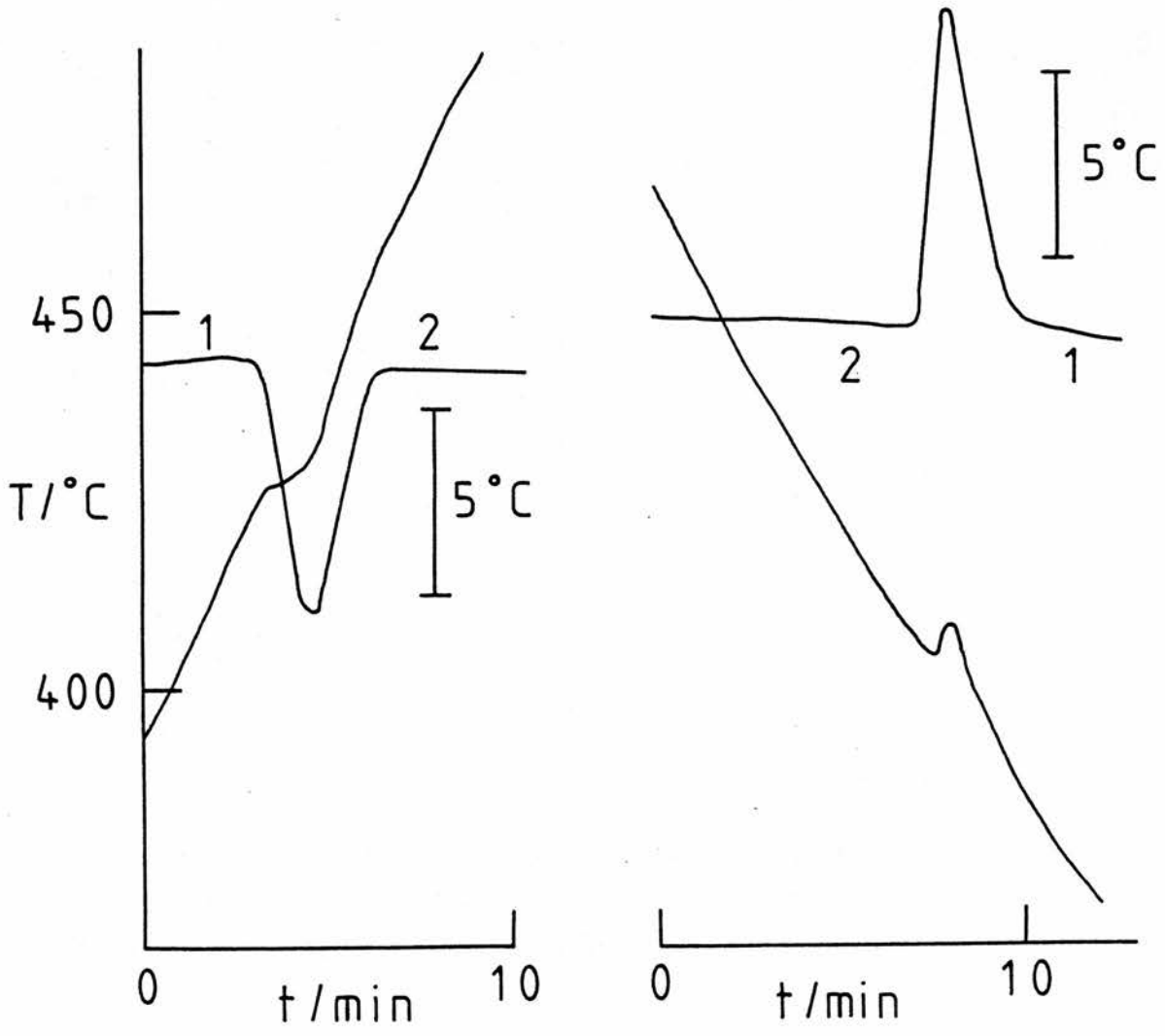

Fig. 64. DTA curves of Ag_2SO_4. 1 = α -Ag_2SO_4 ; 2 = β -Ag_2SO_4. The solid was not melted.

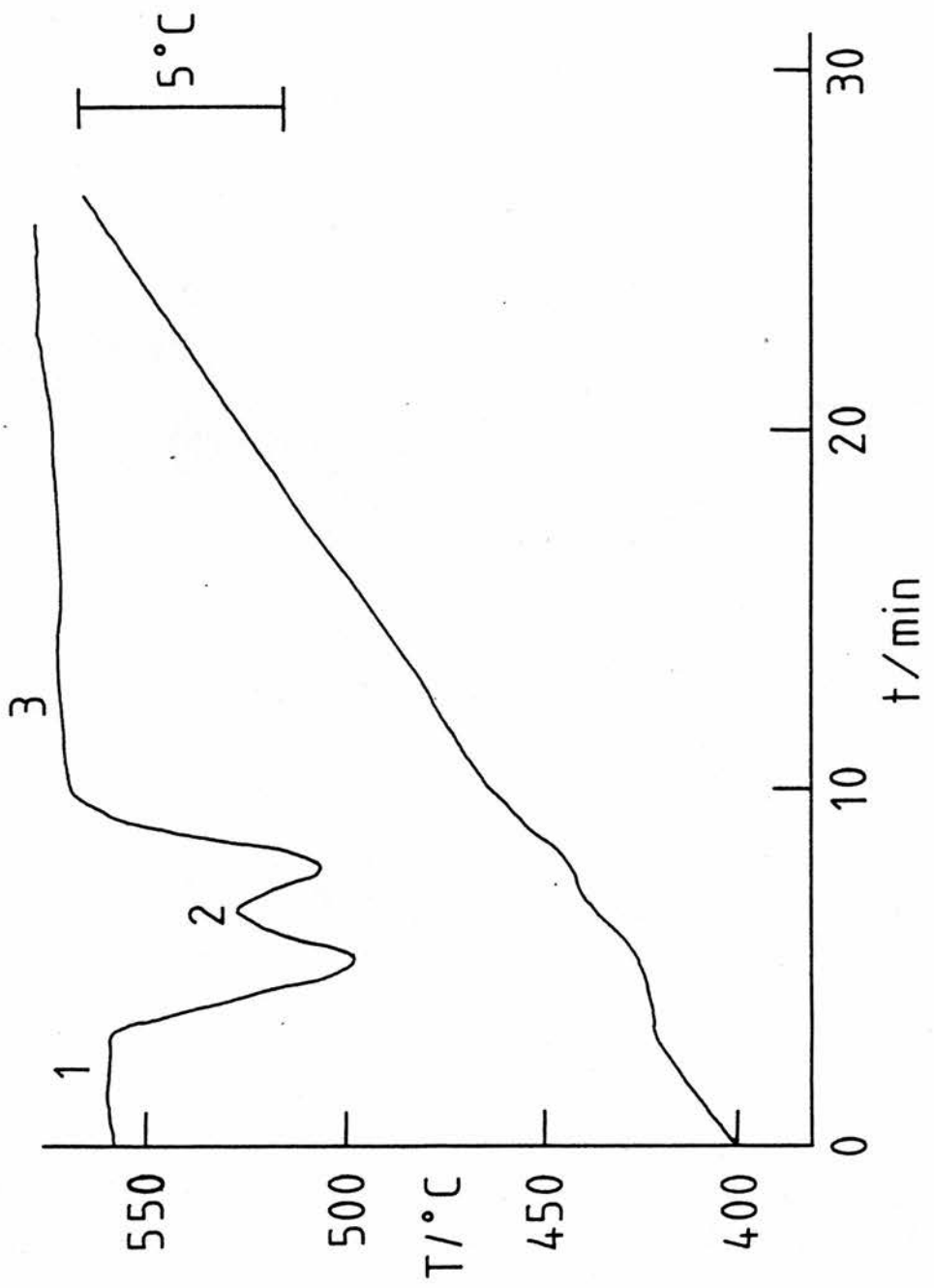

Fig. 65(a). DTA curves of a {23 mol% $BeSO_4$-77 mol% Ag_2SO_4} mixture. 1 = α -Ag_2SO_4+α-$BeSO_4$; 2 = β -Ag_2SO_4+α-$BeSO_4$; 3 = β -Ag_2SO_4+ l.

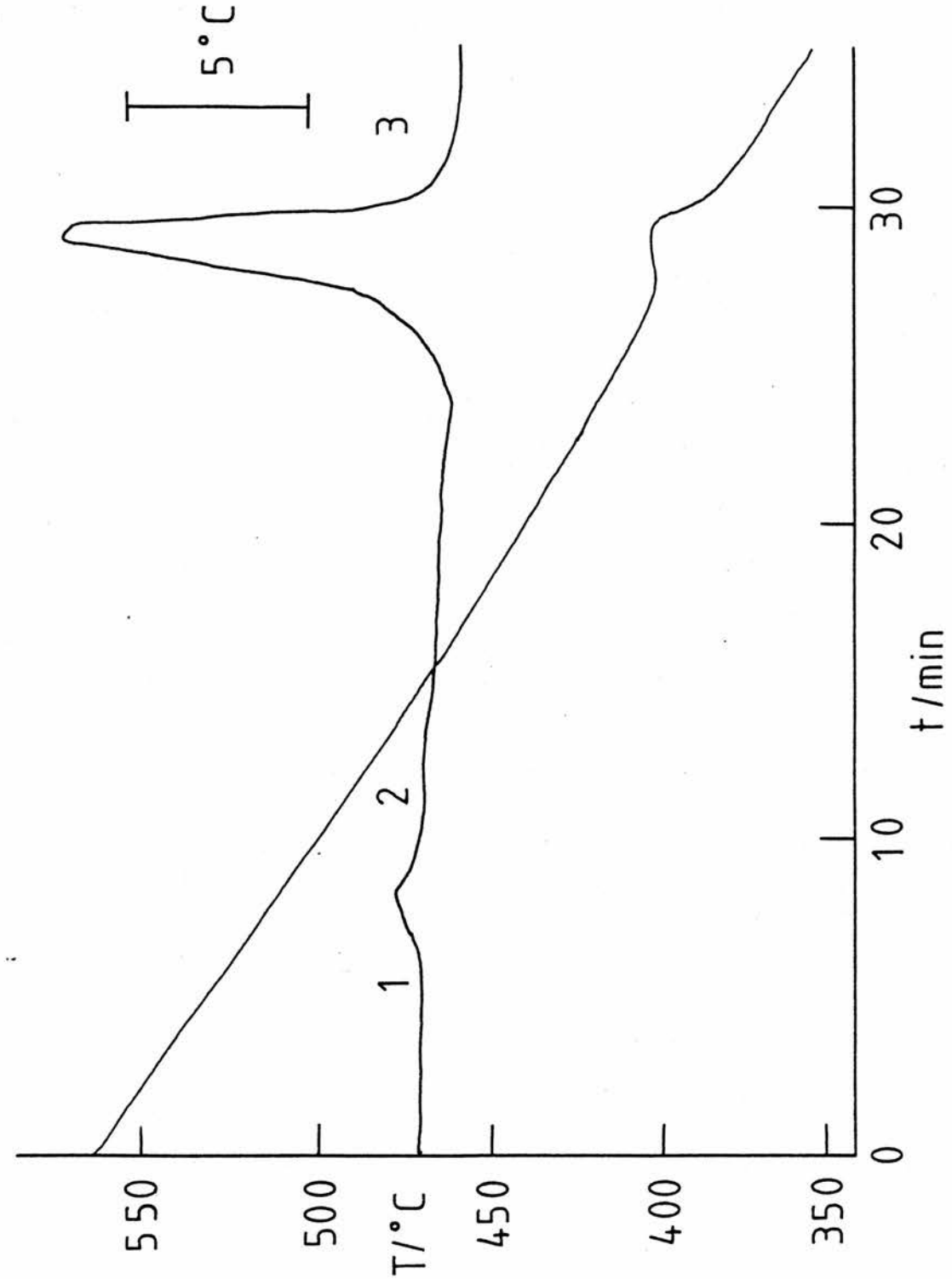

Fig. 65(b). DTA curves of a {23 mol% $BeSO_4$-77 mol% Ag_2SO_4} mixture. 1 = λ ; 2 = $\lambda + \beta$-Ag_2SO_4 ; 3 = α-$BeSO_4$ + α-Ag_2SO_4.
The small exothermic effect occurs on crossing the liquidus line.
The eutectic and Ag_2SO_4 $\beta \rightarrow \alpha$ transitions are not resolved.

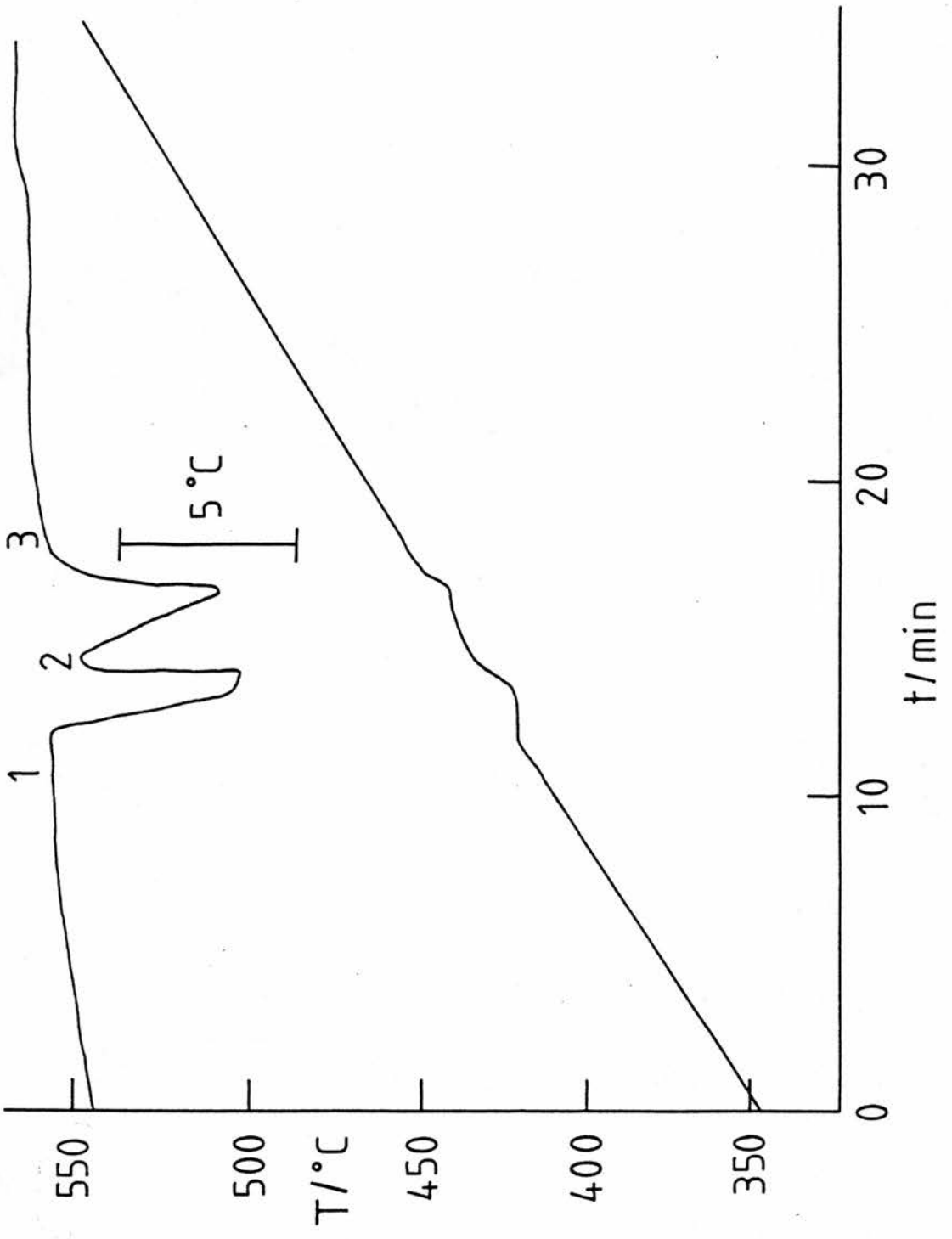

Fig. 66(a). DTA curves of a $\{65$ mol% $BeSO_4$-35 mol% $Ag_2SO_4\}$ mixture. 1 = α-$BeSO_4$+α-Ag_2SO_4 ; 2 = α-$BeSO_4$+ β-Ag_2SO_4 ; 3 = ℓ + α-$BeSO_4$.

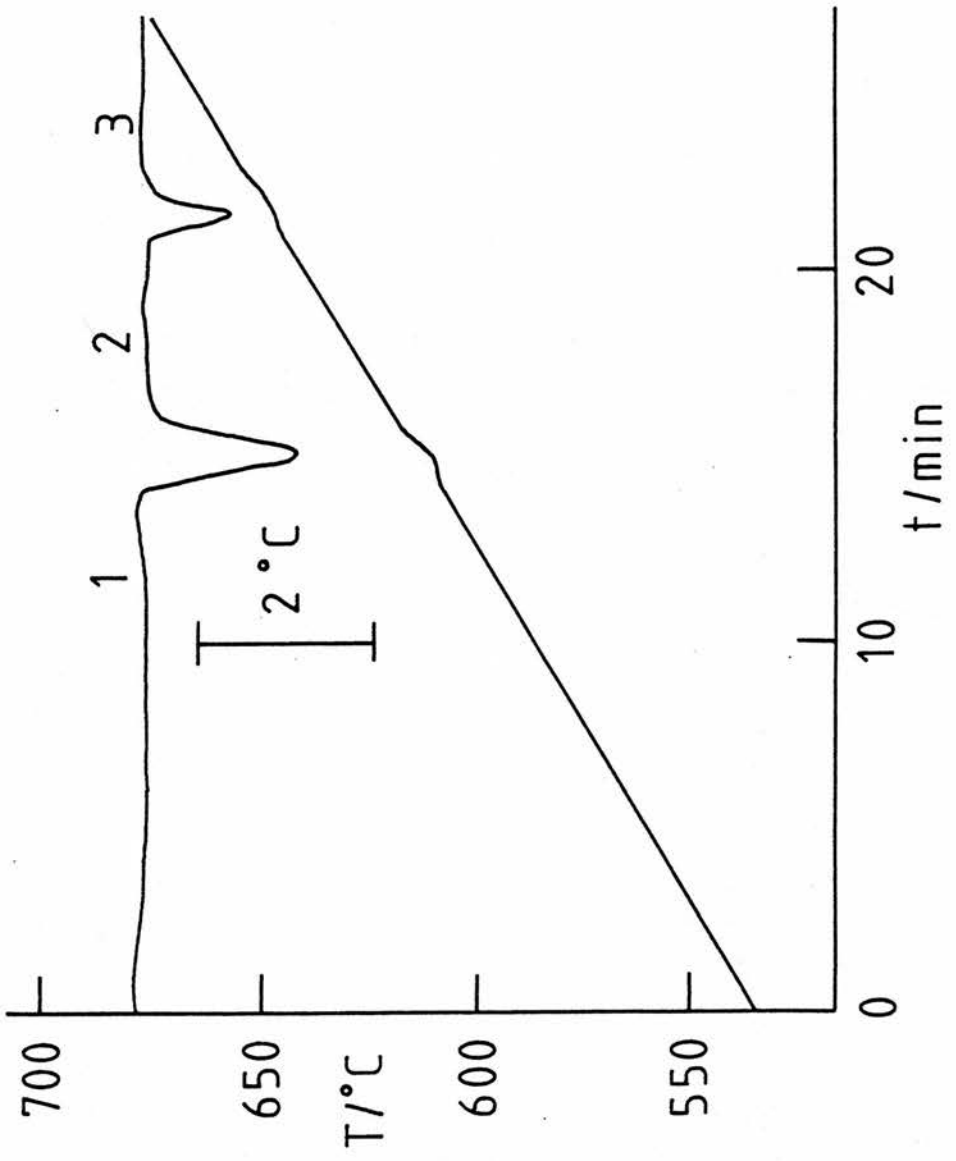

Fig. 66(b). DTA curves of a {65 mol% $BeSO_4$-35 mol% Ag_2SO_4} mixture. 1 = $\ell + \alpha$-$BeSO_4$; 2 = $\ell + \beta$-$BeSO_4$; 3 = ℓ + γ-$BeSO_4$.

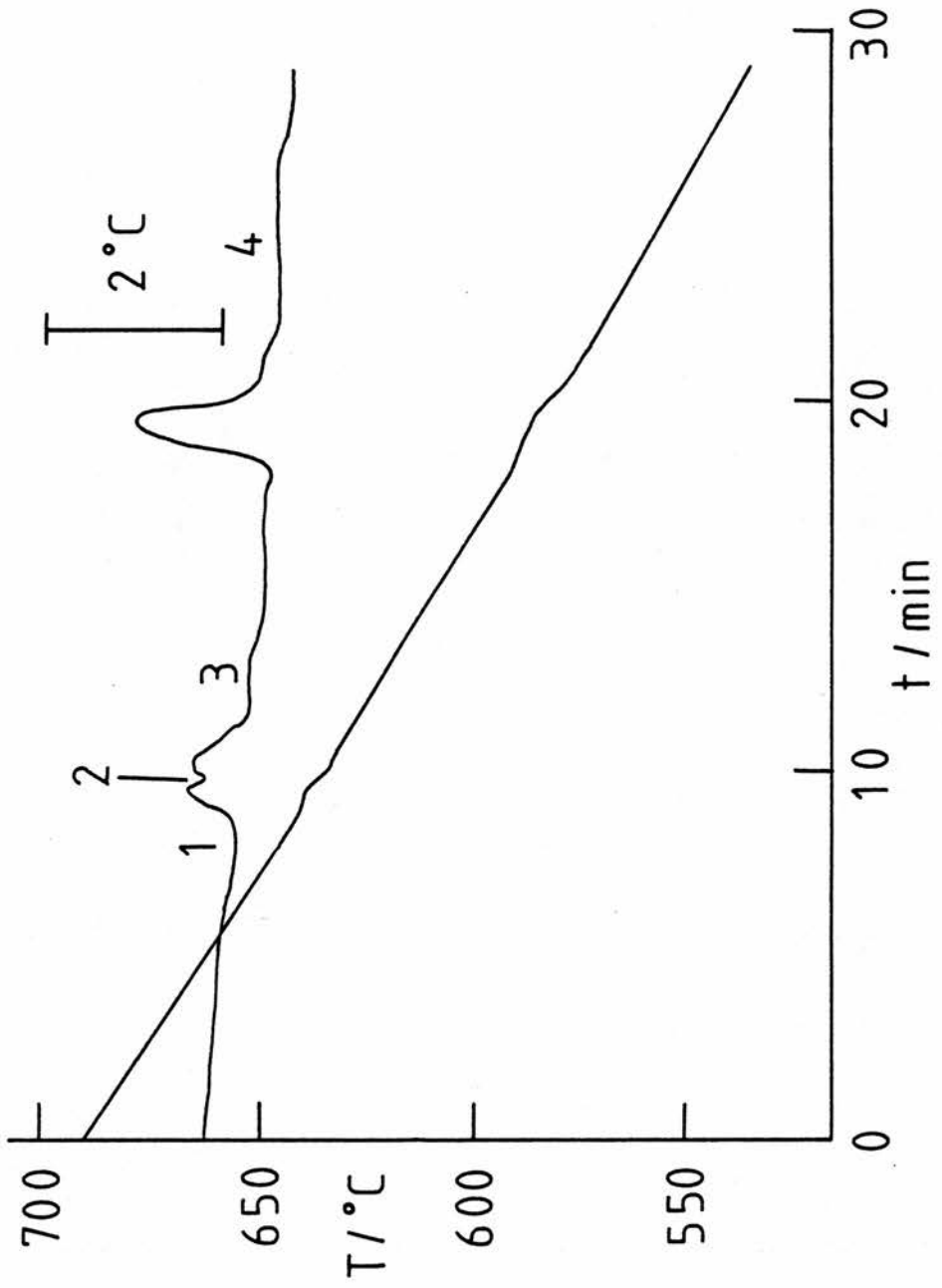

Fig. 66(c). DTA curves of a {65 mol% $BeSO_4$-35 mol% Ag_2SO_4} mixture. 1 = $l + \gamma$-$BeSO_4$; 2 = $l + \delta$-$BeSO_4$; 3 = $l + \beta$-$BeSO_4$; 4 = $l + \alpha$-$BeSO_4$.

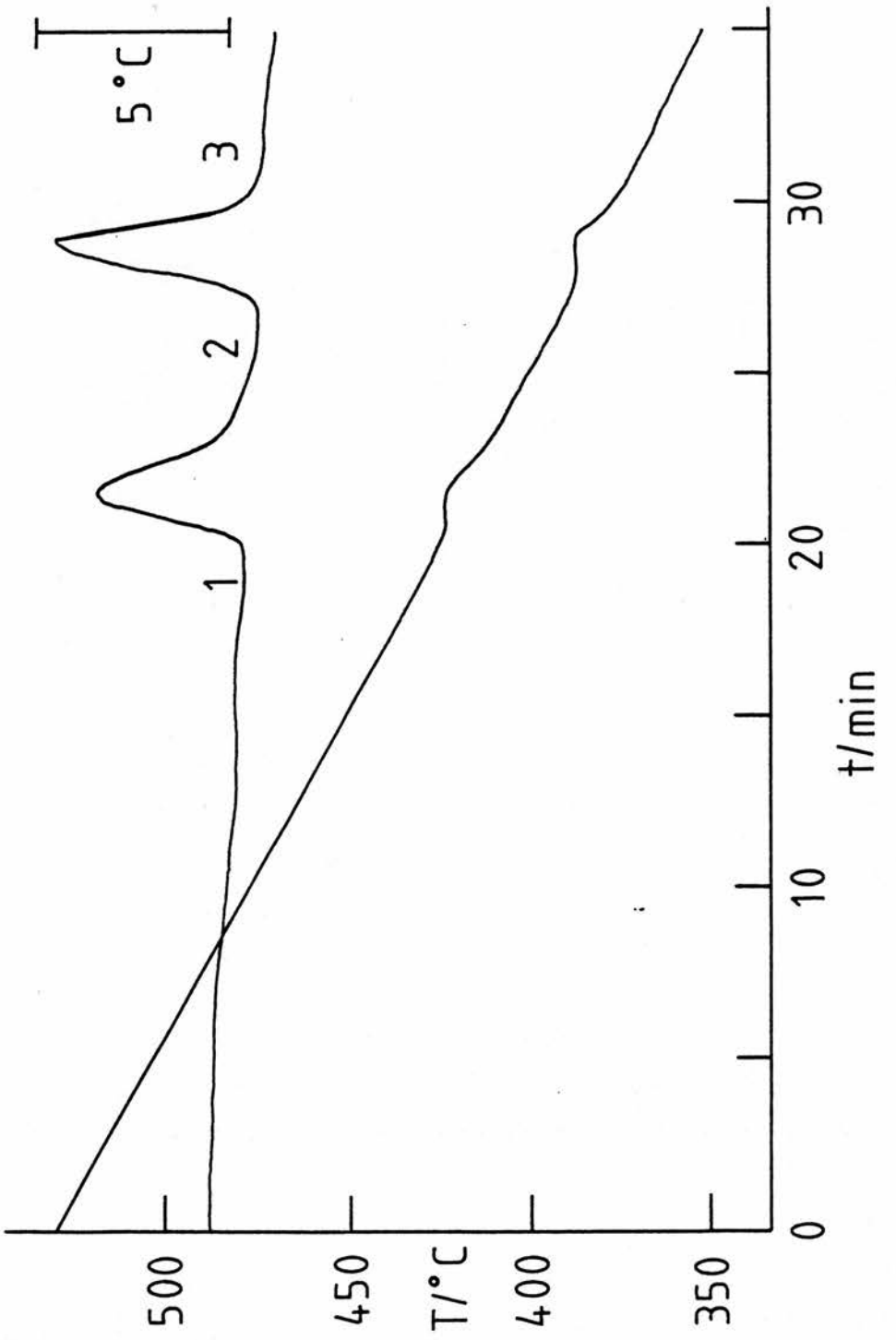

Fig. 66(d). DTA curves of a {65 mol% $BeSO_4$-35 mol% Ag_2SO_4} mixture. 1 = α + α -$BeSO_4$; 2 = α -$BeSO_4$ + β -Ag_2SO_4 ; 3 = α -$BeSO_4$ + α -Ag_2SO_4.

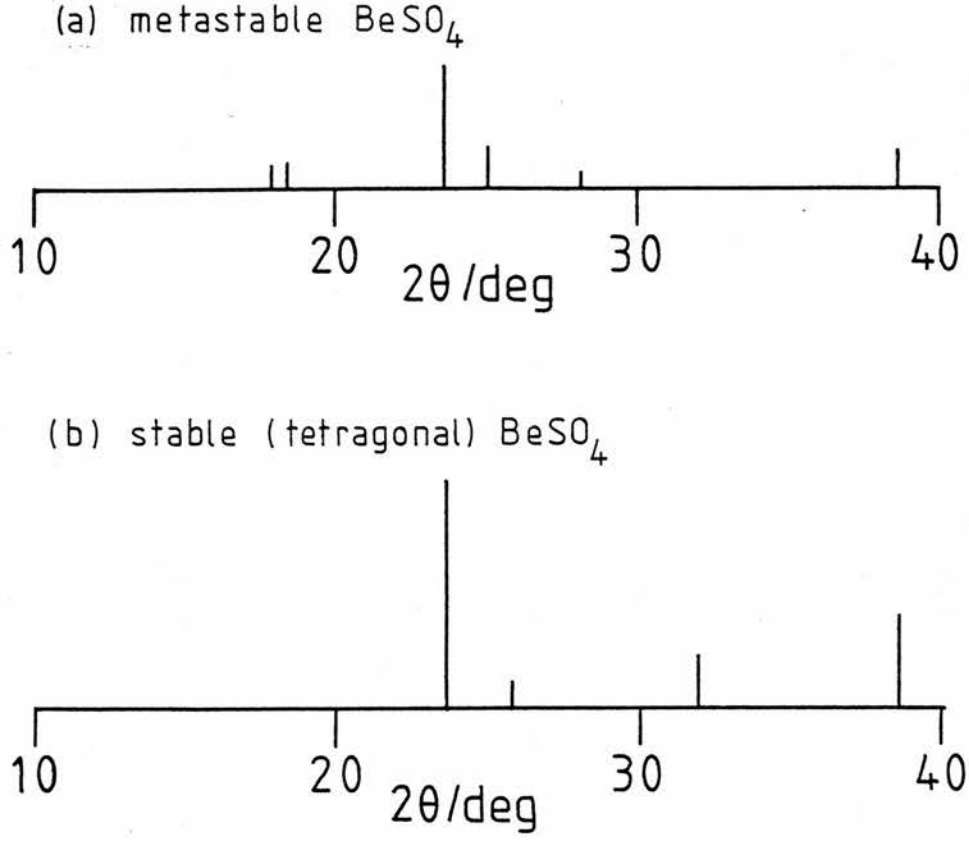

Fig. 67. (a) the powder X-ray diffraction pattern of $BeSO_4$ obtained by dehydrating $BeSO_4.4H_2O$; (b) the pattern for the stable form of $BeSO_4$ obtained by recrystallisation from a 98 mol% mixture with Ag_2SO_4 above the eutectic temperature for 4 h (Ag_2SO_4 lines omitted). CuK_α radiation was used.

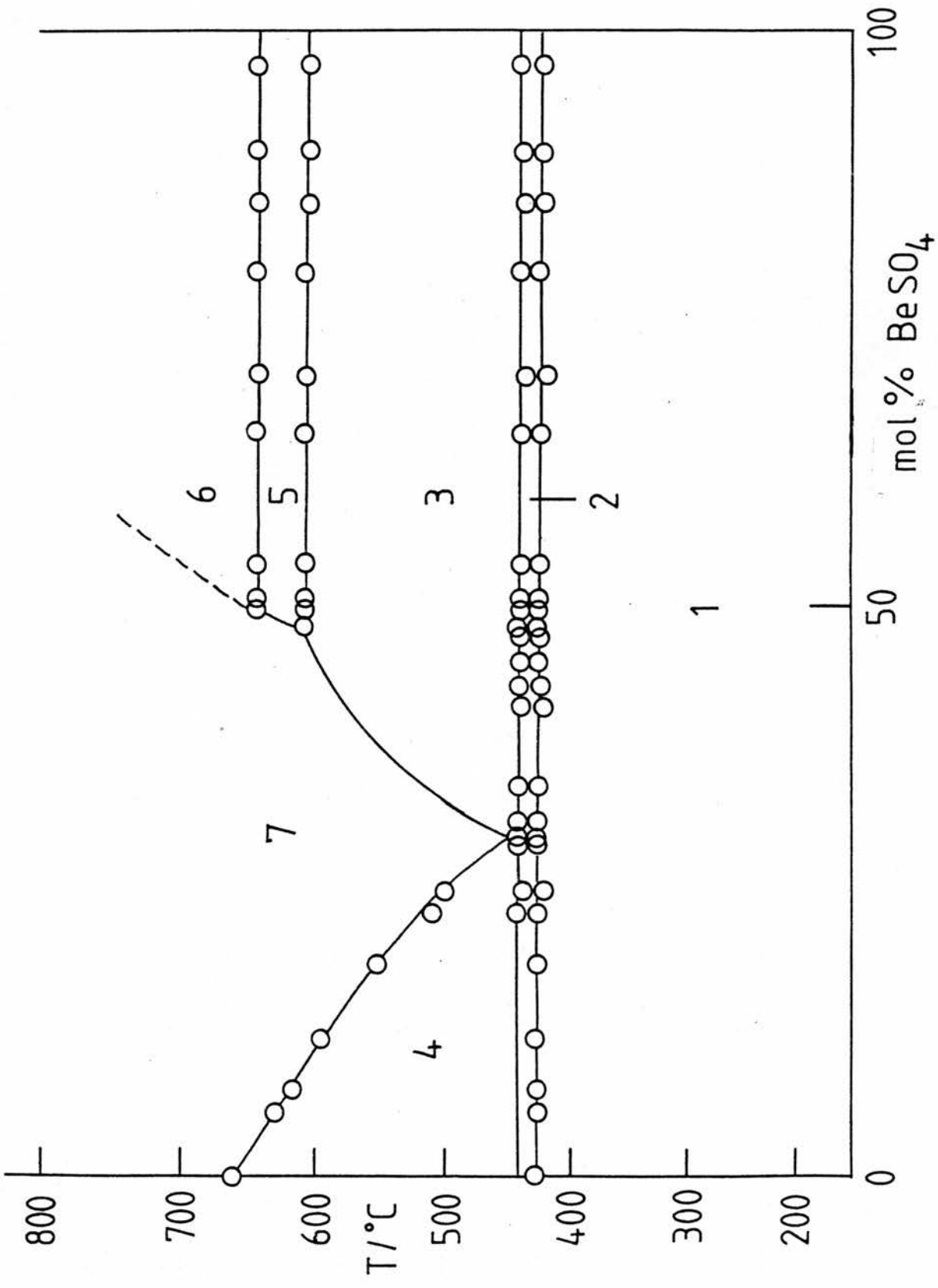

Fig. 68. The phase diagram for the system Ag_2SO_4-$BeSO_4$.
1 = α-$BeSO_4$ + α-Ag_2SO_4 ; 2 = α-$BeSO_4$ + β-Ag_2SO_4 ; 3 = *l* + α-$BeSO_4$;
4 = β-Ag_2SO_4 + *l* ; 5 = *l* + β-$BeSO_4$; 6 = *l* + γ-$BeSO_4$; 7 = *l* .

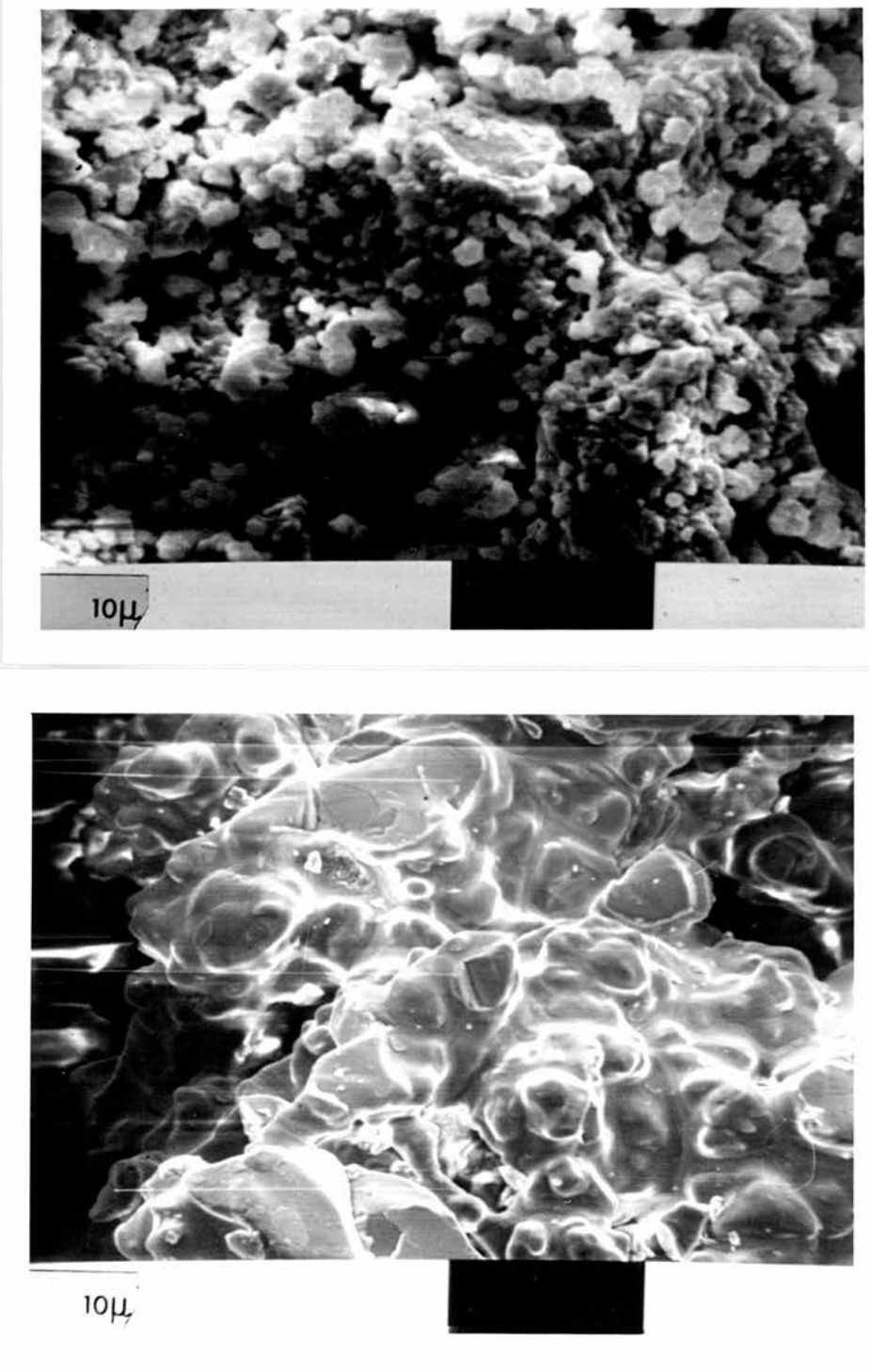

Fig. 69. Electron micrographs of (a) a powdered mixture of composition {98 mol% $BeSO_4$-2 mol% Ag_2SO_4} and (b) the above mixture held at 550 °C (above the eutectic temperature) for 1 h and quenched. In (b) , $BeSO_4$ crystals are coated in glass.

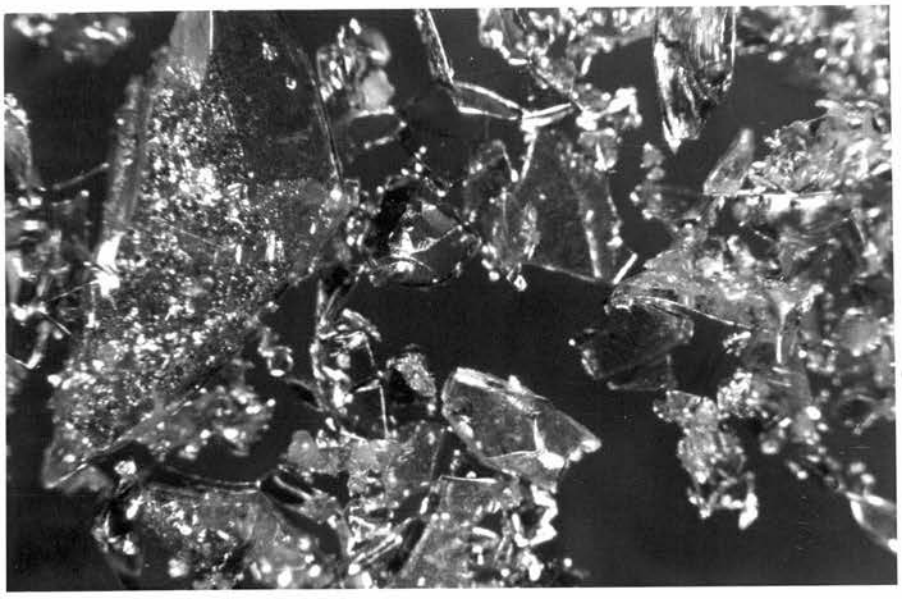

(a)

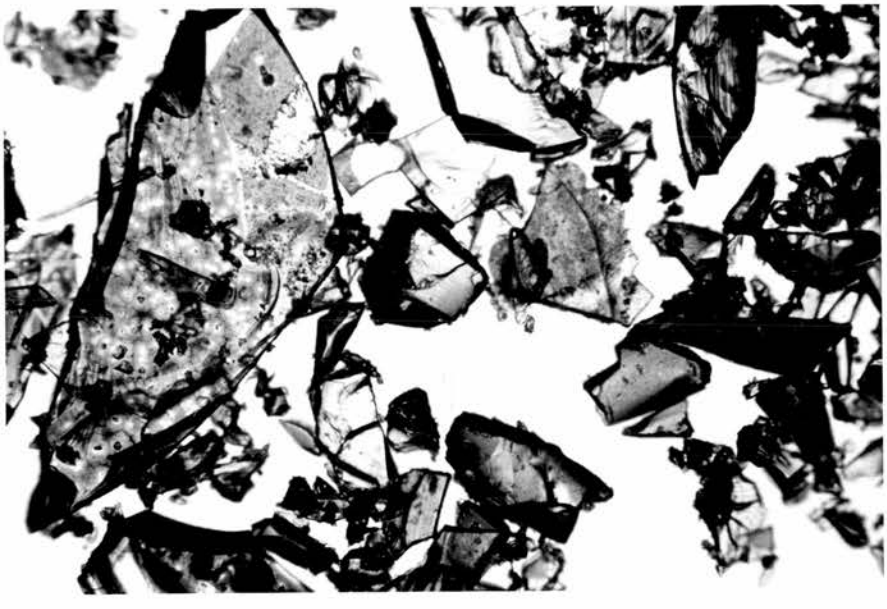

(b)

Fig. 70. Optical micrographs at x50 of a mixture of composition {42 mol% $BeSO_4$-58 mol% Ag_2SO_4} held at 606 °C (20 °C above the estimated liquidus line) for 20 h and quenched. Examination in (a) crossed polars and (b) normal transmitted light. The sample is essentially glass (dark in crossed polars) with very few crystalline regions.

REFERENCES

(1) I.Langmuir , J. Amer. Chem. Soc. , 38(1916)2263.

(2) P.W.M.Jacobs and F.C.Tompkins , in W.E.Garner (Ed.) , Chemistry of the Solid State , Butterworths , London , 1955 , p. 184.

(3) D.A.Young , Decomposition of Solids , Pergamon , Oxford , 1966.

(4) F.C.Tompkins , in N.B.Hannay (Ed.) , Treatise on Solid State Chemistry , vol. 4 , Plenum , London , 1976.

(5) A.W.Searcy and D.Beruto , J. Phys. Chem. , 80(1976)425 ; 82(1978)163.

(6) T.L.Hill , An Introduction to Statistical Thermodynamics , Addison-Wesley , London , 1960.

(7) J.J.Burton , in B.J.Berne (Ed.) , Statistical Mechanics , part A , Plenum , London , 1977 , p. 195.

(8) N.B.Hannay , Solid State Chemistry , Prentice-Hall , London , 1967.

(9) W.E.Garner and T.J.Jennings , Proc. Royal Soc. , A224(1954) 460.

(10) P.J.Herley , P.W.M.Jacobs and P.W.Levy , Proc. Royal Soc. , A318(1970)197.

(11) N.F.H.Bright and W.E.Garner , J. Chem. Soc. , (1934)1872.

(12) J.A.Cooper and W.E.Garner , Trans. Faraday Soc. , 32(1936)1739.

(13) D.Beruto and A.W.Searcy , J. C. S. Faraday I , 70(1974)2145.

(14) P.Mohazzabi and A.W.Searcy , J. C. S. Faraday I , 72(1976)290.

(15) E.T.Turkdogan , Physical Chemistry of High Temperature Technology , Academic , London , 1980.

(16) W.E.Garner , in W.E.Garner (Ed.) , Chemistry of the Solid State , Butterworths , London , 1955 , p. 213.

(17) D.Nicholson and J.H.Petropoulos , in S.J.Gregg , K.S.W.Sing and H.F.Stoeckii (Eds.) , Characterization of Porous Solids , Society of the Chemical Industry , London , 1979 , p. 211.

(18) F.W.Sears , M.W.Zemansky and H.D.Young , University Physics , Addison-Wesley , London , 5th ed. , 1976 , p. 233.

(19) E.H.Kennard , Kinetic Theory of Gases , McGraw-Hill , London , 1938.

(20) H.A.Lorentz , Lectures on Theoretical Physics , vol. 7 , MacMillan , London , 1927 , chp. 3.

(21) I.Langmuir , Ann. Physik , 14(1913)1273.

(22) A.N.Nesmeyanov , Vapour Pressures of the Chemical Elements , Elsevier , London , 1963.

(23) T.D.Sandry and F.D.Stevenson , J. Chem. Phys. , 53(1970)151.

(24) P.Clausing , Ann. Physik , 12(1932)961.

(25) I.M.Sobol , The Monte Carlo Method , The University of Chicago Press , London , 1974.

(26) R.A.Alberty and F.Daniels , Physical Chemistry , Wiley , New York , 5th ed. , 1980 , p. 227.

(27) R.M.Barrer and J.A.Barrie , Proc. Royal Soc. , 213A(1952)250.

(28) R.M.Barrer and T.Gabor , Proc. Royal Soc. , 256A(1960)267.

(29) P.C.Carman , Flow of Gases Through Porous Media , Butterworths , London , 1956.

(30) J.L.Margrave , in J.O'M.Bockris , J.L.White and J.D.Mackenzie (Eds.) , Physicochemical Measurements at High Temperatures , Butterworths , London , 1959 , p. 225.

(31) J.V.Lepore and J.R.Van Wazer , Atomic Energy Commission USA Report MDDC-1188 , 1948.

(32) M.Avrami , J. Chem. Phys. , 7(1939)1103 ; 8(1940)212.

(33) B.V.Erofeyev , C. R. Acad. URSS , 52(1946)511.

(34) K.L.Mampel , Z. Phys. Chem. , A187(1940)43.

(35) Handbook of Chemistry and Physics , 61st ed. , The Chemical Rubber Company , 1980.

(36) B.Topley and M.L.Smith , Nature , 128(1931)302.

(37) R.Giovanoli and R.Brütsch , Thermochim. Acta , 13(1975)15.

(38) R.D.Shannon , Trans. Faraday Soc. , 60(1964)1902.

(39) R.D.Schultz and A.O.Dekker , J. Chem. Phys. , 23(1955)2133.

(40) K.J.Laidler , Chemical Kinetics , McGraw-Hill , London , 1965.

(41) J.E.Burke and J.H.Rosolowski , in N.B.Hannay (Ed.) , Treatise on Solid State Chemistry , vol. 4 , Plenum , London , 1976.

(42) W.D.Kingery and B.Francois , in G.C.Kuczynski , N.A.Hooton and C.F.Gibbon (Eds.) , Sintering and Related Phenomena , Gordon and Breach , New York , 1967.

(43) J.M.Bijovoet , X-ray Analysis of Crystals , Butterworths , London , 1951.

(44) V.C.Farmer (Ed.) , The Infra Red Spectra of Minerals , Mineralogical Society Monograph no. 4 , London , 1974.

(45) E.G.Prout and F.C.Tompkins , Trans. Faraday Soc. , 40(1944)488.

(46) W.W.Wendlandt , Thermal Methods of Analysis , Wiley-Interscience , London , 1964.

(47) C.B.Murphy , Anal. Chem. , 42(1970)268R ; 36(1964)347R.

(48) H.E.Kissinger , Anal. Chem. , 29(1957)1702.

(49) J.H.Sharp , in R.C.Mackenzie (Ed.) , Differential Thermal Analysis , vol. 2 , Academic , 1972.

(50) P.P.Budnikov and A.M.Ginstling , Solid State Chemistry , Maclaren , London , 1968.

(51) H.Schmarlzried , in N.B.Hannay (Ed.) , Treatise on Solid State Chemistry , vol. 4 , Plenum , London , 1976.

(52) S.F.Hulbert , J. Brit. Ceram. Soc. , 6(1969)11.

(53) J.L.Margrave , in J.O'M.Bockris , J.L.White and J.D.Mackenzie (Eds.) , Physicochemical Measurements at High Temperatures , Butterworths , London , 1959 , p. 6.

(54) International Practical Temperature Scale of 1968 (English Version of the Official French Text) , HMSO , London , 1969.

(55) D.R.Stull and H.Prophet , JANAF Thermochemical Tables , US Department of Commerce , Washington , 1971.

(56) P.D.Garn , Thermoanalytical Methods of Investigation , Academic , London , 1965.

(57) K.H.Stern and E.L.Weise , National Bureau of Standards Report NSRDS-NBS 7 , US GPO , Washington , 1966.

(58) H.H.Kellogg , Trans. Met. Soc. AIME , 230(1964)1622.

(59) V.V.Pechkovskii and M.S.Gaisinovich , Zh. Neorg. Khim. , 9(1964)2299.

(60) M.M.Shokarev , F.I.Vershinnia and E.V.Margulis , Zh. Strukt. Khim. , 11(1970)151.

(61) T.R.Ingraham and H.H.Kellogg , Trans. Met. Soc. AIME , 227(1963)1419.

(62) G.Hoschek , Monat. Chem. , 9(1962)826.

(63) B.Nam , C.R. , 249(1959)1108.

(64) K.Friedrich and A.Blicke , Metallurgie (Halle , Ger.) , 7(1910)323.

(65) G.A.Kolta and M.H.Askar , Thermochim. Acta , 11(1975)65.

(66) G.V.Jagannathan , D.G.Powell and P.A.H.Wyatt , J. Chem. Research , (S)(1978)372.

(67) A.M.Alper (Ed.) , Phase Diagrams : Materials Science and Technology , vols. 2 and 3 , Academic , London , 1970.

(68) T.I.Barry (Ed.) , The Industrial Use of Thermochemical Data , Chemical Society Special Publication no. 34 , London , 1980.

(69) G.A.Chadwick , Metallography of Phase Transitions , Butterworths , London , 1972.

(70) R.E.Smallman and K.H.G.Ashbee , Modern Metallography , Pergamon , Oxford , 1969.

(71) M.L.McGlashan , Physicochemical Quantities and Units , Royal Institute of Chemistry Monograph for Teachers no. 15 , London , 1968.

(72) M.L.McGlashan , Chemical Thermodynamics , Academic , London , 1979.

(73) O.Kubaschewski, in J.O'M.Bockris , J.L.White and J.D.Mackenzie (Eds.) , Physicochemical Measurements at High Temperatures , Butterworths , London , 1959.

(74) N.Temkin , Acta Physicochim. URSS , 20(1945)411.

(75) O.Kubaschewski , E.L.Evans and C.B.Alcock , Metallurgical Thermochemistry , Pergamon , Oxford , 1967.

(76) H.K.Hardy , Acta Met. , 1(1953)202.

(77) J.J.Van Laar , Z. Physik. Chem. , 63(1908)216 ; 64(1908)257.

(78) CALPHAD , Pergamon , Oxford.

(79) L.Kaufman and H.Bernstein , Computer Calculation of Phase Diagrams , Academic , London , 1970.

(80) L.Kaufman and H.Nesor , in N.B.Hannay (Ed.) , Treatise on Solid State Chemistry , vol. 5 , Plenum , London , 1976.

(81) W.W.Liang , P.-L.Lin and A.D.Pelton , High Temp. Science , 12(1)(1980)41 ; 12(2)(1980)71.

(82) L.Kaufman and H.Nesor , CALPHAD , 2(1978)35.

(83) L.Kaufman , CALPHAD , 27(1979)3.

(84) P.-L.Lin , A.D.Pelton and C.W.Bale , J. Amer. Ceram. Soc. , 62(1979)414.

(85) C.W.Bale and A.D.Pelton , Met. Trans. , 5(1974)2323.

(86) G.W.Toop , Met. Trans. , 233(1965)850.

(87) F.Kohler , Monat. Chem. , 91(1960)738.

(88) G.V.Raynor , in R.W.Cahn (Ed.) , Physical Metallurgy , North-Holland , Amsterdam , 1970.

(89) J.B.MacChesney and P.E.Rosenberg , in A.M.Alper (Ed.) , Phase Diagrams : Materials Science and Technology , vol. 1 , Academic , London , 1970.

(90) W.Kauzmann , Chem. Rev. , 43(1948)219.

(91) A.Ishii and K.Aikawa , Reports-Research Lab. of Ashai Glass Co. Ltd. , 15(1965)1.

(92) M.E.Fine , Phase Transformations in Condensed Systems , MacMillan , London , 1964.

(93) C.N.R.Rao and K.J.Rao , Phase Transitions in Solids , McGraw-Hill , London , 1978.

(94) W.Gutt and A.J.Majumander , in R.C.Mackenzie (Ed.) , Differential Thermal Analysis , vol. 2 , Academic , London , 1972.

(95) H.S.Yoder , Trans. Amer. Geophys. Union , 31(1950)827.

(96) G.C.Kennedy and R.C.Newton , in W.Paul and D.M.Warschauer (Eds.) , Solids Under Pressure , McGraw-Hill , London , 1963.

(97) C.W.F.T.Pistorius , J. Chem. Phys. , 43(1965)2895 ; 44(1966)4532 ; 46(1967)2167.

(98) F.P.Bundy , W.R.Hibbard and H.M.Strong (Eds.) , Progress in Very High Pressure Research , Wiley , New York , 1961.

(99) R.Powell , Equilibrium Thermodynamics in Petrology , Harper and Row , London , 1978.

(100) J.L.McNaughton and C.T.Mortimer , in H.A.Skinner (Ed.) , Thermochemistry and Thermodynamics , Physical Chemistry Series 2 , vol. 10 , International Review of Science , Butterworths , London , 1972.

(101) A.Stingele , Thermodyn. Nucl. Mater. , Proc. Symp. , Vienna 1967 (pub. 1968) 92-24. From Nuc. Sci. Abst. 22(15)(1968)31448. International Atomic Energy Agency , Vienna , Austria.

(102) R.P.Miller and G.Sommer , J. Sci. Inst. , 43(1966)293.

(103) N.H.Hartshorne and A.Stuart , Crystals and the Polarising Microscope , Edward Arnold , London , 3rd ed. , 1960.

(104) E.M.Chamot and C.W.Mason , Handbook of Chemical Microscopy , vol. 1 , Wiley , New York , 1958.

(105) D.Shelly , Manual of Optical Mineralogy , Elsevier , Oxford , 1975.

(106) H.J.Goldschmidt , High Temperature X-ray Diffraction Techniques , Bibliography 1 , International Union of Crystallographers Commission on Crystallography Apparatus , 1967.

(107) E.M.Levin , C.R.Robbins and H.F.McMurdie (Eds.) , Phase Diagrams for Ceramists , The American Ceramic Society , Ohio , 1964.

(108) J.F.Schairer , in J.O'M.Bockris , J.L.White and J.D.Mackenzie (Eds.) , Physicochemical Measurements at High Temperatures , Butterworths , London , 1959.

(109) J.J.Rowe , G.W.Morey and I.D.Hansen , J. Inorg. Nucl. Chem. , 27(1965)53.

(110) E.W.Dewing and F.D.Richardson , Trans. Faraday Soc. , 55(1959)611.

(111) E.T.Turkdogan , Met. Trans. , 5(1974)1537.

(112) S.Gal , G.Pokol and E.Pungor , Thermochim. Acta , 16(1976)339.

(113) R.C.Mackenzie , Talanta , 16(1969)1227.

(114) R.C.Mackenzie , C.J.Keattch , D.Dollimore , J.A.Forrester , A.A.Hodgson and J.P.Redfern , Talanta , 19(1972)1079.

(115) S.D.Shargorodskii , Ukr. Khim. Zh. , 15(1949)332.

(116) C.R.M.Rao and P.N.Mehrota , Thermochim. Acta , 29(1979)180.

(117) B.R.Conrad , T.B.McAneney and R.Shridhar , J. Chem. Thermodyn. , 10(1979)889.

(118) C.W.F.T.Pistorius , J. Chem. Phys. , 46(1967)2167.

(119) B.N.Mehrotra , W.Eysel and Th. Hahn , Acta Crystallogr. , Sect. B , B33(1)(1977)305.

(120) I.J.Bear and A.G.Turnbull , Aust. J. Chem. , 19(1966)751.

(121) I.I.Bosik , A.V.Novoselova and Yu.P.Simanov , Russ. J. Inorg. Chem. , 6(1961)1295.

APPENDIX 1.

Notation used in part two

(1) The partial molar free energy (chemical potential) of component A in a binary solution of structure α at temperature T and a pressure assumed to be 1 atm , is written ${}^{\alpha}G_A(T,X)$. X is the mole fraction of a specified component , say A. For a solid solution , the symbol α indicates the structure of the lattice. For pure component A of structure α, the molar free energy is equivalent to the chemical potential , that is

$$ {}^{\alpha}G_A^*(T) = {}^{\alpha}G_A(T,X=1) $$

Similarly , the molar enthalpy , molar constant pressure heat capacity , etc. are written ${}^{\alpha}H_A^*(T)$, ${}^{\alpha}C_{p,A}^*(T)$, etc. .

(2) $\Delta_{\alpha}^{\varepsilon}G_A^*(T)$ is equivalent to ${}^{\varepsilon}G_A^*(T) - {}^{\alpha}G_A^*(T)$.

(3) The molar integral free energy of a binary solution of structure α is written as ${}^{\alpha}G_m(T,X)$. To avoid confusion , m must not be used to label a component.

(4) The temperature at which phases α and ε coexist in equilibrium is written as $T^{\alpha+\varepsilon}$.

APPENDIX 2. Results referred to on pages 102-103.

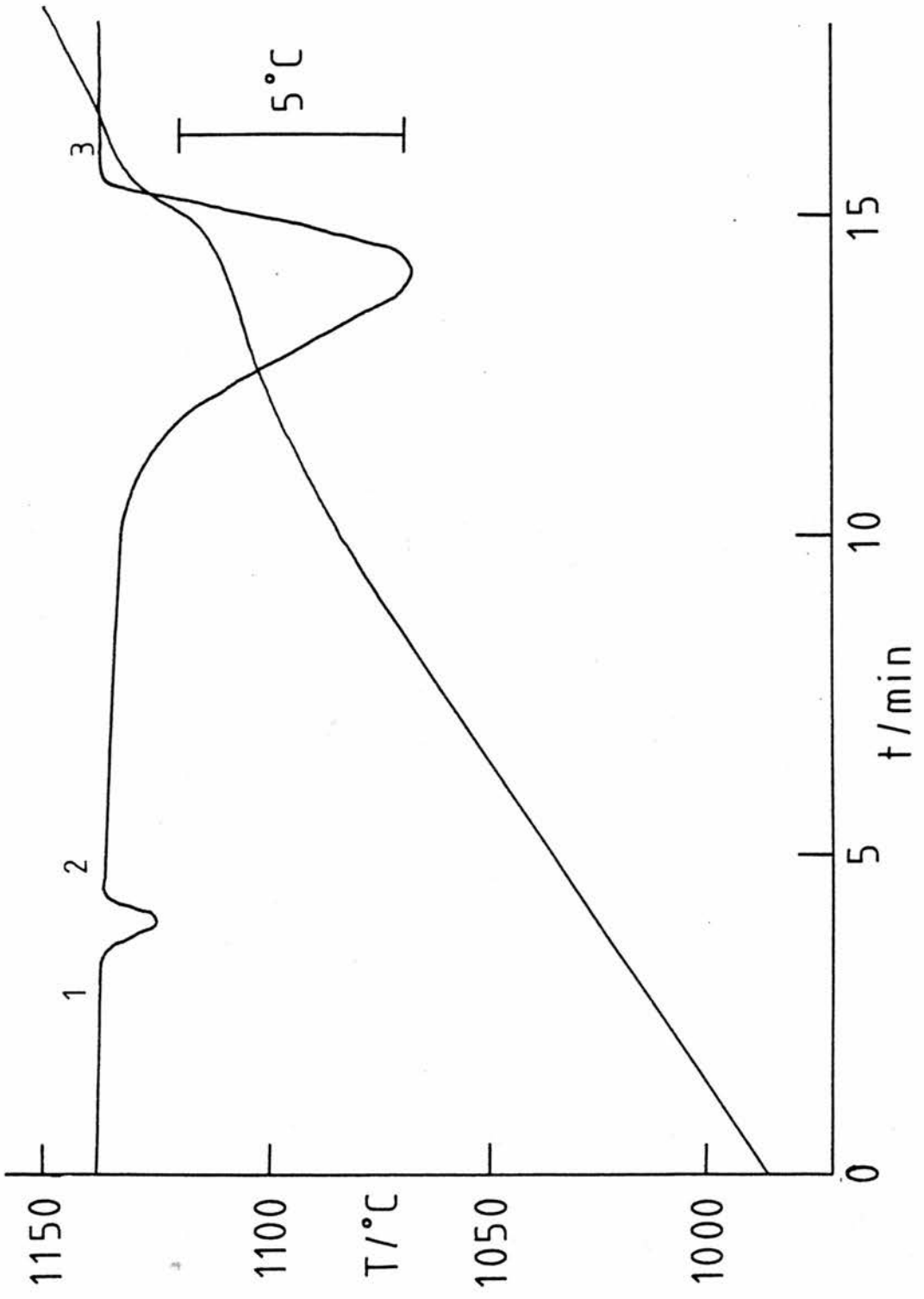

Fig. 71. DTA curves for the $\alpha \rightarrow \beta$ transition and decomposition of $MgSO_4$ in a flowing atmosphere of SO_2 , O_2 and N_2 with a Pt catalyst present. Thermocouple arrangement (a) in fig. 55 was used and the heating/cooling rates were 9 K min^{-1}. 1 = α-$MgSO_4$; 2 = β-$MgSO_4$; 3 = MgO.

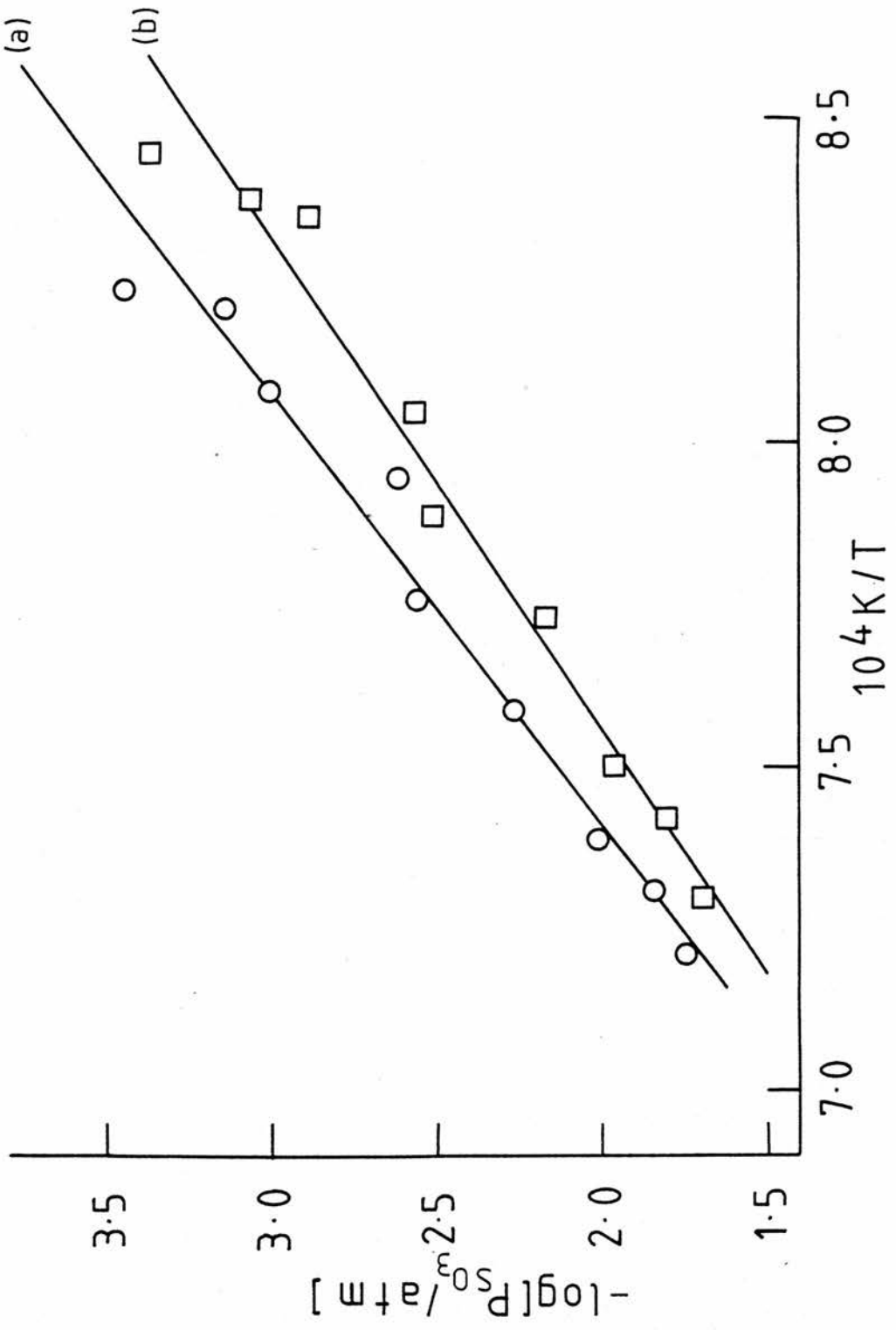

Fig. 72. Dependence on SO_3 pressure of the temperature of onset of reaction : (a) $MgSO_4 \rightarrow MgO$ on heating the sulphate ; (b) $MgO \rightarrow MgSO_4$ on cooling the oxide.